Analysis and Practical Assessment of Converter-Dominated Power Systems: Stability Constraints, Dynamic Performance and Power Quality

Luis Reguera Castillo

Wind & Marine CDT

Electric and Electronic Engineering

University of Strathclyde, Glasgow

September 12, 2018

Declaration

This thesis is the result of the author's original research. It has been composed by the author and has not been previously submitted for examination which has led to the award of a degree.

Signed:

Date:

Acknowledgments

I have to begin by saying thanks to the EPSRC for providing me with the opportunity of doing a PhD with a decent stipend, making me feel welcome in a society which appreciates the values of the university. Unfortunately, this is not the case in my country of origin. Thus, I would like to thank the EPSRC in particular, and the UK in general, for giving me this opportunity.

I ought to extend my gratitude to my supervisor Dr. Andrew Roscoe. He has dealt with my stubbornness and temper with absolute mastery enlightening at the same time my PhD path with the necessary inspirations. To continue, I also would like to thank to my colleagues in the Wind & Marine CDT and the EEE department in general for those good drinks after-work; they had the highest amount of patience in the world dealing with my broken English. Thanks to my colleagues in my cohort for the good times together and the ones which will come after this adventure. In particular I would like to thank Euan; he introduced me to his family with no regret (so far). Also, Alice, my fifth sister, for providing me with the support and the conversations that I needed at the right time. Additionally, my other dinner-club colleagues, Anthony and Alex I have the feeling of bringing with me something big having you as friends.

Now on the more personal side my Spanish community in Glasgow: Esther, Carlos, Carmen, Nuria, Jorge, Efren and Marta. The moment I met you, I began to feel at home in another country and you all know that feeling is one of those things which can help you coping with the Scottish weather. Finally my dear reader, allow me to say some words in Spanish for my family.

GRACIAS en mayúsculas a mis hermanas, Noelia, Diana, Patricia y Olivia y a mi tía Vicenta, por hacerme crecer como persona, como hermano, sobrino, hacerme tío e incluso a veces padrino. He tenido la suerte de que vosotros seas mi familia. Me habéis hecho creer que valgo mucho más de lo que soy o podría llegar a ser.

Sin ellas saberlo, un trozo de este pastel de agradecimientos es para mis sobrinas Irene, Ainara, María e Itzíar. Puedo estar en el extranjero pero siempre estáis conmigo si veo vuestras fotos. Por último, a mis padres, Luis Reguera Muñoz y María Teresa Castillo Pascual. Ellos merecen que ponga sus apellidos porque son a los que debo prácticamente todo lo que soy. Han sufrido mi ausencia con estoicismo sin dejar de alentarme a seguir adelante y conseguir mis metas.

A ellos les dedico y les debo este y cualquier éxito profesional. GRACIAS Papá, GRACIAS Mamá.

Abstract

For years, large power systems have been predominantly managed using the very well known synchronous machine on the generation side. With the increasing penetration of load and generation interfaced by converter-based systems, the conventional synchronous machine is being gradually replaced by these new devices. However, this slow and steady change of the generation technology has led to side-effects which can affect to the local stability and, if no remedial action is taken, system-wide stability.

The main objective of this thesis is to understand, expose and overcome the weaknesses of converter-dominated grids within a laboratory environment. To do so, a converter of 10kVA has been built implementing the standard D-Q axis Current Injection (DQCI) control and, for first time to date, the Virtual Synchronous Machine with Zero Inertia (VSM0H). Further developments have been made to this control strategy to implement this theoretical algorithm into a real system.

The solutions proposed in this thesis for converter-dominated grids are based on the Grid Forming Nodes (GFN) solution. This composition suggests the usage of a combination of DQCI and Virtual Synchronous Machine (VSM) converters to achieve stability within converter-dominated grids. However, there is limited understanding about VSM functioning. Initially, the application of VSM-style converters was proposed as a natural replacement of the real synchronous machine present in the system without understanding which are the specific weaknesses that affect to this type of grid. Due to the aforementioned reasons, this thesis aims to provide a more scientific and rigorous explanation of why the GFN solution can provide stability for converter-dominated power systems. Using the converter built, it is possible to recreate scenarios where the technical challenges involved in power systems can be understood.

Going from well-established solutions for relatively low Levels of Penetration (LoP), such as grid-friendly or smart converters, to an insightful explanation of why these solutions are not valid for converter-dominated grids with high values of LoP. This thesis puts more emphasis on the latter case, assessing experimentally the GFN solution for representative scenarios and control strategies used in the converter built explicitly for this project.

Initially, three experiments are conducted to identify the weaknesses of converter-dominated grids. During these initial scenarios, it has been found that DQCI converters behave as current sources from the grid point of view, following an already imposed voltage signal. As current sources, DQCI converters do not provide effective voltage regulation. On the contrary, GFN/VSM converters behave as voltage sources behind an inductance from the grid point of view. Thus, they contribute to the entire grid stability by assuring the local voltage stiffness. However, further experiments with unbalanced and non-linear loads have found that this capability is finite and directly dependent on the equivalent converter filter impedance.

During the execution of the experiments, there have been additional contributions explained throughout this thesis:

- The virtual resistor technique. Incorporating an additional feed-forward term into the inner current loop, the stabilizing effect of the parasitic inductor resistance is simulated. As result, the inner control loop operates in a more stable manner.

- The explanation, implementation and validation of a novel control strategy which makes the converter operate with variable speed response depending on the grid events. This adaptive functioning leads to a more robust operation for both the converter and the grid.

- A new control strategy based on the VSM0H (so called in this thesis as VSM0H+). Measuring the negative sequence voltage present in the grid, it is possible to add a compensation term which can provide an almost perfect voltage regulation under the presence of heavily unbalanced loads.

Contents

List of Figures

List of Tables

List of Tables

List of Acronyms and Symbols

AC	Alternating Current
APF	Active Power Filter
C_f	Converter filter capacitor
DC	Direct Current
DNO	Distribution Network Operator
DPSL	Dynamic Power Systems Laboratory
DQCI	D-Q Axis Current Injection
F_c	Crossover frequency
GFN	Grid Forming Node
HVDC	High Voltage Direct Current
IGBT	Insulated-Gate Bipolar Transistor
LED	Light Emitting Diode
L_f	Converter filter Inductor
L_{trf}	Equivalent leakage inductance
LoP	Level of Penetration
LV	Low Voltage
LVRT	Low Voltage Ride-Through
MIMO	Multiple Input Multiple Output
MV	Medium Voltage
PCC	Point of Common Coupling
PD	Proportional-Derivative
PI	Proportional-Integral
PLL	Phase Locked-Loop

PM	Phase Margin
PSC	Power Synchronization Control
PV	PhotoVoltaic solar energy
ROCOF	Rate Of Change Of Frequency
R_{Cf}	Damping frequency resistor
R_{trf}	Equivalent core losses resistance
SCR	Short-Circuit Ratio
SFR	Synchronous Referenced Frame
THD	Total-Harmonic Distortion
TSO	Transmission System Operator
VSM	Virtual Synchronous Machine
VSM0H	Virtual Synchronous Machine with Zero Inertia
VSM0H+	Enhanced Virtual Synchronous Machine with Zero Inertia
ω_{res}	Resonance frequency of the converter filter

Chapter 1

Introduction

1.1 Problem definition

In 2018, the relevance of the renewable energies in many countries around the world is undeniable. Since the beginning of the 2000s, many power systems started to replace carbon or gas plants by renewable generation for two reasons: reduction in carbon footprint, and energy independence. For instance, as of 2015, wind energy represents the second largest form of generation in Europe in capacity terms, with gas being the largest [1]. In total, 168.7 GW of net installed capacity is based on wind energy in Europe as of 2017. The PhotoVoltaic (PV) solar energy is experiencing a huge growth as well. In 2017, the total net capacity of this technology experienced a spectacular 28% increase, reaching a total of 8.61 GW of energy installed in Europe [2].

However, these new technologies give rise to technical challenges. Since wind and solar energy use converters to produce grid-compliant electricity, every single time a gas, carbon or oil plant is replaced by a wind or solar farm there is a greater deviation from the well-understand classical power system. If the aggregated nominal power of converters connected to the grid is not relevant compared to the total, the implications and drawbacks caused by these systems are not significant. However, as these converters begin to represent significant proportions of overall energy mix, conventional tasks which assure the grid stability, traditionally undertaken and inherently provided by synchronous generators, must be supplied by the converters.

Due to the aforementioned reasons, countries with a high amount of renewable energy are also countries with a high amount of converter-based generation. Thus, they are gradually transforming from conventional synchronous-dominated power systems, to converter-dominated power systems. This progression has major implications on grid stability if the converter-based generation reaches certain level and, if nothing is done, they can lead to additional costs in the electricity price. In [3], these costs are calculated for the UK system, reaching up to 3000 m per year due to additional charges caused by technical constraints in the grid.

In this thesis, these implications will be analyzed and exposed, proposing solutions to overcome the side-effects of converter-based generation, and, lastly, allowing the possibility of a technically feasible electric system based solely on converters.

1.2 Background

The evaluation of the side-effects caused by the renewable energy integration has a long history of studies since it has been a topic of major interest in academia and industry. The first indication that converters were producing grid instabilities for Transmission System Operators (TSO) and Distribution Network Operators (DNO) was the major drop of the aggregated inertia of the electric system.

If a short-circuit or sudden loss of load occurs in the network, conventional machines naturally react injecting a current surge. This additional current is created by the sudden acceleration of the rotor caused by a combination of the mechanical inertia of the rotating elements of the generator and the loss of electric torque in the stator. This also contributes to the grid stability since it helps to recover the system from the grid event avoiding a major cascade failure which could end in the disconnection of a lot of generators in the neighborhood or, in the worst case, a local or total blackout.

Before TSOs and DNOs realized about this drop in inertia, no duties were demanded to the renewable generation. Therefore, these wind or solar farms only should inject the energy produced to the grid. Consequently, no contribution to the grid stiffness or inertia was required from these producers. In an equivalent way, no reactive power was required from these systems, causing also local voltage instability and displacing

these duties to the remaining synchronous generators present in the system. Since, as it has been mentioned previously, no additional task was required initially to the renewable energy, the same delegation of responsibilities was applied for other grid ancillary functions which conventional synchronous generators provided naturally and at no cost such as inertial response and frequency or voltage regulation.

TNOs and DNOs, witnessing this loss of management of the system, began to evaluate the possibility of requiring that converters to provide a set of functionalities which could help to mitigate the side-effects caused by the converter/renewable generation. These ancillary functions would be included into the national grid codes, and would be imposed on new generators connected to the grid (explained more profusely in Chapter 4). Converters performing these additional tasks would be baptized as grid-friendly or smart-converters. Nonetheless, although there has been a communal effort between TSOs to perform an homogenization of the grid codes, the exact definition and performance of these tasks vary across Europe, making it difficult to manage at continental level.

Depending on the total nominal power based on converters installed in the specific electric system of interest, these grid-friendly converters can be the solution to solve the instability of electric systems where converters and synchronous machine have to coexist in a stable manner. However, if the number of converter-based generation is relatively high, grid-friendly converters are only a temporary solution to the problem. As reference, in [4], one of the first books where the grid supporting functions were explained, a Level of Penetration (LoP) of 10% is considered high (although this parameter will be further explained in section 1.4, at this point consider LoP as the percentage of the total generation based on converters). Therefore, there is a certain limit beyond which, the application of grid-friendly converters is not practical. It is at this point where more drastic solutions have to be considered and these grids begin to be recognized as converter-dominated grids.

Stability within converter-dominated grids is an active area of research, 11 countries have already hit the objectives for 2020 [5] of 20% of renewable energy [6]. Excluding hydro power, the vast majority of renewable energy is converter-based. Thus, the vast

majority of the 20% of renewable power is converter-interfaced. Such systems have, due to their novelty, not been studied extensively. One of those few ones is a project realised in Strathclyde University in collaboration with National Grid about the limits of converter-dominated grids, nonetheless, it is enclosed in the simulation scope [7, 8].

1.3 Providing stability in converter-dominated grids

In order to begin assessing the stability of converter-dominated grid, it isalways good to start from the basics. In his book Power System Stability and Control [9], P. Kundur states that grid stability is assured for power systems if three main pillars are controlled. These are depicted in Figure 1.1.

If frequency, rotor angle, and voltage stability are guaranteed, the electrical grid can be considered stable. Therefore, special emphasis has to be made to these three parameters. However, the weight and importance of these factors will depend on the type of electrical grid. If, for instance, a power system is based on synchronous machines, frequency stability and rotor angle stability play a major contribution. To illustrate this, equation 1.1 is presented. It defines the active power injected by a synchronous machine connected to a grid.

$$P_{Sync} = \frac{|\,E\,||\,V\,|}{X} sin\delta \tag{1.1}$$

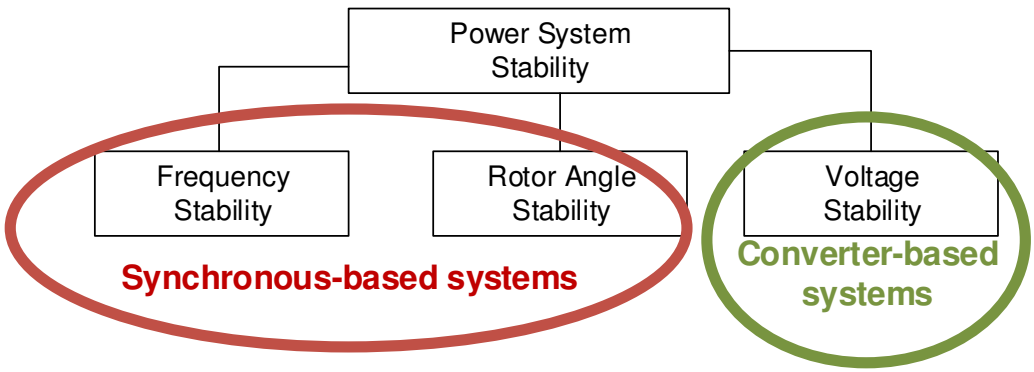

Figure 1.1: Power system stability according to [9].

where E is the voltage set by the machine, V the grid voltage, X the reactance that is between them and δ is the difference of angle between the machine and the grid. From equation 1.1, it is straightforward to observe that if the rotor angle is not stable, δ would be ungovernable and, consequently, the active power. The same can be said about frequency stability. If sudden changes of frequency were to occur, there would be jumps or transitory shifts in the difference of angle δ, which would create power shifts as well. These oscillations could potentially drive the synchronous machine to an unstable region where it would be forced to disconnect. However, the importance of voltage stability is low relative to synchronous generator-based grids. Since a synchronous machine behaves as a source of positive sequence voltage, it imposes its nominal voltage regardless of the grid events. Naturally, if the voltage deviations are large, this would affect V in equation 1.1. However, relative to δ, the net change in P_{Sync} would be relatively lower. In other words, for the same variation of driving angle or voltage ($\Delta\delta$ or ΔV), the variation in the resulting output power (ΔP_{Sync}) is much higher for the case of the driving angle.

Now, moving to the other extreme of the case where a grid is completely based on converters the importance of these parameters seems opposite. The converter is a system based on semiconductors which is steady and does not have to respect any mechanical inertia to inject its energy. Therefore, without considering the internal stability of the control algorithm and taking into account exclusively the physics of the generator, this element can deal without major problems sudden changes of frequency or instantaneous grid angle. However, these elements are especially sensitive to the voltage noise or weak networks with a low Short-Circuit Ratio (SCR). Conventional-controlled converters based in the vectorial current control on the D-Q axis (DQCI converters) use a Phase Locked Loop (PLL) to provide a reference of synchronism to the system. This subsystem is especially sensitive to the voltage, being prone to disconnect when the voltage is not stiff or it contains much noise coupled to the main signal.

To summarize, in order to assure the stability of power systems dominated by synchronous generators, more attention will have to be paid to the frequency and

rotor angle stability. On the contrary, for converter dominated grids, voltage stability will be the main contributor to the entire stability. Because of the aforementioned reasons, when a conventional grid is moving on from a synchronous-based system to a converter-based grid, the importance of the frequency and rotor angle stability to the entire system stability is being translated to the voltage stability. Having this evidence clear, special measurements can be taken to guarantee that the voltage is stable and free of noise coupled.

1.3.1 The Grid Forming Nodes solution

The pursued voltage stiffness can be provided by what has been called *Grid Forming Nodes* (GFN) and initially cited in [8]. In principle, just with a replacement of the internal algorithm, it is possible to transform a converter into a GFN and make it behave as a source of positive sequence voltage. Consequently, this will mitigate automatically the lack of voltage regulation and will guarantee the pursued voltage stability to the nearby converters. These new algorithms are called Virtual Synchronous Machine (or VSM). However, although the solutions based in the VSM algorithm are several (more deeply analyzed in Chapter 2), only one of these solutions, the Virtual Synchronous Machine with Zero Inertia (VSM0H) has been evaluated in this thesis.

The structure of the GFN solution is better illustrated with Figure 1.2. Assuming the majority of the existent and future converters are controlled using the conventional DQCI algorithm, only a fraction of the nominal power generated and connected should behave as GFN to assure the stability of the entire grid. This fraction is defined in [8] as 10% for marginal stability and 20% as a more realistic value.

1.4 Level of Penetration

In previous sections, the loose concept of Level of Penetration or LoP was introduced but not explicitly defined. LoP aims to encapsulate the idea of how much demand can be supplied by converters while maintaining robust and feasible operation. However, as it will be shown along this section, this idea can be difficult to express in a single parameter since the particularities of a large interconnected grid can be too expansive

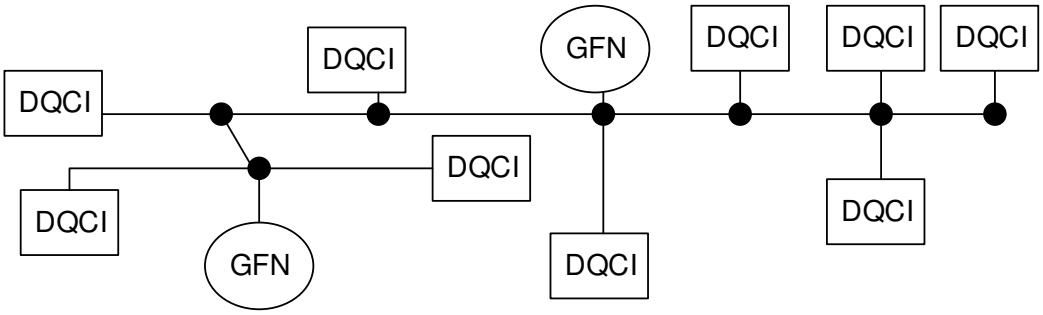

Figure 1.2: Architecture of the Grid Forming Nodes solution.

for LoP to be condensed in a single number. Thus, several definitions of this parameter will be explained.

The most straightforward definition of this parameter can be obtained dividing the total power provided into in two groups: one for all the generators based on converter systems, and another for the ones based on synchronous generators. If the power of each group is combined, it is possible to find a percentage or *LoP*. This is explained in equation (1.2):

$$LoP(\%) = \frac{\sum |P_{Conv}|}{\sum |P_{Conv}| + \sum \mid P_{SG} \mid} \tag{1.2}$$

where P_{Conv} is the total active power provided by converters installed in the system, P_{SG} is the total active power provided by synchronous generators or generators not-based in converters.

However, this research topic involves the study of large power systems, much more intricate and complicated than the small-scale recreations performed in this thesis. Such systems have many particularities in an electric market that evolve to, each time more, larger and more interconnected systems that exchange energy using high power rated connections. Although these connections can be done also in AC, usually they are done in DC due to its higher transmission capacity [4]. Thus, an equation that would take into account this particularity can be expressed as follows:

$$LoP_{exp}(\%) = \frac{\sum P_{Conv} + HVDC_{Imports}}{P_{Demand} + HVDC_{Exports}} \tag{1.3}$$

where P_{Conv} is the power injected based in converters, $HVDC_{Imports}$ is the contribution of power generation from external systems, $HVDC_{Exports}$ is the power exported to other systems and P_{Demand} is the total demand of the system, in watts, regardless of the energy origin necessary to provide it. This equation is used for many organizations such as National Grid or Eirgrid [3].

Additionally, according to the evidence found in the experiments conducted in Chapters 5 and 6, a new equation for LoP is proposed in this thesis. Due to its relevance to this section, it will be introduced here. For further explanation refer to the aforementioned chapters or, alternatively to the paper of the author in [10].

$$LoP_{conv}\left(\frac{W}{VA}\right) = \frac{\sum |P_{DQCI}| + \sum |P_{GFN}|}{\sum |S_{DQCI}| + \sum S_{SG} + \sum S_{GFN}} \tag{1.4}$$

where P_{DQCI} and P_{GFN} are the aggregated active power injected or absorbed from the system such as; converter-connected generation, energy storage devices or HVDC systems controlled using the DQCI strategy or regulating as GFN, respectively. S_{GFN} is the aggregated rated power of every GFN converter. S_{DQCI} is the aggregated nominal power of the DQCI-controlled converters and, finally, S_{SG} is the aggregated nominal power connected into the system based on real synchronous systems.

1.5 Objectives

Having explained the potential issues associated with the integration of converter-interfaced generation into large power systems, the main objective of the thesis is to understand which are the weaknesses of converter-dominated grids and once these are understood, propose new solutions which will be validated in the laboratory environment. If the GFN solution is going to be implemented, experimental assessments have to be made in order to validate this solution. Part of this work is to choose representative scenarios where these aforementioned weaknesses can be exposed providing evidences of the conclusions obtained.

To perform this task in the laboratory, a customized converter of 10 kVA has been built and integrated into the microgrid of the Dynamic Power Systems Laboratory

(DPSL) [11]. This converter requires the capability of reconfiguration such that, without any change in the hardware used, the converter can switch its internal control algorithm from one where the system is controlled using the conventional DQCI control strategy to one where the inverter behaves as a GFN using a style of VSM algorithm. This functionality allows the realization of experiments such as the evaluation of maximum LoP using different control strategies, or the contribution of the GFN solution to the power quality.

1.6 Structure of the thesis

The project is outlined as following:

Chapter 2 introduces the concepts of Virtual Synchronous Machines and expose the weaknesses and strengths of different algorithms which can potentially make the converter to work as GFN. It provides further insights about the problematic of converter-dominated grid, and which are the specific features of synchronous machines required to provide absolute stability for this type of grids.

Chapter 3. For the realization of this project a 10 kVA converter has been built and integrated into the DPSL. This Chapter explains details about its design and construction including the two logics of control embedded in this converter, the standard DQCI and the VSM0H.

Chapter 4. As it was explained in the introduction, there is a middle step solution between synchronous-dominated and converter-dominated electrical grids which can provide stability to power systems with a relatively low LoP; the grid-friendly converters. These converters provide some ancillary functions to the grid which are sufficient to maintain the grid stability. In this Chapter these functions will be explained and implemented in the aforementioned converter providing at the same time two additional contributions to the thesis; the grid-friendly converter with customizable response and the virtual resistor.

Chapter 5. In this Chapter several laboratory experiments are described which assess the operation limits of a small-scaled representation of a converter-dominated grid, evaluating the capability of islanding and the dynamic behaviour of the converter using

the conventional DQCI control strategy and the VSM0H. Also, the GFN architecture will be evaluated as solution for electrical grids highly dominated by converters.

Chapter 6. Additionally, the GFN solution will be assessed further against, this time, challenging loads which differ significantly from the previously assumed linear and balanced loads. The experiments conducted with unbalanced and non-linear loads provide an insightful and deep understanding of the GFN solution and the measures necessaries to eliminate or mitigate their side-effects.

Conclusions, further work and main contributions. The project ends with the key findings of the thesis, evaluating the fulfillment of the objectives previously set and proposing future work.

Bibliography

[1] Wind Power in 2017. "Annual combined onshore and offshore wind energy statistics. Wind Europe Annual Statistics." Internet: https://windeurope.org/wp-content/uploads/files/about-wind/statistics/WindEurope-Annual-Statistics-2017.pdf [Consulted May 2018].

[2] SolarPower Europe Press. "European Solar Market Grows 28% in 2017." Internet: http://www.solarpowereurope.org/fileadmin/user_upload/documents/Media/090218_press_release_European_Solar_Market_Grows_28__in_2017.pdf [Consulted in May 2018]

[3] Helge Urdat el all. "System strength considerations in a converter dominated power system" presented at the Wind Integration Workshop, London, 2015.

[4] T. Ackermann et all. *Wind Power in Power Systems*, England, Ed. Wiley, 2005, pg. 144.

[5] European Comission in Renewable energy. "Moving towards a low carbon economy". Internet: https://ec.europa.eu/energy/en/topics/renewable-energy [Consulted May 2018].

[6] Eurostat. "Eleven EU countries hit 2020 renewable energy targets". Internet: http://ec.europa.eu/eurostat/documents/2995521/7905983/8-14032017-BP-EN.pdf/af8b4671-fb2a-477b-b7cf-d9a28cb8beea [Consulted May 2018].

[7] Yu, M, Roscoe, AJ, Dysko, A, Booth, CD, Ierna, R, Zhu, J & Urdal, "Instantaneous penetration level limits of non-synchronous devices in the British power system". *IET Renewable Power Generation*, vol. 11, page 1211-1217, 2017.

[8] Ierna, R, Zhu, J, Roscoe, AJ, Yu, M, Dysko, A, Booth, CD & Urdal, H 2016, "Effects of VSM convertor control on penetration limits of non-synchronous generation in the GB power system" presented at 15th Wind Integration Workshop, Vienna, Austria, 2016.

[9] P. Kundur. *Power system Stability and Control*. Ed. McGraw-Hill. USA, 1994.

[10] L. Reguera Castillo, A.J. Roscoe, "Experimental Stability Assessment of Converter-Dominated Electrical Grids" presented at the 16th Wind Integration Workshop, Berlin, 2017.

[11] University of Strathclyde. "webpage of the Dynamic Power Systems Laboratory". Internet: https://pure.strath.ac.uk/portal/en/equipment/dynamic-power-systems-laboratory(d81dbaed-713c-440b-a5ee-11d8052f1a63).html [Consulted May 2018].

Bibliography

Bibliography

Chapter 2

Review of VSC control strategies and Problem insight

2.1 Introduction

In the previous chapter, the topic under study in this thesis has been explained, exposing the main weaknesses of converter-dominated grids and which are the main concepts of the solutions proposed. In section 1.3.1, the so-called Grid-Forming nodes solution was mentioned and briefly explained as an architecture which can provide the necessary stability for large converter-dominated grids. These solutions were based on the usage of converters controlled in a different manner from the conventional vectorial D-Q Converter Injected controlled (DQCI) control. These new algorithms are enclosed within the Virtual Synchronous Machines (VSM) since partially or totally behave similarly to a synchronous generator. The variant VSM0H, which provides voltage stability but no inertia, is investigated in this thesis.

The initial motivation for the creation of these algorithms was the progressive decay of the total inertia present in large power systems due to the replacement of synchronous machines by converter-based generation and the inability of the latter to mitigate increasing values of ROCOF. Initially, the solutions created were focused on providing synthetic inertia embedded inside the control algorithm [1–4] (Something enclosed within the ancillary functions of grid-friendly converters explained with further

detail in section 4). However, research projects of the University of Strathclyde in collaboration with National Grid already identified voltage stability or stiffness as a much more stabilizing factor than inertia [5].

A possible solution to overcome this was the modeling of a synchronous machine. This solution can be easily explained and developed since the theory of large power systems based on synchronous machines is well-established, and so could then be directly applied to converters.

Nevertheless, the methods used to implement this logic differ severely between authors, from describing a complete model of a synchronous machine to using only the most critical features. These strategies will be explained in this chapter including a discussion which includes the strengths and weaknesses of the algorithms.

2.2 Review of VSC control strategies

A lot of work in academia has been done regarding Virtual Synchronous Machines (VSM). The number of implementations available online has even triggered surveys about their characteristics and their respective comparisons between them [6]. Since many models have been proposed, the study done in this chapter will focus on the four main control strategies enclosed within the VSM techniques.

2.2.1 Virtual Synchronous Machine (VISMA)

The first algorithm shown in academia trying to replicate the behavior of synchronous machines is the concept so-called by the authors VISMA and presented in [7]. Here, a full parametrized model of synchronous machine is embedded inside the converter. Figure 2.1 shows the schematic of the VISMA control strategy. The measurements of current and voltage are used to compute the real active and reactive power.

Subsequently, the reference signals and the aforementioned computed instantaneous power values are introduced into a full 5th order electrical model together with a 2nd order for the mechanical part. This produces a 7th order model to describe completely the synchronous machine. The controller sets the current references ($Iabc*$) which are passed through using a hysteresis comparator.

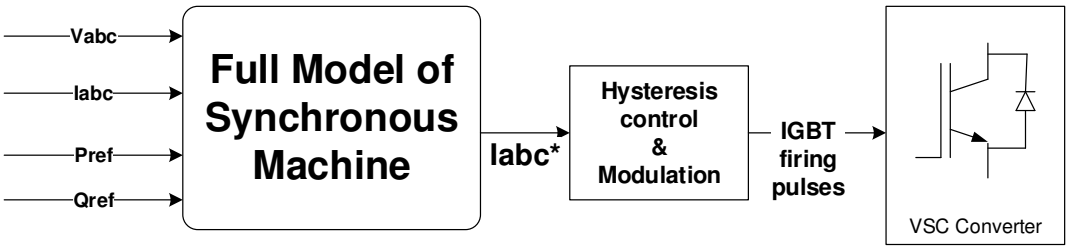

Figure 2.1: Schematic of the VISMA control algorithm.

However, this control strategy does not provide one of the best features of synchronous machines from the grid point of view. Since the references obtained from the models are values of currents, it still behaves as a current source. This is later fixed in the following publication and in [8] it explains how the model implemented is slightly modified to produce as control outcome the voltage references.

This transformation is vital. Now, the converter behaves as a real voltage source, and like traditional machines do, provides stiff positive sequence voltage regardless of the grid events. Since the model is completely numeric, so it is the internal modeled virtual machine. Consequently, full customization of the internal parameters can be obtained. This feature is later exploited in [9] and [10] where this model is connected to a weak and faulty grid. Since traditional parameters which contribute to the inertia like virtual rotor mass or rotor damping are only numbers inside the synchronous machine model, this value can be completely configurable to provide more inertia or contributing with more damping into the system. This is better illustrated in Figures 2.2 and 2.3.

Figure 2.2 shows the different converter response for different values of virtual rotor mass against a drop in frequency. According to these figures, if this parameter is higher, the virtual generator will have more inertia, resulting in an increased power support which leads to a higher overshoots than a lighter one. Figure 2.3 compares two values of damping virtual rotors. Here, higher damping will lead to fewer power oscillations which otherwise should be mitigated by the remaining generators present in the system.

Also, as a voltage source, the converter can provide more reliably islanding capabilities (something that is very difficult to obtain in DQCI controlled converters). This feature is assessed in [10] proving very good results and improving the dynamic response

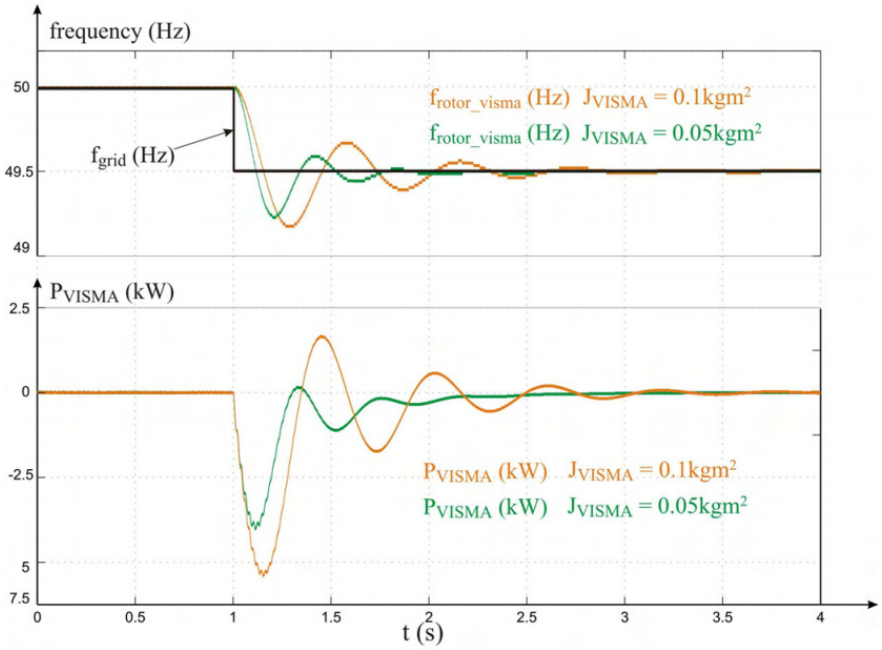

Figure 2.2: Effect of the virtual rotor mass (Extracted from [10]).

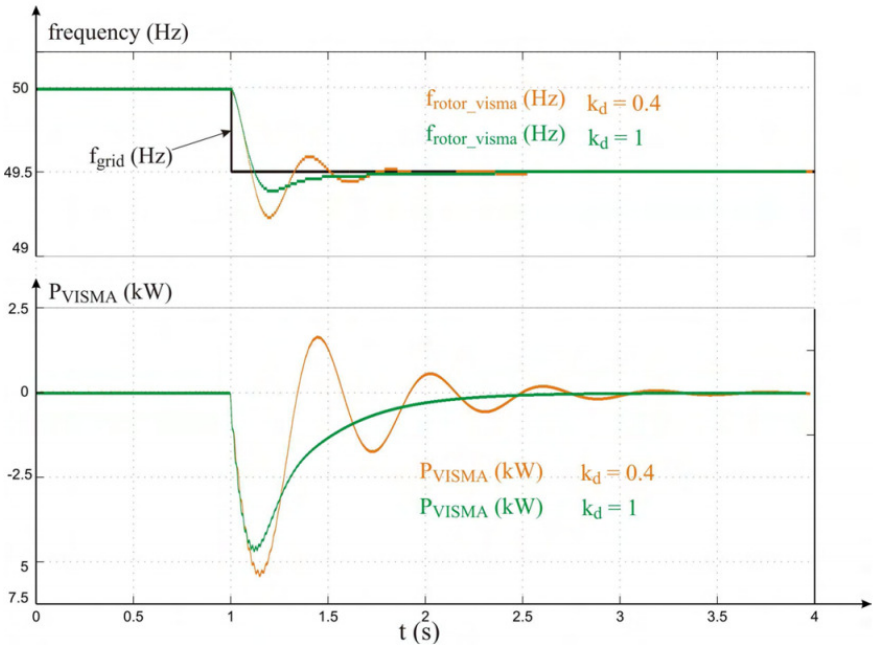

Figure 2.3: Effect of the virtual damping (Extracted from [10]).

of systems where other synchronous machines are present in the system.

2.2.2 Synchronverter

Very similar to the VISMA, the synchronverter concept also attempts to model a synchronous machine, but this time a less complex architecture is detailed inside of the logic of control. Instead of using a model of 7th order, the synchronverter is based on the swing equation of traditional machines giving as result a second order model. This reduces massively the complexity of its implementation maintaining the good features of conventional machines such as inertia contribution or voltage regulation. This simplification removes unnecessary calculations such as instantaneous internal virtual fluxes into the control algorithm. The control architecture is presented in Figure 2.4.

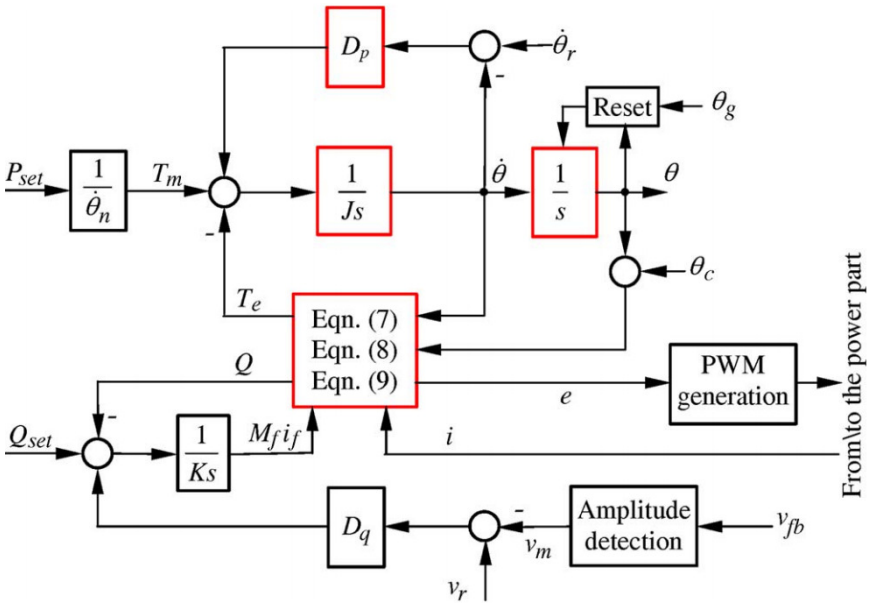

Figure 2.4: Control architecture (Extracted from [12]).

where the most relevant parameters are defined as following: D_p is the damping coefficient, θ_r the rotor angle, θ_g is the instantaneous voltage grid angle, θ is the converter voltage angle, J is the moment of inertia, e is the resultant electromotive force from the model which is equivalent to the voltage magnitude imposed by the converter, and, finally, P_{set} and Q_{set} are the active and reactive power references. Equations noted as (7)-(9) in the original paper are the following:

$$T_e = M_f i_f \langle i, \widetilde{sin}\Theta \rangle \tag{2.1}$$

$$e = \dot{\Theta} M_f i_f \widetilde{sin}\Theta \tag{2.2}$$

$$Q = -\dot{\Theta} M_f i_f \langle i, \widetilde{cos}\Theta \rangle \tag{2.3}$$

where T_e is the electric virtual torque, M_f the virtual mutual field inductance and i_f the field current running through the virtual armature of the virtual generator.

As it can be observed from Figure 2.4, the damping characteristics of the virtual machine (for instance) is maintained and this parameter is completely configurable thanks to D_p. Equally, the inertia is still provided thanks to the moment of inertia J. Consequently, the resultant control, although still quite complex compared to the conventional vectorial control or DQCI, is much simpler than the VISMA concept, maintaining the main features demanded in a virtual synchronous machine. Finally, since the control algorithm still imposes a voltage magnitude and angle, the converter can be observed as a voltage source behind an inductance.

So far, the control logic of this strategy has been explained in its most simple terms. However, this algorithm has triggered many studies in academia looking for further refined models which improve and evaluate its performance during various scenarios. For instance, from the same authors in [13], the model is refined to allow the synchronization with the grid without using any PLL or external grid to pre-synchronize. Also, the operation is more robust using more stable values of the voltage imposed by the converter.

A modification of the control structure is presented in [14]. Here, the synchronverter concept is extended to an HVDC link showing good results. However, the chosen scenario is not very representative; a converter of 200 MW is inserted in an 800 MW grid based on synchronous machines. Therefore, the scenario is not very challenging since it is not a weak grid nor it is the most relevant generator nearby.

Another implementation of the synchronverter can be found in [15] and [16]. In [15],

a non-linear controller is introduced into the control logic. This regulator provides grid connection without the intervention of the operator since the transition between grid-connected and islanding is done very smoothly. It provides a small-signal stability assessment of the model working as a current source (PQ node) or voltage source (PV node). Depending on the mode of operation, the internal variables are tuned differently to provide more stability. In this analysis, here it is taken into account the possibilities of the synchronverter to regulate voltage and provide stability to very weak grids. A similar control strategy is followed in [16] where the system is implemented into a converter hardware very similar to the one used during this thesis.

2.2.3 Power Synchronization Control (PSC)

Although the synchronverter concept provides a simplification compared to the VISMA control strategy, it still includes some complexity which may be unnecessary for the converter control. Since an IGBT converter is fully controllable and it does not have any mechanical inertia or rotating element, a semiconductor-based system should be able to perform additional tasks which would be unbearable for a physical synchronous machine such as large grid phase jumps or sudden changes in frequency. Thus, modeling a synchronous machines seems like limiting the dynamic capabilities of a fully controlled converter to certain well-known dynamics. On the contrary, only the most interesting features of this machine should be taken and not necessarily defined by the physics of a synchronous generator.

One of the main advantages of the VSM algorithms is that it gets rid of the weakest subsystem inside a conventional DQCI converter; the Phase Locked Loop (PLL). Using the active power as means of communication, it is possible to get synchronism with the grid voltage. This method is used inherently by all the synchronous machine and the PSC algorithm presented in [18] explains in an easy manner how this is implemented in a converter. Figure 2.5 illustrates better the schematic in blocks of this control strategy.

As it can be observed from Figure 2.5, this control strategy does not model any of the electrical or mechanical parts of the synchronous machine. It only reproduces the basic synchronization process that occurs in synchronous machines. Measuring

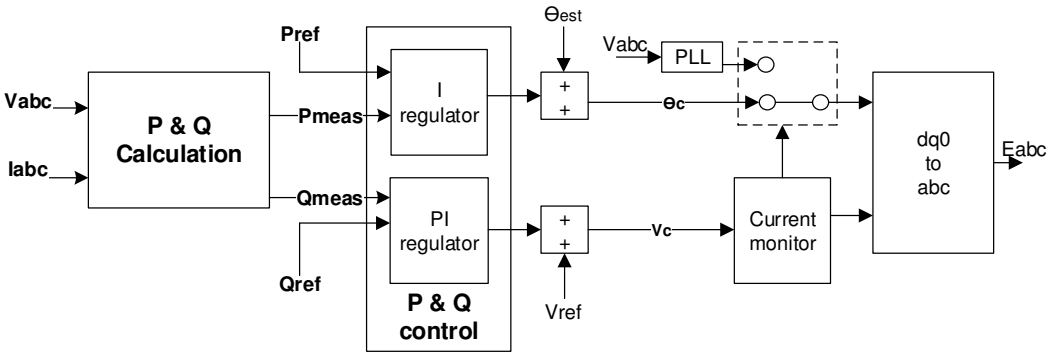

Figure 2.5: Control architecture for the PSC algorithm.

the active and reactive power, it is possible to add a regulator to impose a voltage magnitude and angle at its output.

This control strategy also deals with one of the most problematic events which can occur in a VSM-controlled converter (and applicable to any of the aforementioned VSM algorithm). Since now the converter is controlled by voltage and angle, if there is a short circuit or a sudden increase of the current injected to the grid, the converter will trip due to overcurrent, otherwise, its own integrity will be compromised. Conventional synchronous generators can provide briefly a current of up to 5 pu, while IGBT-based converters can only provide up to 2 pu and on the exchange of some lifespan. For the PSC algorithm, the *current monitor* block provides damping of the filter frequency and limits the amount of current injected to the grid. If an event occurs, this is detected and the control algorithm automatically switches to a backup standard DQCI control that is operating all the time in parallel.

Later, in [19], the PSC technique is implemented in an HVDC explaining the cross-coupling between the active and reactive power with the voltage magnitude and angle imposed by the converter for both HVDC converters. In other terms, in Figure 2.5, the active power was controlled by the angle and the reactive with the voltage magnitude. For weak systems, both magnitudes are mutually dependent and therefore, Multiple Inputs Multiple Outputs (MIMO) control has to be applied. Although more complex, the resulting converter performs very well against very challenging scenarios with Short-Circuit Ratio (SCR) lower than 1.5.

Additionally, in [19] it also mentions something that still has not been covered by the previous VSM solutions. So far, PSC and the remaining algorithms have assumed infinite energy available on the DC bus. Since now the inverter behaves more as a voltage source, it will inherently provide energy when it is necessary and therefore, if the grid is weak, the converter will require more DC capacitance in order to store more energy to mitigate the multiple and frequent oscillations of such electrical grids.

Finally, in [20], the system is evaluated with a different type of weak electrical grid. Now the weak grid is defined as an electrical grid with low inertia having also a high chance of disconnection and, therefore, of getting islanded. Here also, a short circuit is applied whilst being islanded proving its resilience against such events.

2.2.4 Virtual Synchronous Machine with Zero Inertia (VMS0H)

Still, further simplifications and modifications can be done from the PSC algorithm. First of all, PSC has one weakness. In order to be able to compute the instantaneous active and reactive power, at least four signals have to be obtained with their respective noise coupled. Since a small shift in angle can produce a high amount of power, these signals have to be introduced free from that coupled noise. VSM0H introduces a boxcar filter (defined and explained in [21]) which has an almost ideal response. Taking the average signal over a grid cycle, it gets rid of all the unbalanced voltages and harmonics out of the fundamental one, resulting in a confident measured value of P and Q.

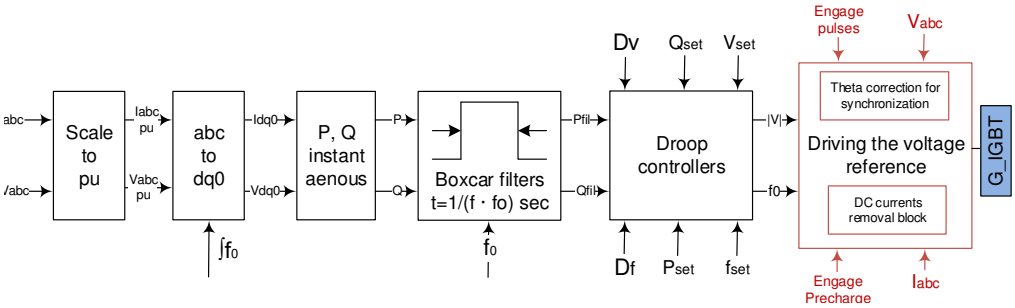

Figure 2.6: Control architecture for the VSM0H algorithm.

Figure 2.6 shows the control logic of the VSM0H scheme. Once P and Q are filtered, droop controllers can be applied to the error of power similarly to the PSC algorithms.

Although, in this case, the regulators only contain the proportional term. Operating with droops can give weights to generators in the system allowing at the same time a more robust operation. Although very simple, this configuration provides very good results against challenging scenarios and it has been chosen as the alternative control to the standard DQCI algorithm throughout this thesis.

Similar to other VSM algorithms, and as it was already mentioned in the PSC section, VSM0H can provide difficult responses against short circuits or sudden changes of current. As a voltage source, the current is not limited or controlled; therefore, large inrush currents can occur during these events. However, in this case, the reference [22] provides methods to accommodate such events. Monitoring the observed dq components of the voltage and current measured, it is possible to detect these events and therefore, actuate putting the converter in self-protection mode. As result, the IGBTs and the converter integrity will not be compromised. Unlike other VSM algorithms, this method does not switch to a standard DQCI type algorithm to control the current but keeps the device in voltage-source mode.

For full internal details about this algorithm and the modifications made for its practical implementation in this thesis, refer to Chapter 3, section 3.5.

2.3 Discussion

There seems to be a progression in the VSM algorithms. Going from the initial VISMA concept to the VSM0H control strategy, although all of them provide the necessary functionalities to provide stability within converter-dominated grids, the control logic seems to have evolved from the most complicated algorithms where a 7th order model of a synchronous machine was implemented, to the most simple but still effective algorithms which only take the necessary features of the synchronous machine.

As it was mentioned in the previous chapter, as power systems evolve and progress to converter-dominated grids, the grid angle stability takes less importance since semiconductor-based systems do not have to respect mechanical inertias typical from synchronous machines. Therefore, these dynamics only have to be respected in order to provide stability to the remaining synchronous generators present in the system. Bringing this

concept to the most extreme case, if a grid would be 100 % converter based, frequency and angle stability would be almost negligible since silicon-based converters can easily do jumps in frequency or angle. These dynamics can be taken as an advantage since then, converter-based systems could have a step type response against events such as load step. Furthermore, they could potentially provide power damping to the remaining synchronous generators in the system and, by a combination of the converter and the synchronous machine, the voltage at the load would not be altered. These phenomena are evaluated empirically later along the thesis in Chapter 5 section 5.4.3.

At this point and after having explained the different VSM techniques it is good to summarise which are the interesting aspects of a synchronous machines that should be included and really contribute to the stability within converter-dominated grids:

- *A synchronous machine is more stable.* Due to its regulatory role in the system, its stability is less compromised than in DQCI converters. This statement will be observed and proved along the experiments undertaken in this thesis, however, there are also small-signal studies which confirm these observations [23, 24].

- *A synchronous machine is a positive sequence voltage source.* Synchronous machine injects their energy as a voltage source. This means that regardless of the events occurred in the grid, the generator will impose a finite and constant positive sequence voltage, providing inherently‘ at the same time voltage regulation capabilities. Consequently, the grid voltage observed by the load will be freer of noise contributing thus, to the stability of the DQCI converters connected to the grid and consequently, to the entire grid stability.

- *A synchronous machine does not need a source of synchronism.* These machines get its synchronization using active power as means of communication, allowing a more robust operation. This also contributes to the rotor angle stability which guarantees a safe operation to the remaining synchronous generators of the system.

As it can be observed, a converter which could provide these three tasks could contribute to the stability of both the converters and synchronous generators present

in the system, making it eligible as a solution for converter-dominated grids where a huge diversity of generators are connected between them. Obviously, this is performed by a virtual synchronous generator but it seems unnecessary to design a full 7th order model like for example the VISMA solution to develop these duties. PSC or VSM0H are simpler solutions which cover the aforementioned functionalities without being so complex.

Bibliography

[1] J. Zhu, C. D. Booth, A. P. Grain, A. J. Roscoe, and C. G. Bright, "Inertia Emulation Control Strategy for VSC-HVDC Transmission Systems." *IEEE Transactions on Power Systems*, vol. 28, pp. 1277-1287, 2013.

[2] A. J. Roscoe, G. Jackson, I. M. Elders, J. McCarthy, and G. M. Burt, "Demonstration of Sustained and Useful Converter Responses during Balanced and Unbalanced Faults in Microgrids," presented at the IEEE International conference on Electrical Systems for Aircraft, Railway and Ship Propulsion (ESARS), Bologna, Italy, 2012.

[3] K. Sakimoto, Y. Miura T. Ise. "Stabilization of a power system with a distributed generator by a virtual synchronous generator function." presented at the Power Electronics and ECCE Asia (ICPE & ECCE), Kyoto, Japan, 2011.

[4] M. P. N. Wesenbeeck, S. W. H. de Haan, and P. Varela, "Grid tied converter with virtual kinetic storage " presented at the IEEE PowerTech, Bucharest, 2009.

[5] Ierna, R., Zhu, J., Urdal, H., Roscoe, A., Yu, M., Dysko, A., and Booth, C. "Effects of VSM Convertor Control on Penetration Limits of Non-Synchronous Generation in the GB Power System," presented at the 15th Wind Integration Workshop, Vienna, Austria, 2016

[6] S. D'Arco and J. A. Suul. "Virtual synchronous machines Classification of implementations and analysis of equivalence to droop controllers for microgrids," presented at the IEEE Powertech conference, Grenoble, France, 2013.

[7] H. P. Beck, R.Hesse. "Virtual Synchronous Machine", presented at the 9th International Conference in Electrical Power Quality and Utilisation, Seville, Spain, 2007.

[8] Y. Chen, R. Hesse, Dirk Turschner, Hans Peter Beck. "Comparison of methods for implementing virtual synchronous machine on inverters," presented at the Internationcal COnference on Renewable Energies and Power Quality, Santiago de Compostela, Spain, 2012.

[9] Y. Chen, R. Hesse, Dirk Turschner Hans Peter Beck. "Dynamic properties of the Virtual Synchronous Machine (VISMA) in *Proc. ICREPQ*, 2011, vol 11.

[10] Y. Chen, R. Hesse, D. Turschner and H. P. Beck, "Improving the grid power quality using virtual synchronous machines," presented at the International Conference on Power Engineering, Energy and Electrical Drives, Malaga, 2011, pp. 1-6.

[11] Y. Chen, R. Hesse, D. Turschner, H. Peter Beck. "Investigation of the Virtual Synchronous Machine in the Island Mode," presented at the 3rd IEEE PES Innovative Smart Grid Technologies Europe (ISGT Europe), Berlin, 2012.

[12] Q. C. Zhong and G. Weiss, "Synchronverters: Inverters That Mimic Synchronous Generators," *IEEE Transactions on Industrial Electronics*, vol. 58, pp. 1259-1267, 2011.

[13] Q. C. Zhong, G. C. Konstantopoulos, B. Ren, and M. Krstic, "Improved Synchronverters with Bounded Frequency and Voltage for Smart Grid Integration." *IEEE Transactions on Smart Grid*, vol. 9, pp. 786-796, 2016.

[14] R. Aouini, B. Marinescu, K. Ben Kilani, and M. Elleuch, "Synchronverter-Based Emulation and Control of HVDC Transmission." IEEE Transactions on Power Systems, vol. 31, pp. 278-286, 2016.

[15] M. Ashabani and Y. A. R. I. Mohamed, "Integrating VSCs to Weak Grids by Nonlinear Power Damping Controller With Self-Synchronization Capability." *IEEE Transactions on Power Systems*, vol. 29, pp. 805-814, 2014.

[16] M. Ashabani and Y. A. R. I. Mohamed, "Novel Comprehensive Control Framework for Incorporating VSC's to Samrt Power Grids using Bidirectional Synchronous VSC." *IEEE Transactions on Power Systems*, vol. 29, pp. 805-814, 2014.

[17] M. Y. Guan, W. L. Pan, J. Zhang, Q. R. Hao, J. Z. Cheng, et al., "Synchronous Generator Emulation Control Strategy for Voltage Source Converter (VSC) Stations." *IEEE Transactions on Power Systems*, vol. 30, pp. 3093-3101, 2015.

[18] L. D. Zhang, L. Harnefors, and H. P. Nee, "Power-Synchronization Control of Grid-Connected Voltage-Source Converters." *IEEE Transactions on Power Systems*, vol. 25, pp. 809-820, 2010.

[19] L. D. Zhang, L. Harnefors, and H. P. Nee, "Interconnection of Two very weak AC Systems by VSC-HVDC Links Using Power-Synchronization Control". *IEEE Transactions on Power Systems*, vol. 26, pp. 344-355, 2011.

[20] L. D. Zhang, L. Harnefors, and H. P. Nee, "Modelling and Control of VSC-HVDC links connected to island systems." *IEEE Transactions on Power Systems*, vol. 26, pp. 783-793, 2011.

[21] Roscoe, A.J., and Blair. "Choice and Properties of Adaptive and Tunable Digital Boxcar (Moving Average) Filters for Power Systems and other Signal Processing Applications," presented at the IEEE International Workshop on Applied Measurements for Power Systems, Aachen, Germany, 2016.

[22] Roscoe, A.J., and Finney, S.J. "Method of controlling an inverter and a controller for controlling an inverter (Robust control of a grid connected inverter also during grid distortion and faults)". International patent US9270200 (B2) EP2566035 (A2) US2013051103 (A1).

[23] S. D'Arco, J. A. Suul and O. B. Fosso, "Small-signal modelling and parametric sensitivity of a Virtual Synchronous Machine," presented at the Power Systems Computation Conference, Wroclaw, Poland, 2014, pp. 1-9.

[24] S. DArco, J.A. Suul, O. B. Fosso. "Small-signal modeling and parametric sensitivity of a virtual synchronous machine in islanded operation." *International Journal of Electrical Power & Energy Systems*, vol. 72, pp 3-15, 2015.

Bibliography

Bibliography

Chapter 3

Design and Implementation of an inverter with a customizable control strategy inverter

3.1 Introduction

In order to evaluate the dynamics and transients effects occurred within a converter-dominated scenario, a converter with customizable control was built in the laboratory. Once the control design is thoroughly understood, the grid stability can be assessed, evaluating its constraints, identifying the main internal variables which trigger the instability and, ultimately, proposing solutions which will be tested in the laboratory.

In this chapter, the construction of a 10 kVA inverter is described. The description depicted in this chapter starts with a brief summary about the hardware elements used, paying special emphasis on the subsystems which have been specifically designed and implemented for this inverter. Subsequently, it continues explaining the logic of control under study and used in this thesis: the standard vectorial DQCI control strategy and the VSM0H algorithm.

Figure 3.1: Pictures of the 10 kVA inverter with customizable control strategy (front and side view).

3.2 General description of the 10 kVA inverter

The system used, figure 3.2 is presented. It represents in a schematic diagram every element implemented inside the converter.

Starting from the DC side, the inverter is supplied using a DC power supply connected to a custom-made contactor capable of connecting and disconnecting the DC voltage (for more details of the DC side see section 3.3.1). The IGBT's and the DC input capacitor Ci are contained in a black box from the brand Semikron (further details in section 3.3.2), connected in series with its output is the main filter (section 3.3.3) and, following, it is the precharge system and the main converter relay (3.3.4). Finally, the inverter has a step-up voltage transformer in a Delta-Wye configuration which provides galvanic isolation. The voltages and currents are measured at the main filter using LEM sensors (specific location, methods used and boards designed for this purpose are explained in 3.3.5). Finally, signals are collected and used by the logic of

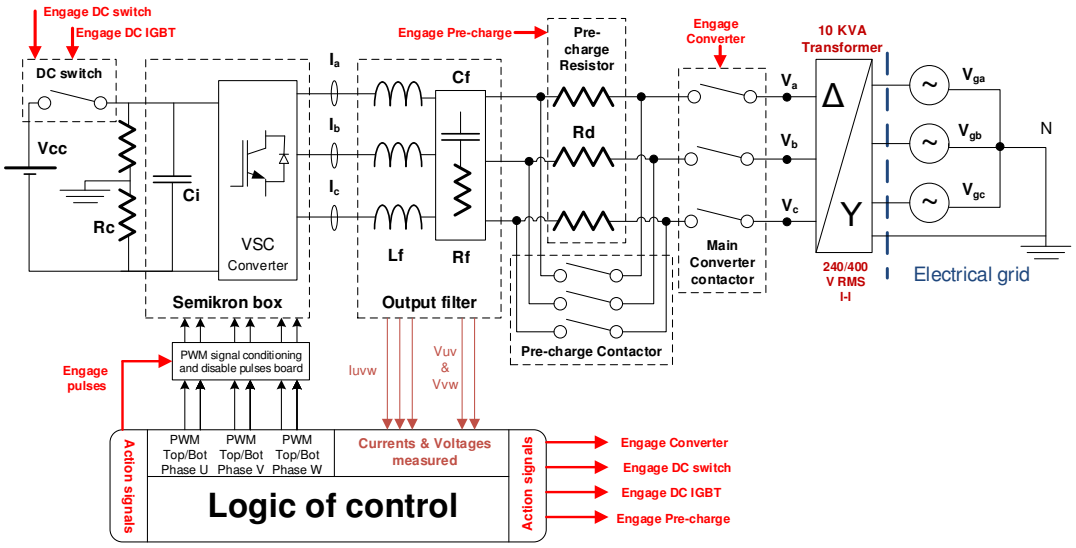

Figure 3.2: Main diagram of the converter.

control (see section 3.4 or 3.5 depending on the algorithm used) implemented inside the dSPACE box (see 3.3.6 for capabilities and constraints).

3.3 Description of the electrical subsystems installed inside the inverter

3.3.1 DC side

What has been cited here as DC side comprehends the DC power supply, the DC contactor, and the DC input resistors, explained as follows:

DC Power supply

The power supply chosen is manufactured by the brand Argantix, KDC series 300-50. It can provide up to 600 Volts, a maximum of 25 Amps and a maximum power of 15 KW. It has several measurements incorporated which can be visualized in its display such as, voltage, current and even the power delivered instantaneously. Also, it incorporates several protections such as maximum current to protect it from unintended faults or overvoltage. For the purpose of this project it is used as a constant voltage source.

Figure 3.3: DC power supply installed in the converter cabinet (Extracted from [1]).

DC Resistors

The DC resistors are needed taking into account how the system has been designed. These resistances provide three functionalities: first, and mainly, the resistors provide a reference voltage for the system; since the output transformer used is delta connected in the converter side, there is no grounding. Second, they divide the single voltage of 600 V into +300 V and -300 V; finally, the resistances also help to dissipate the energy contained in the DC bus when the system disconnects. Accounting a dissipation time of less than 15 seconds, the resistors will have a value of 10 kΩ for a nominal power of 10 W.

DC switch

The main functionality of this element is to provide a controllable connection of the DC bus. However, designing a controllable DC contactor is more challenging than an AC one. Since the voltage value never crosses the zero, the cable is always energized and hence, special procedures have to be taken. The schematic of the designed DC switch is presented in Figure 3.4. The DC switch comprises two sections: the first section is a pair of mechanical contactors that will provide physical separation between the cables; the second part it is a controllable IGBT that will behave as a governable electric switch. Therefore, as it was already presented in Figure 3.2, it is necessary to drive two signals to connect or disconnect the DC bus.

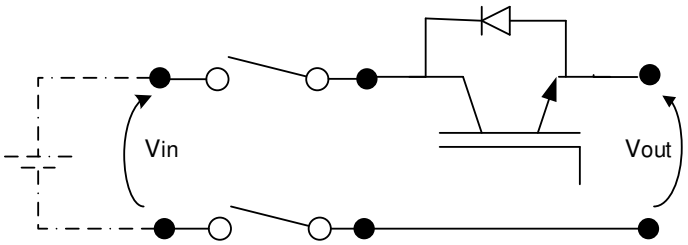

Figure 3.4: Schematic diagram of the DC switch.

However, the diagram shown before is a simplified version of the real one shown in Figure 3.5. Here, it is possible to see the layout of the DC switch with all the sub-components installed in it and how have been mounted in a heat sink that will help to dissipate the heat produced in the IGBT and the freewheel diode (later it will be explained the function of this device).

The circuit to drive the physical contactors consists of a transistor that amplifies

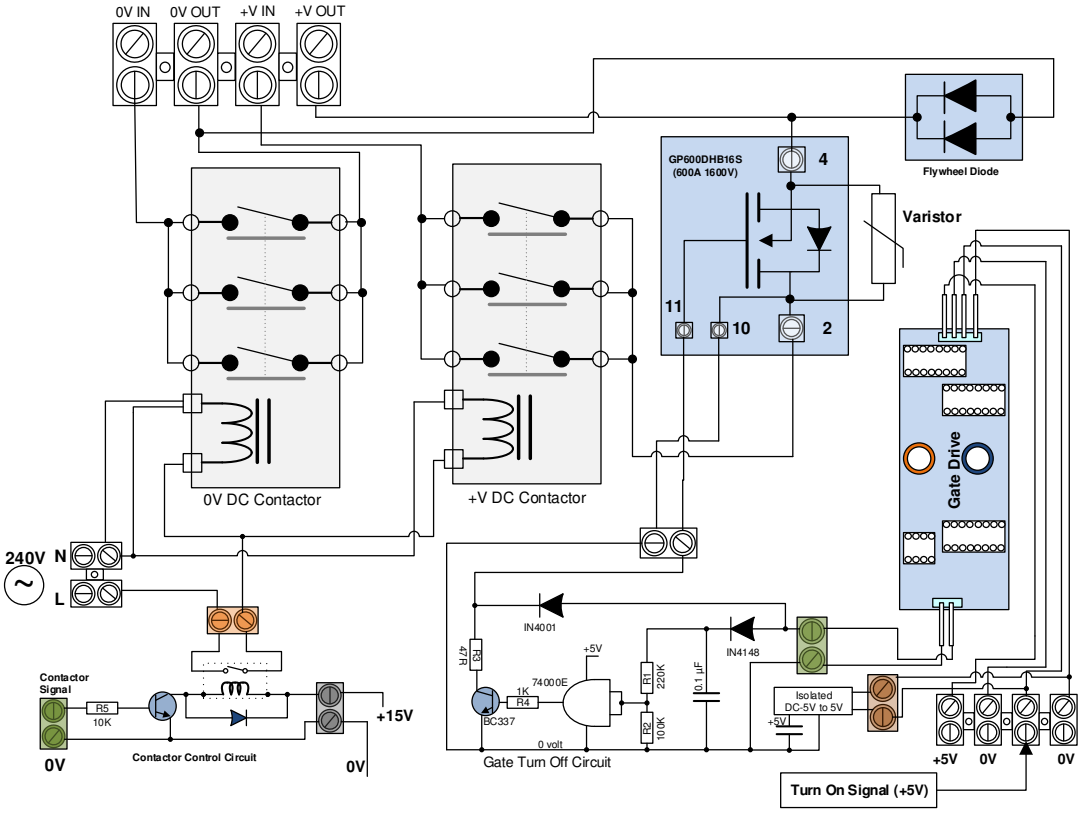

Figure 3.5: More detailed schematic diagram of the DC switch.

the driving voltage signal of 5 V. The amplified signal is now powerful enough to drive a relay which can drive the contactors. The IGBT switch, on the contrary, is more complex. First of all, it requires a gate driver to power up the signal providing optical isolation and, once it is done since it is being used as a controlled switch, it needs a dedicated circuit to force the IGBT's gate terminal to be switched off. Also, it is worth to mention the installation of two additional elements that permit its safe operation. First, a varistor between drain and source of the semiconductor; thanks to this device, the transition of voltage between 0V and nominal voltage is done without unwanted current surges. Secondly, a freewheel diode has been added to the system. In case of unexpected disconnection of the system, the remaining current from the filter inductances will be redirected to the resistances installed in the DC bus, protecting the DC power supply.

3.3.2 Semikron box

This section will describe the performance and internal configuration of the pre-built converter from the brand Semikron, precisely, the subsystem used for this project is the model SKS 25F. This subsystem contains the IGBTs, their drivers, the coiling fans for the heat sink incorporated and the DC input capacitor. Additionally, it contains two current measurements incorporated, however, in the case of the converter implemented these have not been used to obtain a more controllable measurement. All these items are assembled in a black box provided with the connectors necessaries for its control

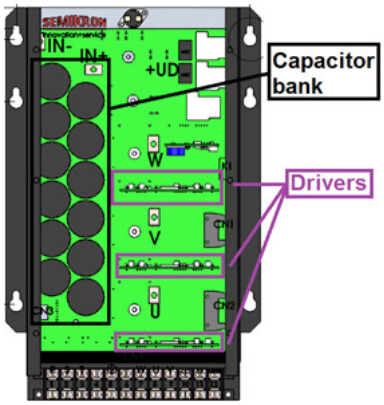

Figure 3.6: Situation of the capacitor bank and the drivers within the Semikron box.

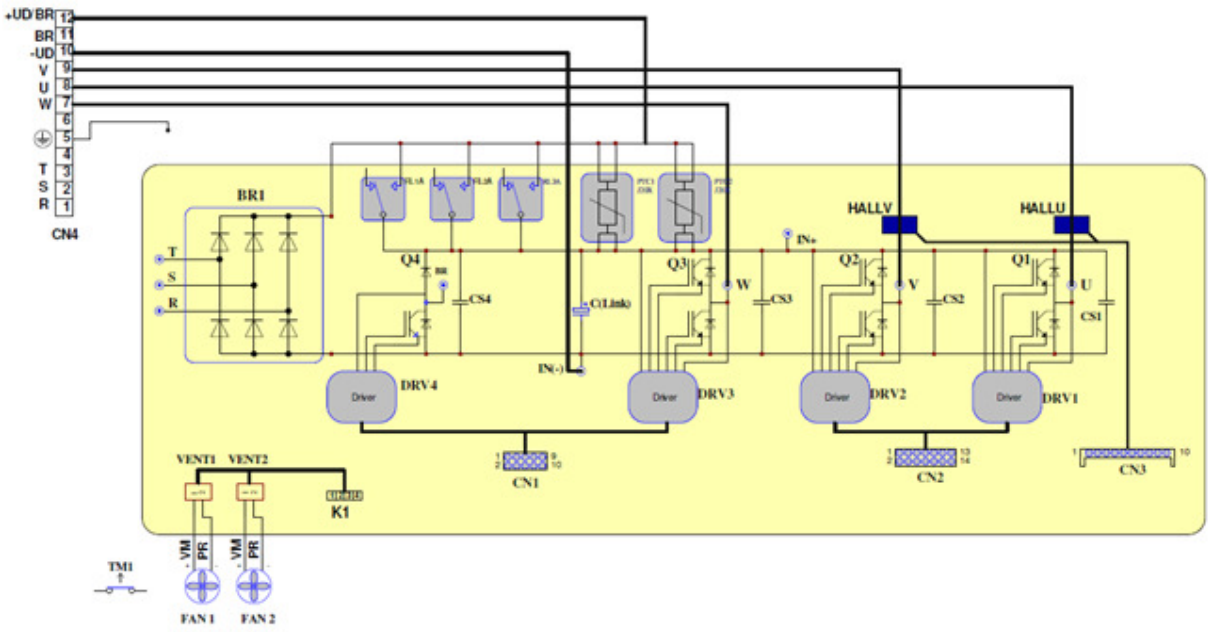

Figure 3.7: Internal wiring of the Semikron box. [2]

and operation. The situation of the capacitors and drivers is presented in Figure 3.6.

Going deeper into the internal characteristics and wiring of the box, it is presented the internal wiring of the VSC is illustrated in Figure 3.7. Here, it is possible to see the terminals where the DC bus will be connected (UD+ & UD-) and the AC side terminals (V, U, W) as well as the current measurements. It is important to remark here that, although in this figure it is represented a diode rectifier, a soft charging circuit for the DC bus and a DC chopper, these elements do not exist in the specific model that it has been used.

Following, table 3.1 contains the most important parameters of the system. Although every parameter has to be accounted, the maximum current that IGBT's can handle is remarked, including the tolerable overloads and the maximum switching frequency. These parameters are especially critical for the converter design and construction in this particular application.

General parameters			
Parameter	**Conditions**	**Values**	**Units**
I_{RMS} T_{amb}=35 C	Maximum current without overload at 5 kHz 150% overload, 60s every 10 min 200% overload, 10s every 10 min	31 41 48	A
V_{CE}	Maximum voltage Collector-Emitter	1200	V
f_{sw}	Advised maximum switching frequency	10	kHz
C_i	Input equivalent capacity	1410	μF
V_{DC}	Max. DC voltage applied to the capacitor bank	800	V
Cooling	Fan, DC power supply Current Consumption (per fan)	24 0.11	V A
Losses	Converter at P_{max}, T_{amb}=35 C Efficiency	550 97	W %

Table 3.1: Semikron characteristics

3.3.3 Grid filter

The converter filter is one of the most critical subsystems inside an inverter since these elements will set the inverter dynamics joined to the control algorithm. As it was already introduced in section 3.2, the filter has an LCL configuration where the second inductance is just the leakage inductance of the transformer used.

Adding the equivalent model of a real transformer and all the parasitic resistances contained in the output filter, the resulting single line diagram is presented in Figure 3.8. Here, the parasitic resistance of the filter inductor Lf has been added as well as the equivalent leakage inductance of the transformer L_{trf} and the core losses in the form of r_{trf}. Since it is very cumbersome to make the proper measurements to obtain the values of L_{trf} and r_{trf}, it has been assumed a value of 0.01 pu for the inductance and 0.005 pu for the resistance. These values are common numbers for laminated steel core transformers.

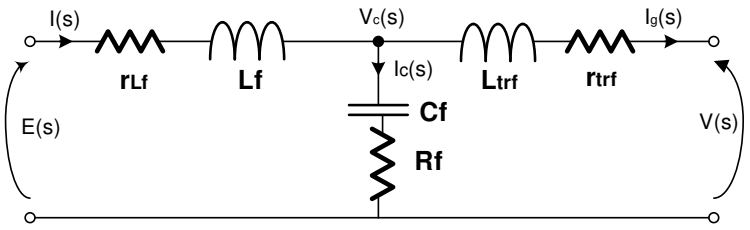

Figure 3.8: Single line diagram of the output filter.

Calculation of the main filter inductor

The filter inductor, Lf, assists with the removal of harmonic content. Therefore, it is vital to choose an inductance high enough that the harmonic content is sufficiently suppressed to not alter the power quality of the grid, but not too high since this element contributes to the active and reactive losses of the system.

There is no specific reference value which dictates the value of this element. An obvious starting point is to limit the amount of ripple in the current injected into the grid. Nonetheless, no grid code or regulation includes this as an actual requirement, instead, the only value which can be linked to this is the Total Harmonic Distortion at the PCC. However, although there are studies that link both parameters ([4], [5]), it is very difficult to link those studies for this specific case. Therefore, since by convention Lf is chosen between 0.1 and 0.2 pu. In this case, a value of 3 mH or 0.18 pu is selected for this converter. Switching and control frequency is set to 2 kHz.

Calculation of the output capacitor and set up of the resonance frequency

Once the main inductance has been set, the following step is to fix the capacitor value Cf for the filter. As it is described in [6], the value of this element will depend on several factors:

- First, and surely most important, the value of the main resonance frequency of the complete filter. Taking into account the capability to be islanded, the resonance frequency must be evaluated for the worst case scenario which is without any load present and connected to the converter. For this case:

$$\omega_{res} = \sqrt{\frac{L_f + Ltrf}{L_{trf} L_f C_f}} \tag{3.1}$$

- *The robustness of* ω_{res} against changes in the grid. Since the converter may be grid-connected, this grid can be changing and the connection or disconnection of systems on the grid can alter the equivalent inductance of the grid.

- *The installed reactive power of the filter.* For a higher value of capacitance, this

will translate into a higher value of reactive energy stored in the filter. Since, usually, the converters command is to maintain a unity power factor, this reactive power will have to be stored on the converter, subtracting with it from the converter's nominal power.

- Lastly, it is important the *space available in the cabinet*. Because it is initially intended to have the possibility of being updated incorporating an additional converter, there must be space available for the present and future elements that will form the back to back converter.

As a trade-off of all the previously discussed considerations, a value of $8.8\mu F$ has been chosen. However, since the capacitors are delta connected, the equivalent single line capacitor is $8.8\mu F * 3 = 26.4\mu F$. This value situates the resonance frequency at approx. 7 kHz which falls in a value much higher than the fundamental (50 Hz). This translates into a reactive power per line of 159 VAr. Multiplying this number by the three phases, the resulting reactive power allocated in the grid corresponds to a 4.7% of the nominal power. Number which is used by convention as a trade-off of losses and reactive provision.

Damping of the resonance frequency

Every filter which consists of an inductance and a capacitor will have a resonance frequency which has to be considered to avoid instability. To do so, [7] has been used as a reference since it is a summary and union of several papers that authors have published about the topic. Also, here it is discussed how an undamped LCL system is very likely to be unstable. Mainly, there are two solutions that can be used to solve this problem:

- *Active damping*. This technique is based mainly on modifying. Two active damping approaches are henceforth presented. The first one is to tune a digital notch filter at the resonance frequency. The second method is based on the addition of a virtual resistance in the filter. Examples of the success of either approach can be found in the literature [7].

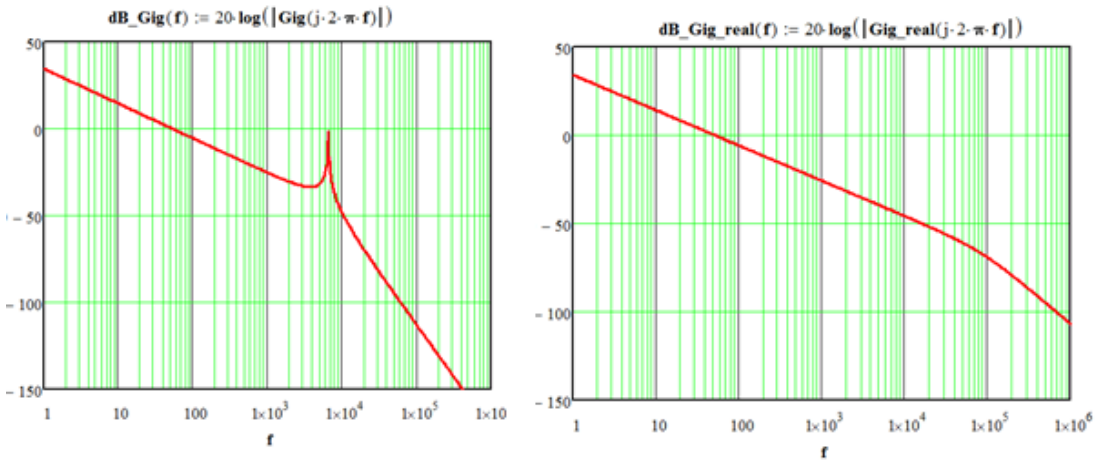

Figure 3.9: Comparison of the amplitude Bode plot for the grid filter without (left and with damping resistance (right)).

- *Passive damping.* Another solution is just to include a real resistance in series with the capacitance (Rf in Figure 3.8). The effect of this resistance can be easily shown in Figure 3.9. Here, on the left, a bode plot of the LCL filter designed for $Rf = 0$ and, on the right, for $Rf = 22\Omega$. As it is observed, the resonance peak of the undamped Bode plot has been eliminated thanks to the addition of the resistance into the filter.

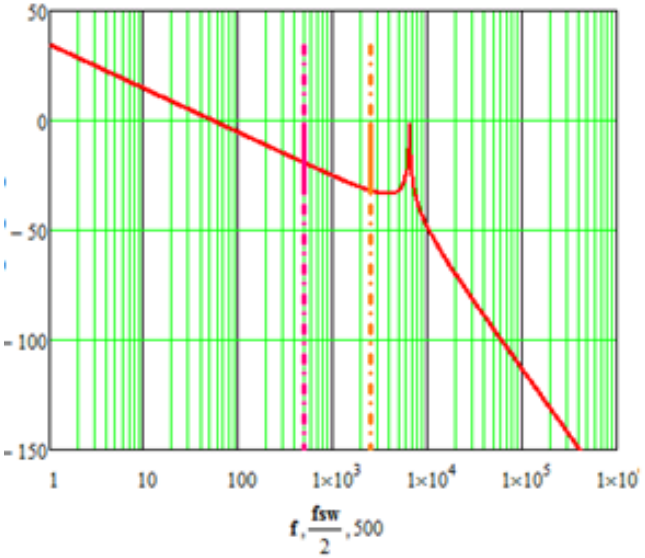

Figure 3.10: Amplitude bode plot incorporating the boarders for the active damping

If possible, always the best solution is the active damping since it does not require any extra element with the inherent losses that it implies. However, to do so, it requires a bandwidth high enough to execute the damping signal. Or, in other terms, the sampling or switching frequency (since the control algorithm is executed only once per switching cycle) will be at least 2 times higher than the resonance frequency. This can be better observed in Figure 3.10.

Here, the amplitude bode plot of the undamped designed grid filter is plot and with it, the borders where the active damping is possible. According to [6], the resonance frequency must be higher than 10 times the fundamental to avoid any significant harmonic but, if active damping is going to be used, this value will not be so high that it cannot be controlled. In Figure 3.10 can be observed that the resonance frequency is far away from than the control bandwidth (500Hz) and therefore the active damping cannot be done. For these reasons, an additional 22 ohm/100 W resistance has been added in series to the capacitor as a compromise between damping and filter effectiveness. The final amplitude bode plot is shown in the previous plot of the damped filter response in Figure 3.9.

Main filter inductor			
Elem./Param.	**Description**	**Values**	**Units**
Lf	Nominal value of the main filter inductance	3	mH
r_{Lf}	Parasitic resistance of the main filter inductor	10	mΩ
Asymmetry between phases.	Variation of the nominal inductance between phases	3	%
Capacitor			
Cf	Nominal value of the capacitors	8.8	μF
R_{Cf}	Resistor added for passive damping	22 100	Ω W
Connection	Delta connected		
Output Transformer			
V1	Primary/Grid side, nominal voltage line to line	400	Vrms
V2	Secondary/Converter side, nominal voltage line to line	240	Vrms
Pnom	Nominal power	10	kVA
Construction	Steel laminated core		

Table 3.2: Grid filter characteristics.

Final filter values

Once the converter installation has been made, the Total Harmonic Distortion (THD) of the converter output current for a stiff grid has been measured using a power quality meter. The THD measured has been lower than 2%, validating the filter effectiveness. To summarize, table 3.2 is presented with the final values of the grid filter implemented.

3.3.4 Precharge and main contactors

This system, with the DC contactor, is another controllable custom-made switch implemented for the converter control. The functions of this subsystem are two: First, it supplies the converter with a controllable switch which provides connection/disconnection with the grid, and second, it allows a soft-connection of the converter due to the

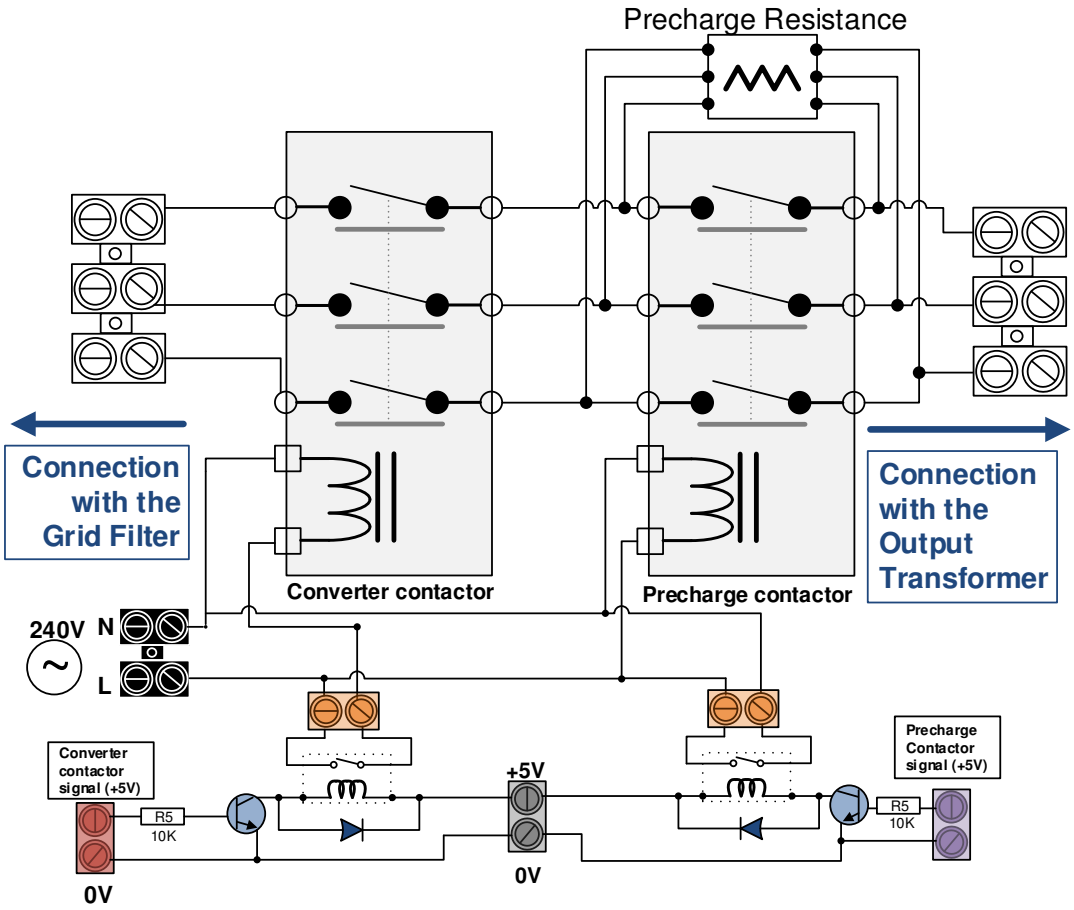

Figure 3.11: Schematic diagram of the precharge and main contactors.

precharge resistors used. Since these resistors limit the amount of current going through the inductors and the DC bus, this low current provides an initial stage of pre-charge where all the elements of the inverters are pre-energized (inductances, capacitors and also the DC bus), avoiding undesirable transients in the current. Naturally, once the inverter is fully connected, these resistors are by-passed using another contactor situated in parallel.

The value of these resistors is a trade-off between two constraints. If the resistance is low, then the damping effect that these resistances add during the initialization process would be almost none but, if the value is quite high, then, the current that would go across them will be so low that the system will take too much time to be energized. Setting an energizing time of 0.2 seconds and using a model created in Simulink to recreate the system, it has been simulated that a resistance of 100 ohms and 100 W is enough to perform the task entrusted.

A schematic of the circuit is shown in 3.11. Here, the internal circuitry of the system is presented. Both signals are driven to circuits consisting of fast transistors which power up the signal enough to drive a relay. This relay provides a new amplification stage on the signal which drives the contactor. As it was requested, if the anti-windup contactor is open, all the electric current will go through the windup resistors and, if the contactor is closed, the resistors will be bypassed by the low impedance path that the controllable switch offers.

3.3.5 Sensors board

A total of three boards are installed in the inverter for control purposes: a three-phase current sensor board to measure the currents going through in each phase, a three-phase voltage sensor and a single measurement voltage board to monitor the DC bus voltage.

Voltage or currents measurements boards are very similar. They both consist, in their most simple terms, of a transducer connected to an amplification stage. The differences between them are the number of measurements taken and the sensor used as a transducer. Therefore, if a current signal wants to be measured, the LA 55-P

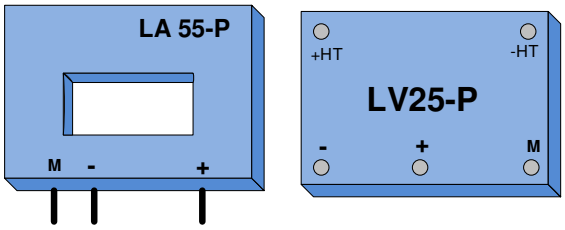

Figure 3.12: Current (left) and voltage (right) sensors used in the inverter.

transducer will be used and if, on the contrary, a voltage is the data to be obtained, the LV25-P will be the sensor to use. Both transducers from the brand LEM are based on the Hall effect to provide the measurement with the proper isolation. In both cases, the signal obtained is contained in the sensor output current.

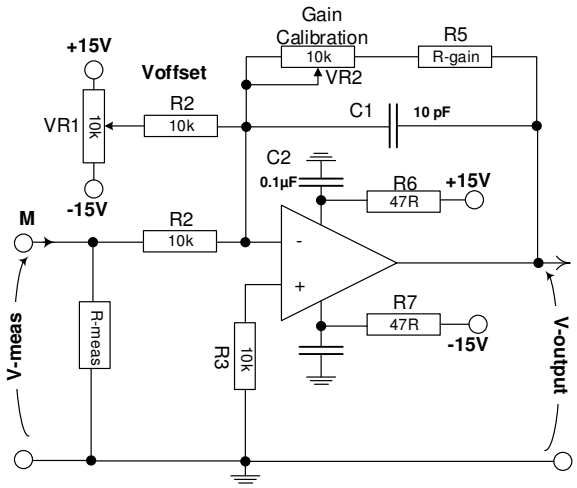

Figure 3.13: Amplification stage of the current/voltage sensor boards.

Since a converter is an environment with a high content of electromagnetic noise, the signals, once obtained from the transducers, must be amplified to make them more resilient against noise coupling. This amplification stage is common for both boards and it is presented in Figure 3.13. As it can be observed, it consists of an operational amplifier in negative feedback with variable gain which also allows the addition of a DC component of the resulting signal. These variable resistors provide adjust in the gain and offset of the resulting amplified signal. The output of these amplifiers is directly connected to the inputs of the dSPACE control box system.

3.3.6 dSPACE control box

This system is a rackable real-time computer that embeds the whole logic of control. It gathers data from the sensor boards, processes them and computes them using the chosen control strategy to produce, as result, the IGBTs firing signals.

Figure 3.14: Main diagram of the converter [3].

This box consists mainly of a processor board (DS1006 card) which manages several ancillary cards installed in its motherboard. Its internal configuration can be observed with the following diagram:

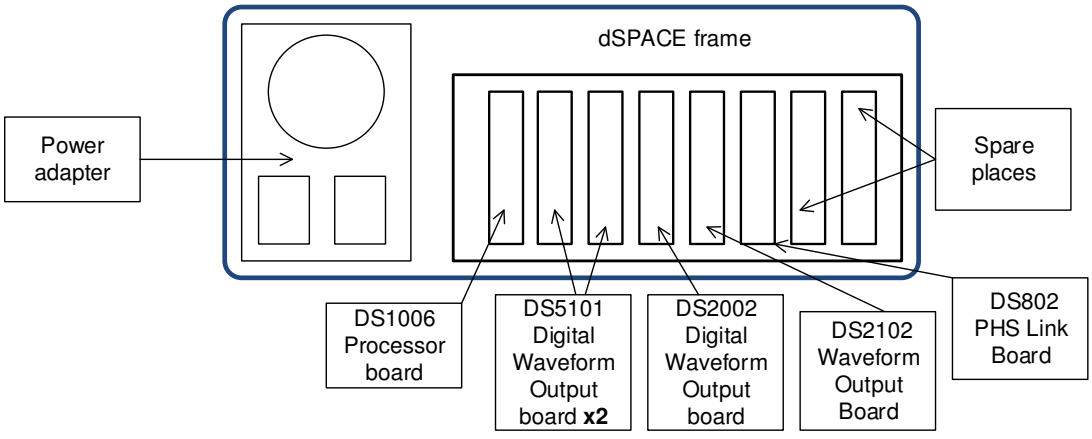

Figure 3.15: Schematic diagram of the back of the dSPACE box.

The dSPACE box used for this inverter has two DS5101 Digital TTL card specifi-

cally designed to generate up to 64 PWM signals in 32-bit resolution. Also, it has one DS2002 card which provides the measurements of up to 32 analog signals, following, the DS2102 card allows the generation of up to 6 analog signals within a programmable range of ±5V, ±10V or 0-10V and a resolution of 16 bits. Lastly, the DS802 card provides the fiber optical link which is connected to the operator computer. This PC monitors the system and presents the required information to the user/operator. Also, it is also responsible for the compiling, building and linking of the Simulink application into the dSPACE box as well as the data collection to export the results obtained in the laboratory.

3.4 Implementation of the DQCI control strategy

This algorithm describes the conventional vectorial current control strategy. It is based on the translation of the rotating phasors abc to a rotatory frame where the vectors abc seem to be static. Then, these three signals can be controlled directly with a much higher bandwidth.

3.4.1 Main control diagram

Figure 6.2 represents the main diagram of the DQCI control strategy. Signals shadowed in green are inputs of the system and in blue, the output of all the control. Framed in red dashed lines are the later described in section 4.2 the ancillary functions which are incorporated now in this control diagram. For the explanation of this section, these can be neglected.

The inputs of the system are the active and reactive power references ($Pref$ and $Qref$). Using the already translated to the rotatory frame Vdq, the power references are translated to current references ($Idqref$) actuating as inputs of the inner current loop (see 3.4.3 for further details about the internal design of the control loop). Following, the modulating signals $dabc$ are produced as an outcome of the control. Finally, they are modulated and transformed into IGBT firing signals. The source of synchronization is obtained using a Phased-Locked Loop (PLL) for this control strategy. Internally a Synchronous-Reference-Frame PLL (SRF-PLL) configuration is used. In parallel to this

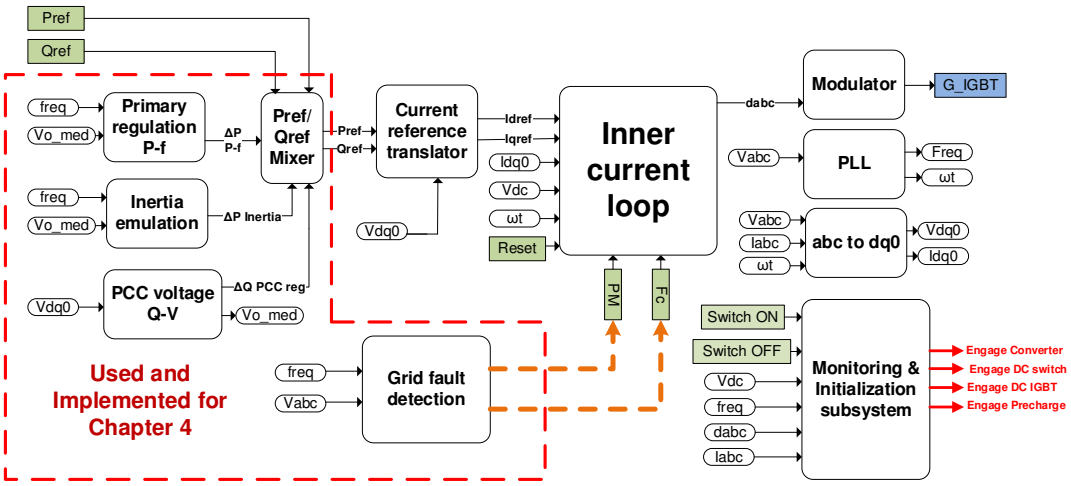

Figure 3.16: Blocks diagram of the DQCI control strategy.

control logic, there is also a monitoring and protection block is constantly operating to protect the converter from harming scenarios. This block is presented as following.

3.4.2 Monitoring and protection block

This block is continuously running in parallel to the control algorithm, protecting the converter from dangerous situations where the system integrity can be compromised. If the inverter enters into a hazardous situation, this block will generate the appropriated signals to the contactors, disconnecting the system and therefore, preventing the converter from permanent damages. Although this section has been explained here for the DQCI control strategy, there is also a replica of this block for the later explained VSM0H control strategy. The block diagram of this block is portrayed in Figure 3.17.

It can be divided into two different subsystems: one which is in charge of monitoring the system seeking possible dangerous situations; and a second block which, in the case of any of the alarms being triggered, will drive the right signals to the contactors to protect the system.

Monitoring check

This block examines any possible situation which can have the potential to damage the equipment. These situations as follows:

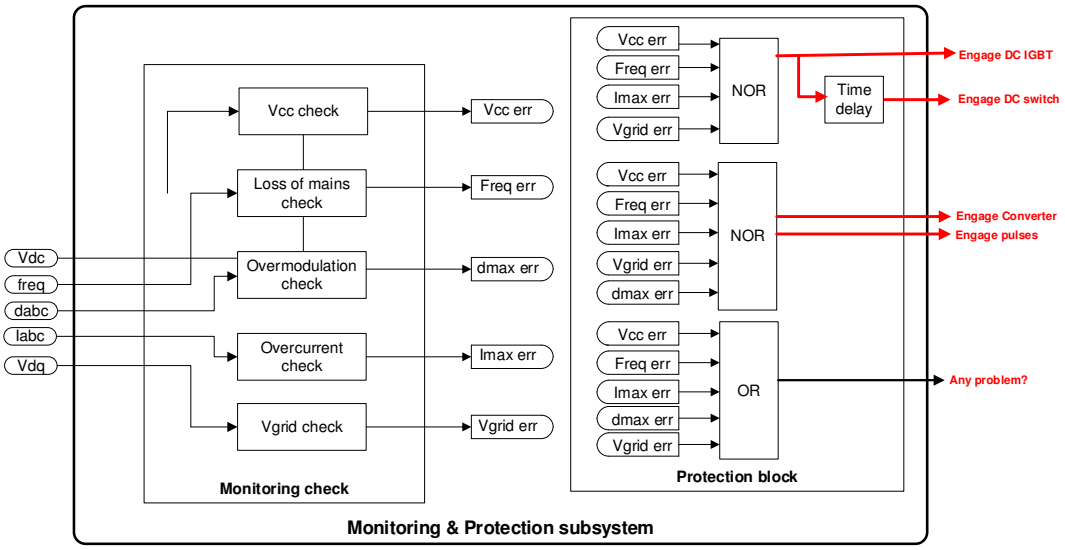

Figure 3.17: Blocks diagram of the Protection system.

- *Vcc check*. Measuring Vcc, the system knows at every moment if the voltage at the DC bus is between a margin of minimum and maximum.

- *Loss of mains check*. Obtaining the frequency from the PLL, this parameter is evaluated to determine if it is situated between the operating margins.

- *Overmodulation check*. This check is in charge of monitoring the system in case of overmodulation, this is made using the resulting output signal of the inner control loop and computing it to obtain a modulation index. If this index is higher than $2/\sqrt{3}$, the system has entered in overmodulation, losing the linear operation zone of the converter.

- *Vgrid check*. Finally, as primary protection, the grid voltage will have to be between some margins to avoid overcurrents. This protection can be disabled if the scenarios to evaluate have deliberately low voltages. For instance, scenarios with unbalanced loads.

Protection block

The monitoring block produces as output a series of flags which can be used to actuate with the contactors. Once the situations are identified and the flags obtained, they can be used to actuate, disconnecting properly the system. Since there are resistances in the converter, these elements can dissipate the excess of energy once the converter is disconnected from the grid. Thus, the only consideration to be taken into account in this block is to follow a correct sequence of disconnection if required. For instance, the DC contactor will always have to be disconnected electrically before doing physically with the contactors.

3.4.3 Design and calculus of the output current loop

The inner current loop is presented in 3.18. It is based almost entirely on the conventional vector current control or DQCI. Framed in red-dashed lines, the standard feed-forward terms are added to the control logic in order to avoid the cross-coupling between the axis dq. In blue-dashed lines, additional terms have been added to improve the control response and robustness.

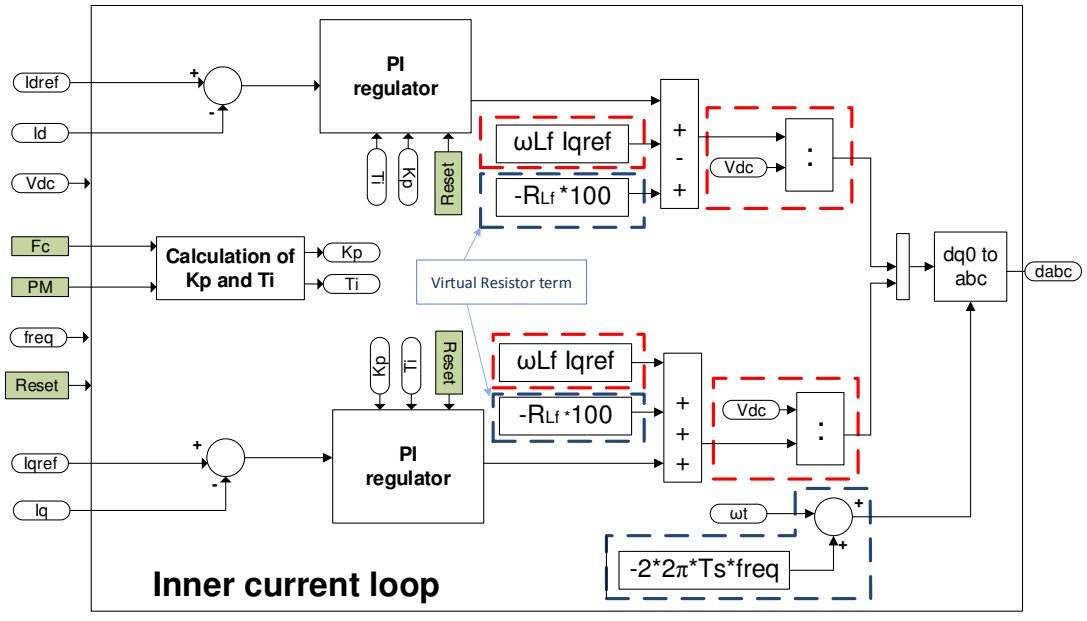

Figure 3.18: Blocks diagram of the inner current loop.

Calculus of the output current loop

The plant used to design the PI regulators is set by the output filter dynamics. For this case, as it was already presented in section 3.2, the inverter makes use of an LCL filter. Authors in [6] observed that the LCL filter plant can be approximated, for the regulation calculation purposes, as one unique equivalent inductance, since it sets the dominant pole of the system that compromises the stability of the system. This equivalent coil is the sum of the filter inductance and the equivalent leakage coil from the transformer used. The resulting plant connected with the regulator in a diagram block has the configuration presented in fig 3.19. Where Lf and R_{Lf} are the inductance and parasitic resistance of the filter.

The blocks presented in 3.19 can be combined to conform one equivalent single block. Having defined the plant and regulator, Kp and Ti can be calculated for a given set of Phase Margin (PM) and crossover frequency (Fc). This process is done calculating the values of Kp and Ti forcing the magnitude of the equivalent total block to zero and the angle equal to the requested PM, in degrees, at the crossover frequency ($s = 2\pi Fc$):

$$Ti = \frac{\left(\frac{-\pi}{2}\right) + \left(PM\frac{\pi}{180}\right) + atan\left(\frac{L_f 2\pi Fc}{r_{Lf}}\right)}{2\pi Fc} \tag{3.2}$$

$$Kp = \frac{(2\pi FcTi)\sqrt{r_{Lf}^2 + (2\pi FcL_f)^2}}{\sqrt{1 + (2\pi FcTi)^2}} \tag{3.3}$$

Equations 3.3 and 3.2, are integrated in one block (as it can be observed in Figure 3.18) which calculates the resulting Kp and Ti for a given set of PM and Fc. This

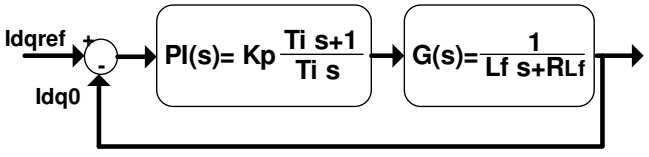

Figure 3.19: Block diagram of the inner current loop.

capability is further exploited in Chapter 4, section 4.4 to produce an inverter with variable response.

Additional compensations to improve the inner current loop response

Since the inner current loop is the core of the control system, additional terms can be added to improve its response and stability. There are two additional compensations added to the logic of control: the first term consists of an advance of two samples on the rotational frame, balancing with it the wide-known 1.5 to 2 sample delay between the references and the actuation signals [10].

The second one is a virtual increase of the parasitic resistance R_{Lf}. As it will be assessed in this paragraph, an increase in the parasitic resistance R_{Lf} is translated to a more stable control of the current.

If the open loop gain of the block diagram of Figure 3.19 is obtained, it is possible to

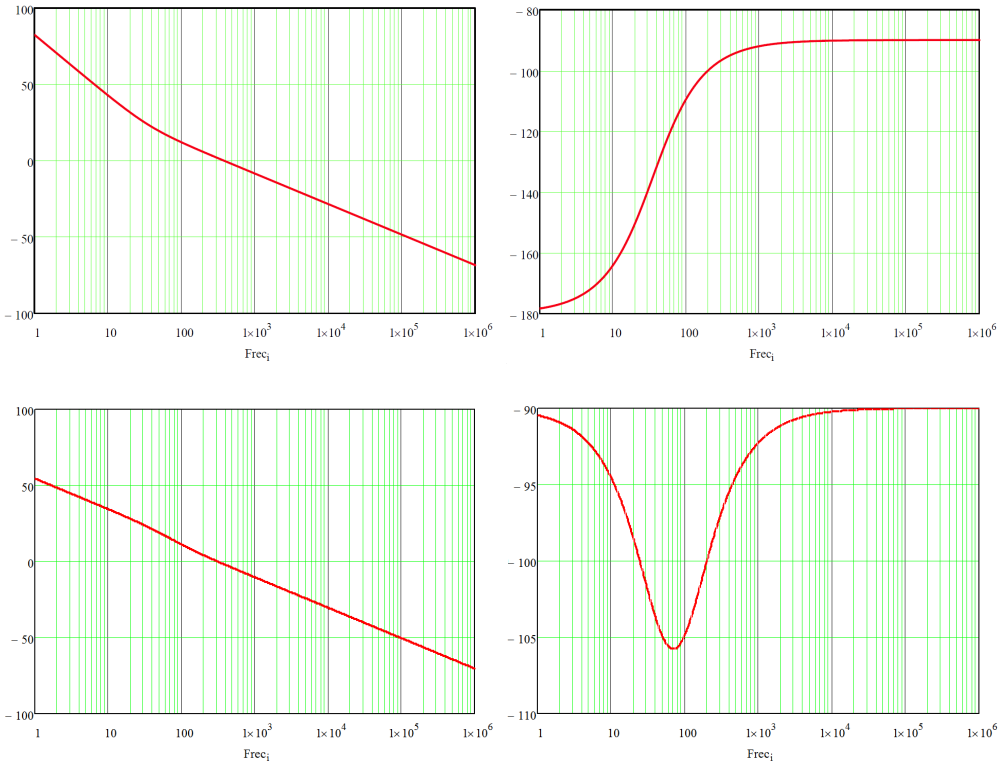

Figure 3.20: Bode diagram in amplitude (left) and phase(right) for $R_{Lf} = 10m\Omega$ (top) and $R_{Lf} = 1\Omega$ (bottom).

assess the control loop stability for different values of R_{Lf}. Figure 3.20, represents the bode diagram in amplitude and phase of the open loop gain of the system for a phase margin of 80 degrees, crossover frequency of 400 Hz and two values of R_{Lf}; The top diagram corresponds to the measured parasitic resistance of Lf ($R_{Lf} = 10m\Omega$) and the bottom one where the same inductance has a fictitious resistance value of $R_{Lf} = 1\Omega$. The differences between both bode plots in the magnitude part are not remarkable, neither affect to this stability assessment. Paying closer attention to the phase plot, for the case where $R_{Lf} = 10m\Omega$, it is observable a situation close to frequency 1 Hz where the phase gets closer to the -180 degrees limit. This does not happen in the case where $R_{Lf} = 1\Omega$ where there is a higher phase margin, and therefore, showing a more stable scenario. Although in both cases (due to the PI regulator), both resulting systems are stable, the scenario where the resistance is higher is more stable thanks to the additional contribution of damping provided by the larger resistance, reverting into a more robust control.

However, there are limits using this technique. If, for instance, seeking for further damping, R_{Lf} is increased up to $100\Omega s$, the entire control loop enters into instability. This can be observed with the open loop presented in Figure 3.21. Here, the -180 degree limit is plotted over the phase response to observe that there are regions over the crossover frequency (400 Hz) where this limit is exceeded.

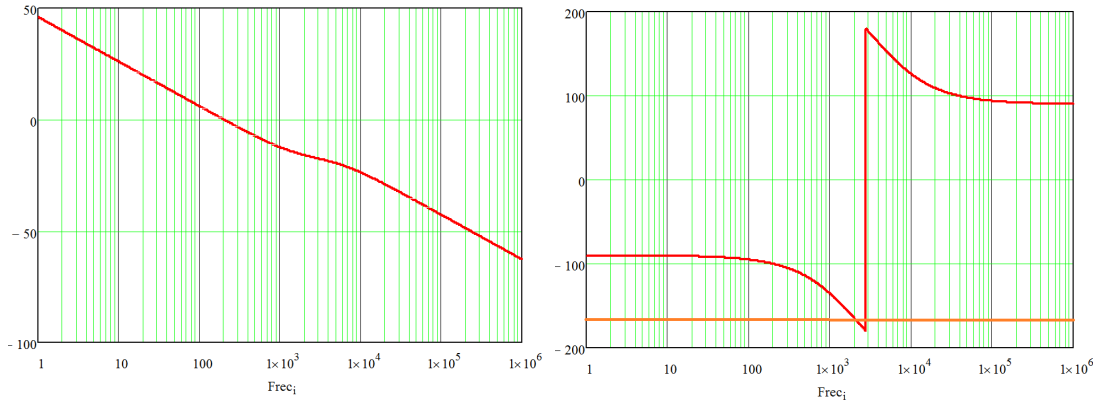

Figure 3.21: Bode diagram in amplitude (left) and phase(right) for $R_{Lf} = 100\Omega$.

A value of a hundred times the natural one has been included into the control loop

(R_{Lf} has been measured obtaining a value of 10mΩ). As it has been observed in Figure 3.20 (bottom) this compensation term provides good results in the stability assessment made in this section. Equally, this has been validated in the simulation and the initial experiments.

3.5 Implementation of the VSM0H control strategy

3.5.1 Main diagram of control

The control strategy used to behave as grid forming node is the Virtual Synchronous Machine with Zero Inertia (VSM0H), more profusely explained in [8] and [9]. Because of its simplicity and effectiveness, it has been chosen as the VSM-type algorithm used in this thesis for the assessment of the GFN solution within converter-dominated grids. In this chapter, only a short summary of this technique will be presented as an introduction for the reader, paying more attention to the blocks which have been developed specifically in this thesis for its implementation into a real converter.

The main diagram of a control for this technique is presented in Figure 3.22. The control starts acquiring the measured currents and voltages, exactly in the same manner as the DQCI control. Later, these signals are translated to pu and the active and reactive powers are calculated. Since, to do so, it is necessary to combine six signals at the same time (three currents and three voltages) with their respective six noises coupled, the measured active and reactive power have to be filtered using boxcar filters (further explanation about this filter in [11]). Filtering also leads to a control bandwidth lower than 50 Hz which has shown as crucial to the VSM0H operation. Once these signals are filtered and reliable, standard droop controllers can be used to obtain as result a voltage magnitude and frequency. Finally, during the last stage, several corrections have to be made to translate this reference into an effective voltage and angle. The author of this thesis in [13] and presented in section 3.5.4 refers about how to implement the theoretical concept of VSM0H into a real connected inverter.

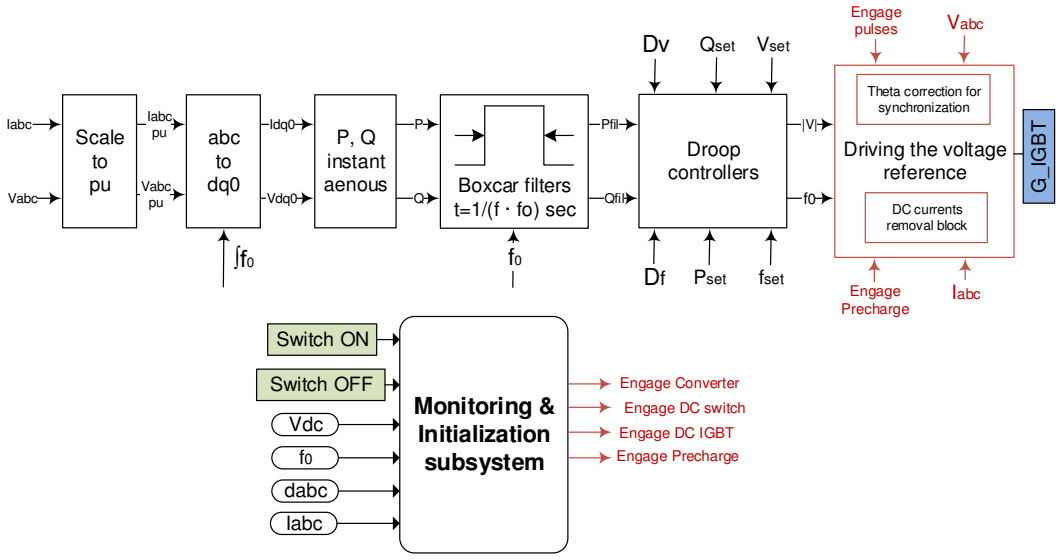

Figure 3.22: Block diagram of the VSM0H technique.

3.5.2 Power synchronization mechanism

One of the main advantages of this algorithm is, as well as the other VSM techniques explained in Chapter 2, the removal of the PLL. Since there is no dedicated block to provide the synchronization reference, the converter can have now its own internal frequency and the deviations of the voltage imposed by the converter from the grid frequency will result in an increase or decrease of the active power injected to the grid. This is the same mechanism that governs the behaviour of traditional synchronous machines (deeply explained in [14]). In their simplest terms it shows that, if the grid with all their generators connected to it is represented as a single synchronous machine with a single electromagnetic force, when there is a change in its angular position, other synchronous machines (virtual or real) will follow it in order to maintain the synchronism. In other terms, the synchronization process is obtained through power flow.

3.5.3 Droop controllers

Once the active and reactive power is measured and properly filtered, simple droop controllers can be applied to set a reference of voltage magnitude and angle. Figure

3.23 presents the internal diagram of this block.

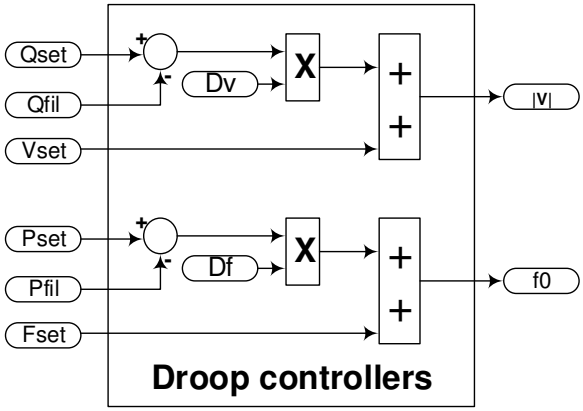

Figure 3.23: Block diagram of the droop controllers.

Using the error of reactive power and the droop for the voltage, a reference of voltage magnitude can be created. Similarly, using the error in active power and the frequency droop, a shift from the nominal frequency is created which results in the target frequency of the converter. In essence, this last droop is using the changes in power as a source of synchronism implementing the power synchronization mechanism explained in the previous section.

3.5.4 Driving the voltage reference

The main aim of this block is to transform the reference of magnitude and frequency voltage into modulating signals to finally translate them into IGBT firing signals. The block diagram of this part is presented in 3.24.

In [8], the previous VSM0H control logic is completely explained, however, as it can be observed from Figure 3.24, two blocks have been added to fully implement this control strategy into a real inverter: The *Theta correction for instantaneous synchronization* and the *DC currents removal block*. These blocks will be explained in the following sections.

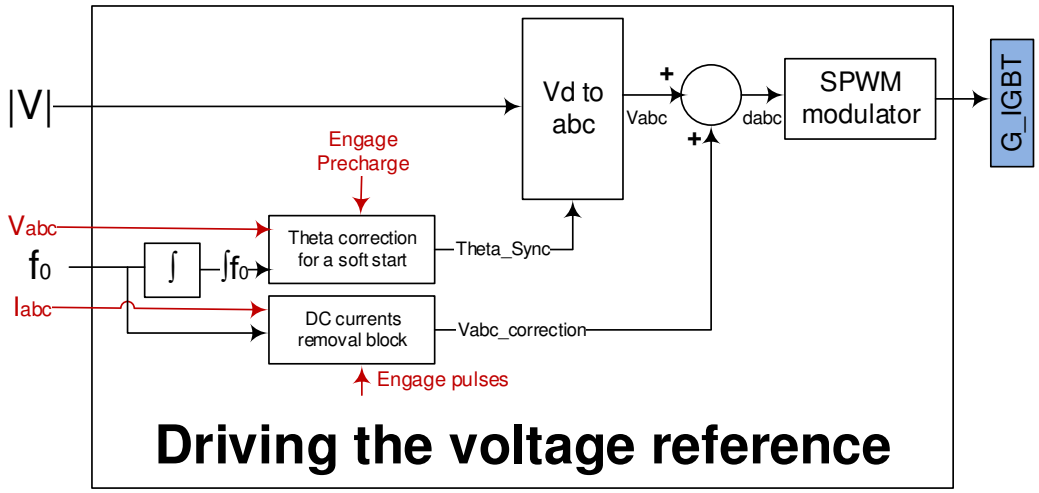

Figure 3.24: Block diagram of the block *Driving the voltage reference*.

Theta correction for Instantaneous Synchronization

The main aim of this block is the correction of the converter instantaneous angle to provide a smooth connection with the grid before injecting any power. Since the VSM0H algorithm transforms the converter into an apparent voltage source of power, the connection process to the grid is especially critical. If a specific block to synchronize is not used huge overcurrents can appear, compromising the converter's IGBTs. The nature of these overcurrents can be easily demonstrated with equation 3.4. This expression quantifies the active power transmitted between two voltage sources.

$$P = \frac{\mid V_c \mid\mid E \mid}{X} sin\delta \tag{3.4}$$

where V_c is the voltage imposed by the converter, E is the grid voltage, δ is the difference of angle between these two voltages and X is the reactance existent between both voltage sources. When the VSM0H is initially started, it begins obtaining its reference of synchronization integrating the initial value of frequency setpoint (50Hz). Although the converter starts with an instantaneous phase equal to 0, this value does not have to match with the instantaneous one of the grid. Since, by default, the VSM0H algorithm does not contain any dedicated block to evaluate the initial difference of angle between

the converter and the grid δ this parameter can take randomly any value, and so will be the active power transmitted immediately at the moment of connection, resulting in a high probability of triggering the protections due to over-currents.

For the aforementioned reasons, it is necessary to add an additional control in the block *Driving the voltage reference* which will manage this situation accordingly. Looking again at equation 3.4, it is observed that, if the difference of angle between the converter and the grid is zero, there will not be any current flowing and, therefore, the connection process would start in the smoothest manner. To do so, it is necessary to create an initial voltage identical to the obtained from the measurements. This process is done using the block diagram presented in Figure 3.25.

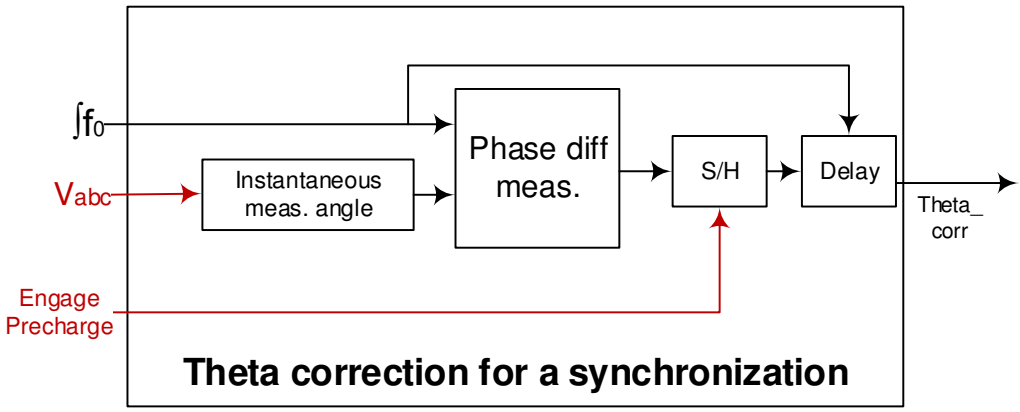

Figure 3.25: Block diagram of the block *Theta correction for a soft start.*

First, using the voltage measured, the instantaneous angle is obtained computing the *arctan* of the α and β components of the grid voltage (as result of using the Clarke transform in the measured voltages $Vabc$ and translating them into $V_{\alpha\beta}$). Although this method is very sensitive to any noise present in the grid, it is a fast, computationally light and therefore efficient for this purpose since it is only used during the connection process. Once the instantaneous grid angle is obtained, a phase difference, measured in samples, is calculated between the angle that the converter initially attempts to drive ($\int f_0$) and the grid angle. While the system is pre-charging, the sample and hold block is transparent for the control logic. Once the initialization process (explained with

higher detailed in 3.5.5) activates this flag (ending with it the initialization process), the last value of delay obtained is maintained until a new connection process is started. The function of the last block is the implementation of the previously calculated delay into $\int f_0$ giving, as result, a corrected instantaneous angle which matches the grid one. The functionality of this block is later assessed within the laboratory in section 3.5.5.

Voltage correction to reduce DC currents

The objective of this second correction is the removal of the DC components which may appear passing through the converter side of the transformer. Depending on the converter filter and the configuration used, DC currents of different nature can appear. If these components are not removed, the transformer used can enter into saturation, losing its linear operation and distorting the resulting currents injected into the grid. For the case of the inverter built during this project, the converter uses a Delta-Wye transformer to connect to the grid, DC components can appear on the converter side of the transformer due to asymmetries between the different elements of the filter, tiny unbalances on IGBT devices or timing errors derived from the discretization in time of the PWM signal. If the inverter would be transformerless, the DC currents would still exist but this time they would flow into the network.

These phenomena do not happen when DQCI algorithm is used since the main variable of control of the system, in that case, is the current. Because the open loop gain is high at frequency 0 (see bode plot in Figure 3.9), the control is very responsive to these DC components removing them without further development. However, in the VSM0H case, the main variable of control is the voltage and therefore, it is not straightforward to remove these undesired currents. Figure 3.26 represents the block diagram of this control.

Figure 3.26 depicts a dedicated control in charge of eliminating the DC components of the current. Starting from the instantaneous value for the measured current, these signals are introduced to a boxcar filter similar to the ones used for the main control of the system. As result, the averaged value of the instantaneous current over a period is obtained, i.e. the DC component of the signal. The error between this averaged

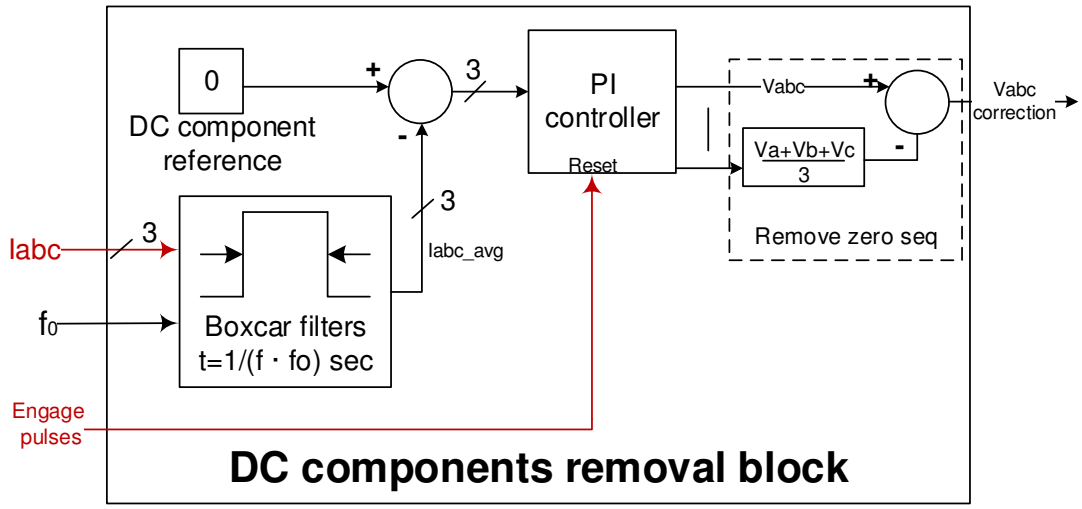

Figure 3.26: Block diagram of the block *DC components removal block*.

signal and the reference is calculated and regulated by a PI controller which provides a deviation of voltage. Finally, in the case of the presence of zero sequence in any of the deviation produced, this is also removed. As result, the aforementioned deviation is added to the voltage initially produced by the main control algorithm (see Figure 3.24), removing the current DC components.

The most challenging part of this block is tuning properly the PI regulator. Since the control variable is an averaged value, a minimum of one entire cycle has to be respected to obtain an updated measurement. This, following Nyquist theorem, translates to a maximum bandwidth for this control of 25 Hz, forcing it to be very slow. Accounting this, the regulator gains can be then calculated in the same manner as it was already described for the DQCI control in section 3.4.3. The plant and the control diagram will be the same as the ones presented in Figure 3.19 and the equations 3.3 and 3.2 are also valid. However, now the crossover frequency must be set to a value lower than 25 Hz. For this thesis, regulator gains were calculated fixing a crossover frequency of 15 Hz and phase margin of 75 Hz. Both values are a trade-off between the necessary stability and speed response. In the same manner as the previous section, this functionality is assessed experimentally in section 3.5.5.

3.5.5 Initialization process

As it has been mentioned in this chapter, the connection process for the now GFN/VSM0H converter is especially critical since now its behavior is very similar to a voltage source behind an impedance. Thus, the connection to the grid must be controlled properly to not provoke any overcurrent. Figure 3.27 presents the results of some critical variables of the system during the connection process. From top to bottom, the following signals are presented: the voltages measured in the converter side V_{abc}, the currents injected to the grid I_{abc}, the references of active and reactive power with their respective real measured outputs (unfiltered), P_{ref}/P_{conv} and Q_{ref}/Q_{conv} and the estimated frequency from the logic of control f_0. Following, a plot of the grid voltage against the modulating signal V_{abc}/d_{abc} is presented for illustration's sake. Continuing, the deviation components to be added for the DC currents removal are shown and, below, the delay adjustment necessary, in samples, to provide a soft start. Finally, the logic signals to drive the five different switches distributed inside the converter are presented.

At $t = 0$, the converter is completely disconnected from any energy source. At $t = 1s$, the connection procedure starts engaging the main contactor of the converter (refer to Figure 3.2 for the exact localization of each contactor/switch), connecting the converter to the grid through the precharge resistors, and pre-charging filter elements and the DC bus. At $t = 1.4s$, the DC switch is engaged, providing physical connection, but it is not until $300ms$ later (when the DC IGBT is activated providing electrical connection) that the DC bus is fully connected and its voltage rises to its nominal value. Even before the connection process would start, the DC currents removal block and the delay adjustment have been working constantly in parallel, providing updated values to add to the driving voltage. However, it is not until the IGBT pulses are activated at $t = 2.52s$ that these two components are applied previously to a reset of the internal PI regulator incorporated in the DC currents removal block. Observe the zoomed view of $Vabc/dabc$ and how, at the moment of engaging the pulses, the phase difference between the driving voltage and the grid angle is almost zero, permitting a smooth connection.

Because of the aforementioned reset applied to the regulators, the resultant DC

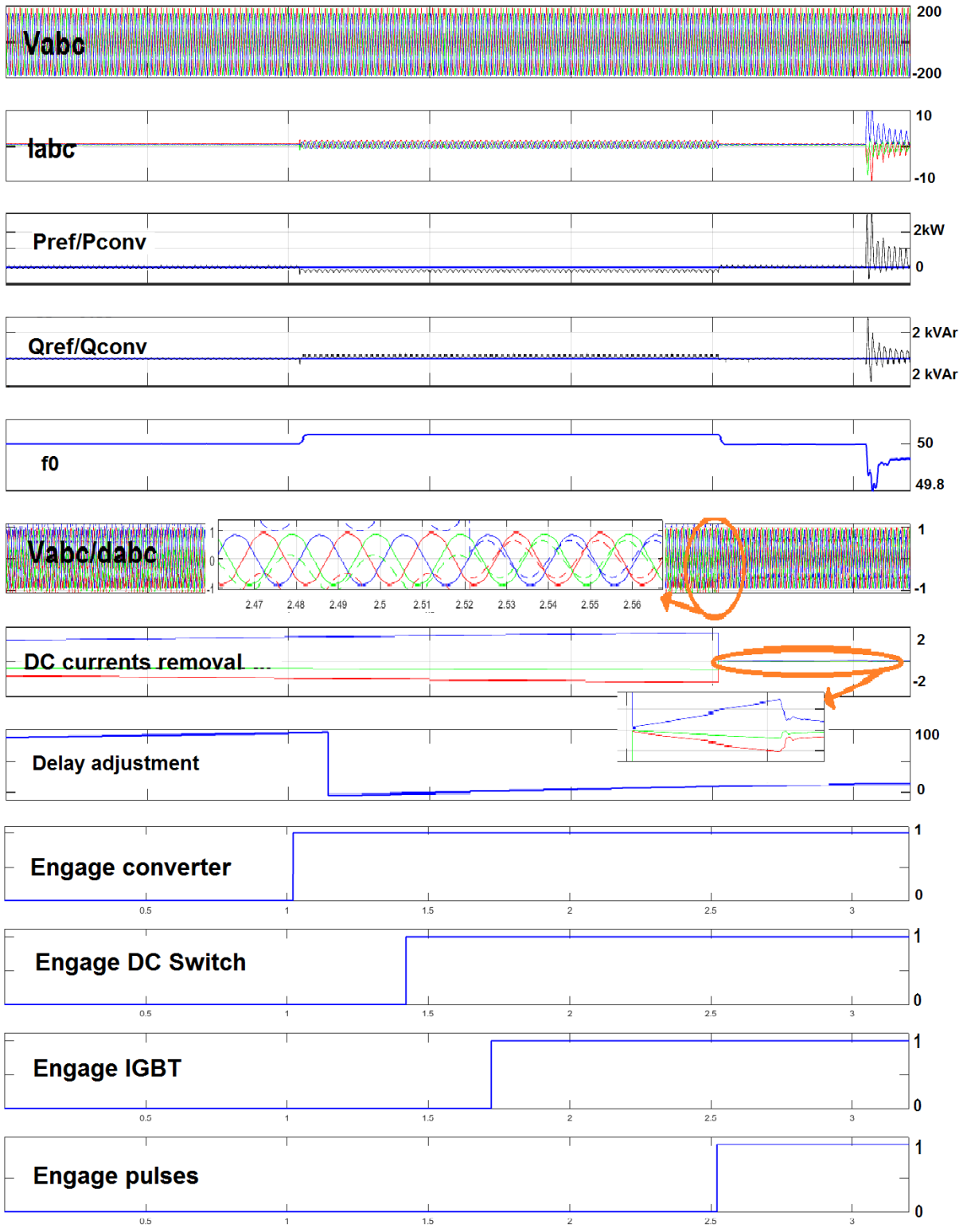

Figure 3.27: Experimental results for the GFN converter during the connection.

components previous to the activation of the pulses are 0 and, it is at this moment when the DC compensation terms are effectively being applied to the driving voltage, trying to remove the observed DC components. However, at this point the converter is still connected to the grid by the precharge resistors, resulting in an ineffective regulation. This situation is corrected when, at $t = 3$, the last precharge contactor is engaged, bypassing these resistors and completing the connection of the converter to the grid. At this moment, DC components converge to 0, removing effectively the DC currents present in the system. It is also at this moment when the last value of the delay adjustment block is held until a new connection procedure is started.

During the experiments, it has been observed that the most sensitive moment is when the precharge resistors are bypassed (the last contactor to engage) and the system is fully energized. This is observable also in the results presented here since, at approximately $t = 3s$, when this contactor is activated, and despite the phase shift applied to the driving voltage, there are short transients which reach up to 10 Amps. Theoretically, this current should be zero as it was already explained in section 3.5.4, However, due to the wrong deviations created from the DC currents removal block and applied to the converter's driving voltage before the last contactor was engaged, these currents are present in the system for some time. This settling time will depend on the dynamics calculated for the DC current removal control loop. In this case, for a crossover frequency of 15 Hz, this settling time is 1 second.

Naturally, the connection procedure has limitations. As it has previously explained, the synchronization is achieved by measuring the instantaneous value of the grid voltage phase. If this signal contains harmonics, the value obtained could not be stable enough to synchronize with the grid, therefore, as requirement for the specific implementation is that the grid voltage must be clean from harmonics at the moment of connection. Once the synchronization is achieved, these do not produce a major harm to the stability of the system (something confirmed in Chapter 6).

If the converter is going to be connected to a point where the grid is weak or contains harmonics, the arctangential PLL installed here can be replaced for more robust PLL architectures such as: The conventional Synchronous Reference Frame PLL (SRF-

PLL) or the Dual Second Order Generalized Integrator PLL (DSOGI-PLL). Since this experiment only aims to validate the correct functioning of the initialization routine, this study has not been included in this thesis.

3.5.6 Changing the power references

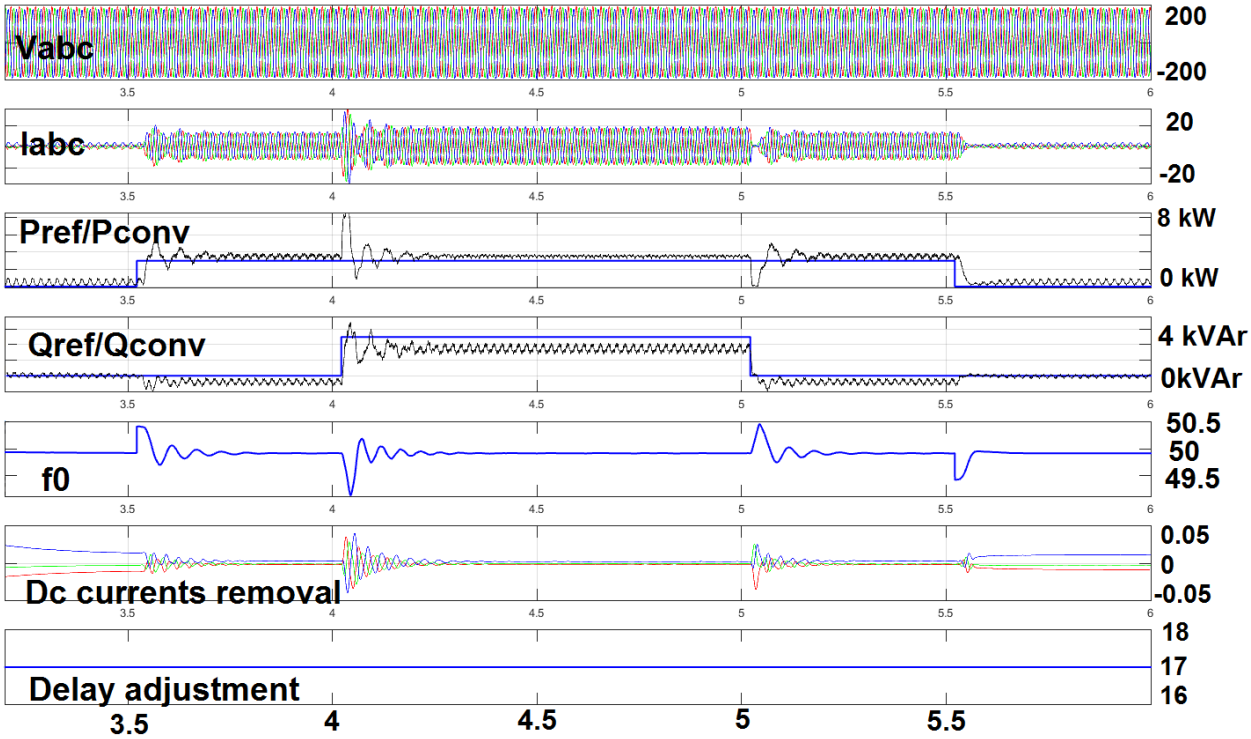

Figure 3.28: Converter results for changes in the power reference using the VSM0H control strategy.

In order to validate the operation of the converter controlled using the VSM0H strategy, an additional experiment showing changes in the active and reactive power reference is presented in this section. The results shown in Figure 3.28 continue in the time from the ones presented in the previous section. Starting at approximately $t = 3.2s$, the converter is fully connected to the grid and the DC currents removal block is still creating little deviations to correct the measured DC components. At approximately $t = 3.5s$, a step of 3 kW is applied to the reference of active power. Following the power synchronization mechanism explained in section 3.5.2, the system increases its frequency to displace its voltage angle. After some transients caused by the DC

removal block, the system satisfies the requested command and the frequency returns to its nominal value. At approximately $t = 4s$, an additional request of 5 kVAr in reactive power is demanded. This time, the control logic reacts by increasing the converter voltage magnitude and, as it can be observed, after new transients, the requested power is obtained. However, since the converter voltage magnitude has increased to provide this reactive power, the active power also increases transiently (observe again equation 3.4, if V_c increases, P rises as well). Thus, the driving frequency has to be reduced temporarily to reduce the driving angle and match the reference of active power set. Although the situation is completely solved by the control logic, it shows a cross-coupling between the reactive and the active power. At $t = 5s$ the command of reactive power returns to 0 and, at $t = 5.5s$, the active power does the same. In both cases, the system reacts in a similar manner with opposite signs.

In reality, the converter can provide a response against load steps on the active or, if necessary, reactive power. Since, either the converter nor the control algorithm contains any inertia, the response could be more similar to the step commanded. However, the synchronous machine present in this experiment creates oscillations in power that are compensated by the VSM0H converter. This feature is more deeply explained in Chapter 5 section 5.4.3.

Bibliography

[1] Argantix. "Argantix official webpage". Internet: http://www.argantix.com [Consulted Aug 2018].

[2] Semikron. "Semikron official webpage". Internet: http://www.semikron.com [Consulted Aug 2018].

[3] dSPACE. "dSPACE official webpage". Internet: http://www.dspace.com [Consulted Aug 2018].

[4] H. Kubo, Y. Yamamoto, T. Kondo, K. Rajashekara and B. Zhu, "Current ripple analysis of PWM methods for open-end winding induction motor," presented at the IEEE Energy Conversion Congress and Exposition (ECCE), Pittsburgh, PA, 2014, pp. 3858-3864.

[5] S. Das, A. C. Binojkumar and G. Narayanan, "Analytical evaluation of harmonic distortion factor corresponding to generalised advanced bus-clamping pulse width modulation." *IET Power Electronics*, vol. 7, no. 12, pp. 3072-3082,2014.

[6] R. Teodorescu, M. Liserre, P. Rodriguez. *Grid Converters for Photovoltaic and Wind Power Systems*, UK: Ed. Wiley, 2011. p. 294-296.

[7] R. Teodorescu, M. Liserre, P. Rodriguez. *Grid Converters for Photovoltaic and Wind Power Systems*, UK: Ed. Wiley, 2011. p. 300-306.

[8] Roscoe, A., Yu, M., Dysko, A., Booth, C., Ierna, R., Zhu, J., and Urdal, H. "A VSM (Virtual Synchronous Machine) Convertor Control Model Suitable for RMS Studies for Resolving System Operator / Owner Challenges," presented at the 15th Wind Integration Workshop, Vienna, Austria, 2016.

[9] M. Yu et al. "Use of an inertia-less Virtual Synchronous Machine within future power networks with high penetrations of converters," presented at the Power Systems Computation Conference (PSCC), Genoa, 2016.

[10] P. Matavelli, S. Buso. *Digital Control in Power Electronics*. USA: Ed. Morgan & Claypool Publishers. 2016. Chapter 3.2.

[11] Roscoe, A.J., and Blair, S.M. "Choice and Properties of Adaptive and Tunable Digital Boxcar (Moving Average) Filters for Power Systems and other Signal Processing Applications." presented at the IEEE Applied Measurements in Power Systems (AMPS), Aachen, Germany, 2016.

[12] P.A. Dahono. "A Control Method to Damp Oscillation in the Input LC Filter of AC-DC PWM Converters," presented at the Power Electronics Specialists Conference, Australia, 2002.

[13] L. Reguera Castillo, A.J. Roscoe. "Experimental validation of a novel inertia-less VSM algorithm" presented at the IEEE Innovative Smart Grid Technologies North America, DC, United States, 2018

[14] L. Zhang, L. Harnefors and H. P. Nee, "Power-Synchronization Control of Grid-Connected Voltage-Source Converters." *IEEE Transactions on Power Systems*, vol. 25, no. 2, pp. 809-820, 2010.

Bibliography

Bibliography

Chapter 4

A solution for power systems with low Level of Penetration, grid-friendly converters

4.1 Introduction

The concept of grid-friendly converters (similar to the term 'smart converter' in America) appears as a natural consequence of the progression of converter-connected generation into large electrical systems. Conventional power plants provide, by default, functions which support the grid with the necessary stability to allow a robust operation. Therefore, when practically the entire generation was dominated by synchronous generators, there was no need to explicitly demand these tasks or even mention them. Since the proportion of these converters were very low, this responsibility could be displaced to the remaining synchronous generators connected to the grid. However, with the gradual progression of renewable energy and its inherent change in the generator device, fewer machines have to compensate for the lack of stability functions of an increasing number of converters connected to the grid.

The need of these functions can be better observed with historical cases where nothing was done ending with disastrous consequences [1]. By 2005 the aggregated nominal power of wind energy in China was 1.3 GW. In that year, the Chinese government

drove a new normative to establish the first grid code (GB/Z 19963-2005). However, this code was not compulsory, it was used more as a reference, and thus, generators ignored it. This lack of regulation led in February 2008 to the disconnection of 598 generators, losing 840 MW of power in the district of Jinquan. The next month, a similar fault disconnected 1000 MW followed by an additional one the next day in a different region. In order to mitigate this cascade of failures, in 2011, the operator created a new grid code, much more ambitious than the previous, now demanding these ancillary functions for new generators and having to request an updated performance to a certain number of wind farms with retroactivity.

Luckily, European TSO's realized about the lack of controllability before the system would become unstable. Thus, they began to demand new converters additional functionalities apart from the mere injection of the energy produced. The term which collects the totality of these tasks is called *ancillary functions* or *grid-supporting functions*. Equally, converters providing these functionalities are called *grid-friendly converters* (also called *smart inverters* in America).

As it should be expected, first TSO's demanding these tasks were the ones which reached sooner high levels of penetration of renewable energy in the system such as: Denmark [3], Spain [4], and UK [5]. However, although nowadays the majority of the European TSO's request these grid supporting functions, there is no consensus between them about the demanded performance or even which is the set of tasks that should be requested. As result, there are a lot of differences between grid codes among countries. Nonetheless, to some extent disparity is required. The demanded performance will not be the same if a converter is connected for instance to Germany than to Ireland. Germany is a very large grid with multiple energy producers in the system and highly interconnected with their neighbor countries. As a whole, it is a much more stable network than Ireland which is much more isolated from the European grid and it is a relatively small grid compared to, for instance, UK or aforementioned Germany. In order to keep the system stable, the performance demanded in smaller grids will be more challenging than in the large ones.

The tempos in North America have been completely different than in Europe. Since

the level of penetration of the vast majority of the states in the USA has not been very high (by 2016 only 5.55% of the energy production came from wind farms [5]), there has not been any actual commitment to establish a set of rules or standards. It has not been until early 2018, that it has just been approved the new IEEE 1547 standard for Grid Integration of Distributed Energy Resources. This document intends to be a reference for converter manufacturers, TSOs and Distribution Network Operators (DNO's).

This chapter begins with a definition of the ancillary functions, describing their main features. Following, there is a discussion about the need for designing fast converters to perform the aforementioned tasks and how this requirement clashes with the converter and grid stability. Later, an inverter with a customizable response is presented as solution to achieve an even more grid-friendly converter. Finally, an experimental assessment of this solution is done in the laboratory.

4.2 Definition of the ancillary functions

As it was already mentioned in the previous section, the ancillary functions are difficult to enumerate since there is no agreement between TSO's and DNO's about which are the main functionalities that must be requested. Therefore, the work done in this chapter focuses on the most common ones, usually present in the majority of the European grid codes. Nonetheless, these are only a fraction of the demanded tasks and they have been accounted here due to its complexity and the issues relative to their implementation.

4.2.1 Virtual Inertia

In conventional power plants, the inertia is only present when there is some event on the grid such a sudden disconnection of the load. If this incident occurs, the synchronous machine loses temporarily some of the electromagnetic torque, causing a small acceleration in the generator rotor due to the accumulated kinetic energy in the rotor. As consequence, the actual production of electrical energy will decrease briefly, providing a contributing factor to the frequency regulation and thus, to the grid stability. Naturally,

the more machines are connected to the system, more inertia will be provided, therefore more contribution to the transient stability. On the other side, since converters are static systems, they do not provide inherently any inertia. Consequently, with the gradual removal of synchronous generators and its substitution by converter-systems, fewer elements of the system provide this stability factor, leading to an electrical grid with lower inertia.

Countries with high levels of penetration are beginning to face the problems entailed in electrical grids with low inertia. Eirgrid in Ireland is already facing some of these problems. In their stability studies it is assumed a ROCOF (Rate Of Change Of Frequency) of more than 2 Hz/sec and a level of penetration of more than 50%. This is a very high number for a country-sized electrical system. As a reference, in the UK, National Grid has a license obligation to control system frequency at 50 Hz with a margin of 0.5 Hz.

In an attempt to mitigate this increasing ROCOF, the request of a virtual or synthetic inertia has been a subject under study among academia. Furthermore, some European grid codes have started to write preliminary drafts about its regulation, thereby, including them in future grid codes modifications. The Spanish grid operator, Red Electrica de Espana, outlined a draft of these tasks which will be used as reference for this chapter [6] [7]. Its block diagram is described in Figure 4.1.

The virtual inertia block consists of a derivative controller which acts with frequency variations, providing as output a shift in active power. In the aforementioned draft, it is expressed the need for an adjustable gain K_d of value between 0 to 15 sec. The

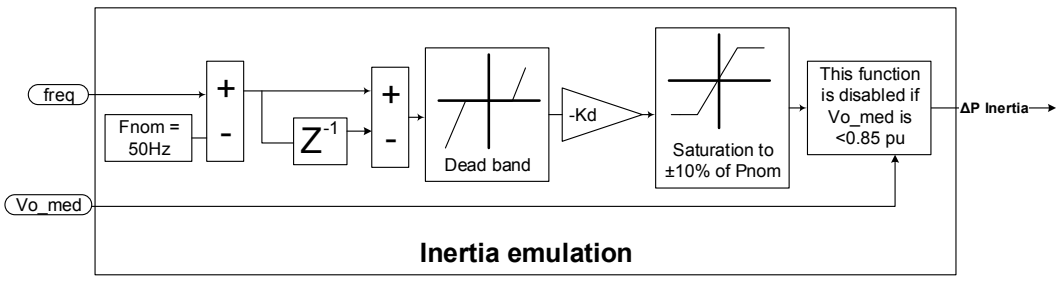

Figure 4.1: Synthetic inertia implementation.

response time should be less than 50 ms to provide a ΔP of 5%. The virtual inertia block will have a limited action to a maximum of 10 % of active power and it can last for 2 sec. Finally, it will have a dead-band of ±10mHz. Although this is the block which has been used in the experiments and simulations, it is worth to explain with further details the problems implementing this ancillary function.

In order to obtain a true inertia it is necessary to execute, immediately as the fault occurs, a shift in the active power injected. As soon as there is some delay until the power drift is present, its effectiveness in the grid stability reduces, getting quickly to the point where the virtual/synthetic inertia has a counter-productive effect increasing the ROCOF values [14] (with 5 ms of delay, the inertia does not contribute positively at all).

The problem using this block is that it requires some time to obtain a reliable value of frequency, typically this measure takes several cycles (10-13 cycles/200-260 ms). If in an attempt to reduce this value this time is reduced, the frequency will not be very stable, and consequently, the derivative term can apply random strong shifts of active power contributing to a further instability.

To summarize, since this inertia cannot be applied when it is exactly needed, it is not a true natural inertia, and the effects of this contribution are only observed as an additional perturbation along the grid. Therefore, it should not be named virtual inertia but short/fast frequency response.

4.2.2 Voltage control at the Point of Common Coupling

Since initially converters injected solely the energy produced, they could only provide active power. With the increased level of penetration, it was necessary more generators which would supply reactive power to maintain the voltage magnitude between some margins. Therefore, grid-connected converters were required to supply reactive power too according to the levels of voltage which they would operate. Here, since there is a huge disparity between TSO's, the same document [6] is used as a reference for this function. Its block diagram is presented in 4.2.

This function consists of an open loop control that will change the value of the reac-

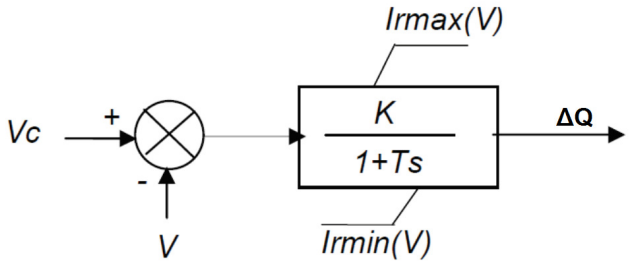

Figure 4.2: Voltage control block according to [6].

tive current depending on the error of voltage in the PCC. The error will be multiplied by a customizable constant (K) that will be executed with a time constant T. The actuation will be limited for the values Qmax and Qmin. These two limit values will change depending on the instantaneous PCC voltage according to the graph in Figure 4.3.

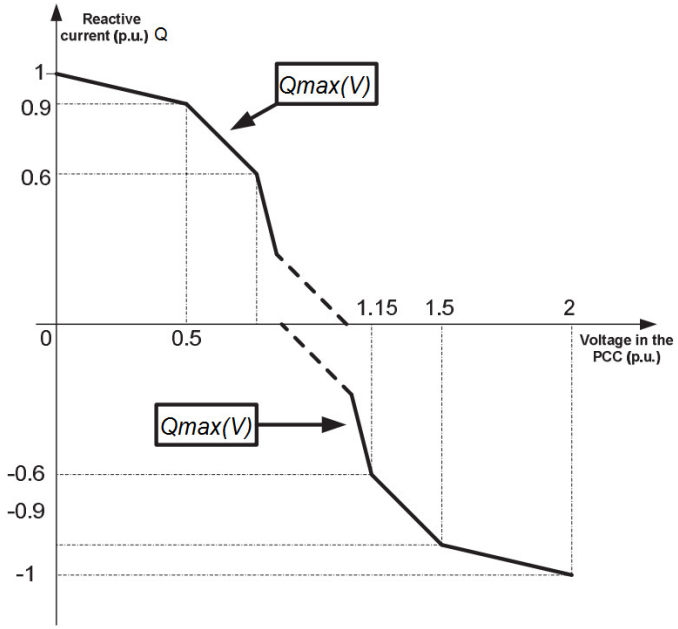

Figure 4.3: Limits depending on the PCC voltage.

4.2.3 Low Voltage Ride-Through

Using the voltage control described in the previous section, this function also demands a certain resilience to the converter against faults. Therefore, an inverter-based genera-

tion has to be capable of riding through voltage dips without disconnection. Moreover, now these systems have to contribute to the voltage recovery during the fault (asymmetrical or symmetrical). The demanded dynamics for this function are usually presented in graphs commonly known as Low Voltage Ride-Through (LVRT) curves. In order to achieve successfully this task, the converter performance against a voltage dip will have to be above the LVRT curve. Figure 4.4 shows several LVRTs for different countries.

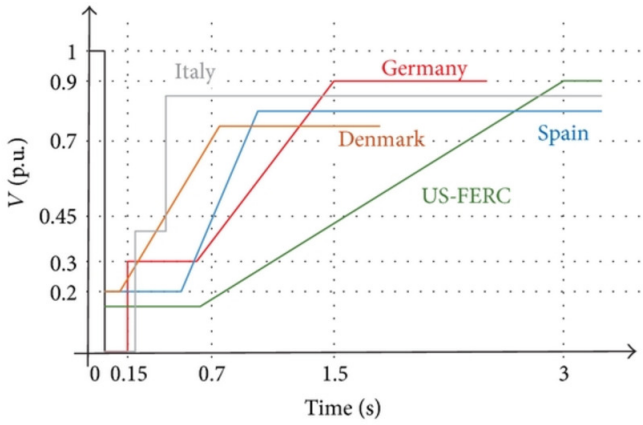

Figure 4.4: LVRT curves for various countries.

Depending on the chosen grid codes, these graphs can be as challenging as being capable of tolerating and recovering up to a full short-circuit (0 pu) like the German grid code. However, if the fault is asymmetrical, unbalanced currents would be demanded from the loads. For this case, the requested response from the converter for these voltage curves according to the grid codes would be a balanced production of reactive power capable of returning the voltage level to nominal values. Nonetheless, this requirement is, to some extent, too limp. If there is a lack of voltage sources in the grid and therefore, a shortage in voltage regulation, converters should also contribute to the grid stability producing unbalanced currents which would maintain the voltage levels between nominal values across the three phases.

In any case, continuing with the keynote followed along this chapter, the Spanish grid code will be used as reference for future experiments.

4.3 A slow converter or a fast converter, what is better?

It is quite intuitive to think that any converter capable of executing control strategies at high speeds will be much more responsive against any event or desired performance, and therefore, it will be much more equipped with all the tools necessary to develop any high-level command. This converter bandwidth is defined by two main parameters; the IGBT switching frequency and the crossover frequency of the inner control loop. Thus, usually, trying to maximize the converter performance, these values tend to be designed as high as possible.

On the contrary, there is evidence enough to think that, if there is no fault or transitory effects on the grid, it is more convenient for the grid to design the inner current loop of the converter with a very low bandwidth [8]- [10]. This low bandwidth will result in a slow response against any change of the current references. Due to the lack of speed on the inner control loop, this strategy has a net averaging effect over the events occurred on the voltage or current signals, responding to these in a much smoother manner than a faster, more nervous control. As result, the system will have a long time response on the exchange of a much more robust operation, especially when connected to weak systems where the voltage quality of the grid is poor, and the voltage transients are frequent. As an illustrative example, the converter with a low bandwidth would behave similarly to a generator with a high stiffness, mitigating possible dangerous overshoots and swings in power that a faster control could provoke. As reference, some studies suggest, if this would be possible, a control bandwidth of less than 5 Hz to get a robust system [10].

Nonetheless, it is necessary to remember that, although in the permanent regime converter may be designed to be slow, the previously explained ancillary functions demand a fast response against events on the grid. As an example, the Low Voltage Ride-Through curve, presented in Figure 4.4, explains how the system has to react against a voltage drop in less than, between 0.15 and 0.6 seconds, depending on the country where the inverter is installed. Therefore, both requirements enter into conflict with each other.

As solution for this, the converter with variable speed response is proposed here.

4.4 The inverter with variable response

Obviously, a converter cannot be slow if a fast dynamic has to be fulfilled. However, if it would be possible, the best behavior in order to make the converter most grid-friendly possible would be as follows; When there is no event in the grid it would have a lower bandwidth, however, if any event is recognized, the ancillary functions will require a fast bandwidth to respond with speed enough to fulfill the requirements.

Using the conventional DQCI control strategy already explained in 3.4.3, the ancillary functions can be supplied installing additional control blocks which will provide shifts in the power references (see Figure 6.2 for a detailed diagram). This author in [11] explained the capability of auto-designing the internal converter dynamics in high detail. For a defined crossover frequency (Fc) and phase margin (PM), equations 3.2 and 3.3 were used to calculate the regulators and embedded in a parameter file that was run before the control and the converter begin to operate. Nonetheless, this functionality was only available before the system was connected and injecting power to the grid, therefore, its response could not be changed live. Assuming the fault detection, the author in [12], exploits this functionality further, allowing the reconfiguration of the internal regulator gains dynamically by changing PM and Fc when needed. If the control notices a change in these values, the regulator gains will be recalculated to satisfy the new dynamics. As a result, the converter will have flexible dynamics, ideal for both the grid and the converter.

In [11] this calculation was done before the converter was connected to the system but in [12], both equations have been included inside the logic of control. Therefore, every single time PM, or Fc, are changed, a new set of Ti and Kp that satisfies these new values are calculated automatically and updated into the controller providing this dynamic behavior.

4.4.1 Performance evaluation of an inverter with variable response

As it was initially discussed in the introduction of this chapter, the aforementioned flexible behavior has been put into analysis implementing this control in the converter used for this thesis. Essentially, this control strategy is very similar to the standard

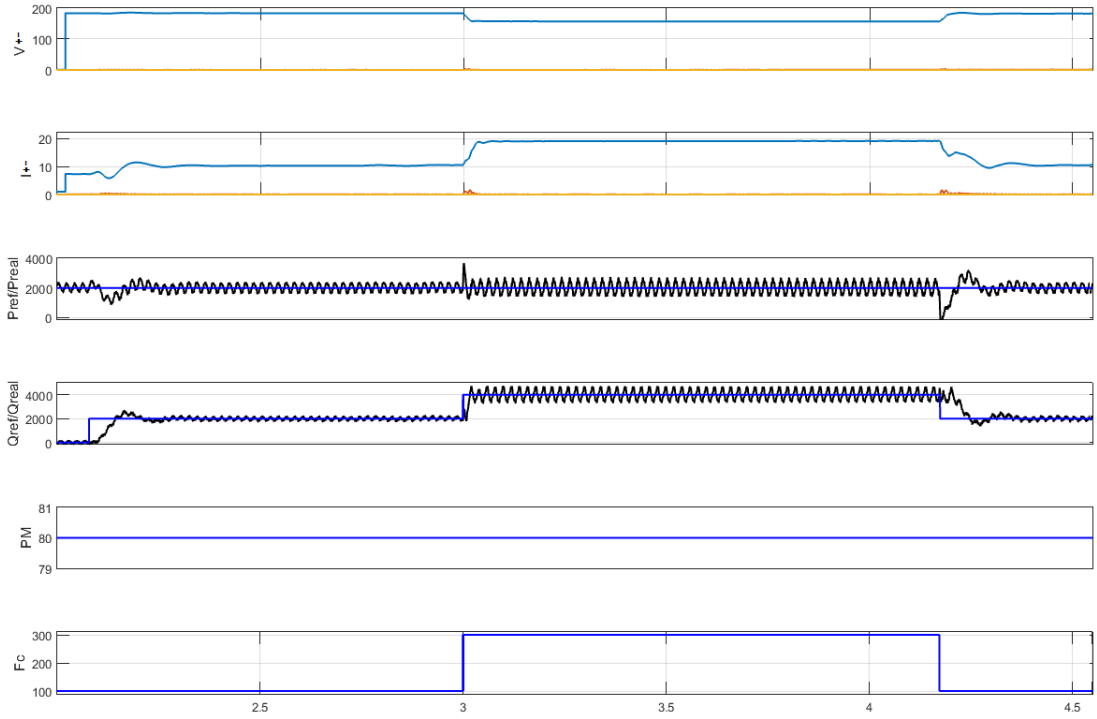

Figure 4.5: Experimental results of an inverter with variable response.

vectorial or DQCI control already explained in 3.4. However, now, the regulator gains (Kp and Ti) are now extracted as variables that are recalculated in case of any grid event. The results of this strategy are presented in Figure 4.5. The graphs shown from top to bottom are as follows: phase voltages (Vabc), current voltages (Iabc), the active power reference and the real one extracted from the measured signals (Pref/Preal); the reactive power reference and the real one (Qref/Qreal), the phase margin (PM), and the crossover frequency of the inner current loop (Fc).

Initially, the experiment starts injecting energy into the permanent regime with a command of the active power of 2 kW and a crossover frequency of 100 Hz. At approximately 2.1 seconds, a change in the demand of reactive power from the transmission/distribution system operator side is executed. After approximately 200 ms, the system begins to inject a total of 2 kW of active power and 2 kVAr of reactive power. At 3 seconds, a symmetrical fault occurs, causing a voltage drop to 0.85 pu for 1.25 seconds. The converter recognizes this event as a fault and the PCC voltage regulation demands more reactive power to overcome this event. As it was already

explained in section 4.2.2, in case of a voltage dip, the inverter has an open loop which reacts against it providing a certain amount of reactive power. This quantity will be conditioned by the graph presented in 4.3. In this case, for illustrations sake, this gain has been calculated so that, for a 15% voltage dip, an additional 2 kVAr are injected (ΔQ PCC reg = 2kVAr).

This additional step at 3 seconds of reactive power is executed immediately, but, since now there is an event in the grid and these functions have to be executed much faster, the crossover frequency is increased to 300 Hz. In order to do so, the gains from the PI regulators are recalculated internally using equations (3.3) and (3.2) without observing any effect on the effective energy injected. As result, for the same step of reactive power (both were intentionally calculated to have 2 kVAr in magnitude), the step commanded from the grid is much slower than the one created by the ancillary function, confirming with it the conditioned behavior of the system depending on the events occurred on the grid.

According to [4], it is required from the generators to respond against this event in less than 150 ms. Since the first step takes 200ms to be satisfied and the second 50ms, if Fc would not change from 100 to 300 Hz when it is necessary, this requirement would not be fulfilled. Thus, the system would not be eligible for connection to the grid. Now, thanks to the customizable behavior, and without having changed any actual hardware in the system, the inverter responds 150 ms faster than before, making it fully compliant with the regulation. For simplicity, only the regulation of the PCC voltage function has been explained but, of course, the same procedure could be done with the remaining ancillary functions. Furthermore, a new set of Fc and PM could be chosen for each ancillary function without any problem as long as this flexibility does not compromise the system stability.

Naturally, this techniques has limits, mainly on the values of Fc and PM that can be set. These limits are determined by the switching and sampling frequency of the converter which set the maximum rate of operation. By convention, the maximum Fc obtained in an inner current loop is about seven times less than the switching frequency. For this particular case, this frequency is 5 kHz which translates into a

maximum crossover frequency of 714 Hz. However, it has been observed empirically in the experiments conducted that the converter can fall into the instability region if this value is higher than 500 Hz, being this its limit. To confirm a safe operation of the converter across the desired values of Fc and PM, a stability assessment must be done to confirm that for the limit values, the system does not enter into instability.

4.5 Summary

In this chapter, a grid-friendly converter has been presented, describing the precise meaning of what grid-friendly is and some detail about the additional functions required in some countries where converters are beginning to take, already nowadays, a significant level of penetration. It has also been presented the most common set of ancillary functions including the misleading term of virtual/synthetic inertia (see section 4.2.1). Finally, it also has been presented an even further grid-friendly functionality which can provide the best response according to the converter and the grid needs to maintain the overall stability.

The set of functionalities presented along this chapter fail in a crucial element, all of them are based in a DQCI control strategy. Thus, they do not provide Grid Forming capabilities like the ones demanded (and explained in section 1.3.1) such as angle or voltage stability to create a stable converter-dominated grid. Since these smart or grid-friendly converters would be still working under a DQCI control, they still would behave as current sources in a grid with a poor voltage grid stiffness being this the main weakness of such power system. Thus, they contribute to the power system stability but with limited effectiveness.

Nonetheless, after having read this chapter the most natural question is; how much grid-friendly converters can we install until the stability is compromised again? which solutions can we take if the Level of Penetration increases to guarantee the stability of a converter-dominated grid?. The answer to these questions are in Chapter 5.

Bibliography

[1] R. Piwko et all. "Penetrating Insights." *IEEE Power & Energy magazine*, 2012.

[2] Energinet. "Regulations for grid connection. Technical regulation 3.3.3 for PV/Wind Power Plants Above 11 kW." Internet: https://en.energinet.dk/Electricity/Rules-and-Regulations/Regulations-for-grid-connection [Consulted March 2018].

[3] Red Electrica de Espana. "Procedimientos de operacion." Internet: http://www.ree.es/es/actividades/operacion-del-sistema-electrico/procedimientos-de-operacion [Consulted March 2018].

[4] National Grid. "National Grid Code". Internet: https://www.nationalgrid.com/uk/electricity/codes/grid-code?code-documents [Consulted March 2018].

[5] U.S. Energy Information Administration. "Electric Power Monthly." Internet: https://www.eia.gov/electricity/monthly/ [Consulted March 2018].

[6] Annex of O.P. 12.2, "Restricted to the Technical Requirements of Wind Power and Photovoltaic Facilities(draft) Red Electrica", www.ree.es (translated into English by Spanish Wind Association AEE in Internet: www.aeolica.es), October 2008.

[7] R. Teodorescu, M. Liserre, P. Rodriguez. *Grid Converters for Photovoltaic and Wind Power Systems.*UK: Ed. Wiley, 2011. p. 165.

[8] L. Zhang, L. Harneforts, H.P. Nee. "Power-Synchronization Control of Grid-Connected Voltage-Source Converters". *IEEE Transactions on Power Systems.* vol. 25, no.2, pp. 809-820, 2010.

[9] L.Harnefors. "Control of a voltage source converter using synchronous machine emulation." U.S. Patent 20110153113A1. Jun. 26, 2011.

[10] A.J.Roscoe , M.Yu , R. Ierna ,J. Zhu ,A. Dyko ,H. Urdal , C. Booth A VSM (virtual synchronous machine) convertor control model suitable for RMS studies for resolving system operator/owner challenges presented at the 15th Wind Integration Workshop, Vienna, Austria, 2016.

[11] L. Reguera , A. Lzaro ,I. Quesada and A. Barrado, Auto-design simulation set up of PV VSC with grid supporting functions," presented at the IEEE 15th Workshop on control and Modelling for Power Electronics (COMPEL), Santander, Spain, 2014.

[12] L. Reguera, A. Lazaro and A. Roscoe, "Experimental analysis of a fully compliant grid inverter with controllable response," presented at the IEEE 12th International Conference on Power Electronics and Drive Systems (PEDS), Honolulu, HI, 2017, pp. 1,167-1,171.

[13] R. Teodorescu, M. Liserre, P. Rodriguez. *Grid Converters for Photovoltaic and Wind Power Systems*. UK: Ed. Wiley, 2011. p. 294-296

[14] M. Rezkalla, A. Zecchino, S. Martinenas, A. M. Prostejovsky, M. Marinelli, "Comparison between synthetic inertia and fast frequency containment control based on single phase EVs in a microgrid," *Applied Energy*, vol. 210, pp 764-775, 2018.

Bibliography

Bibliography

Chapter 5

Understanding the weaknesses of power systems dominated by converters

5.1 Introduction

In the previous chapter, the grid-friendly/smart converters were explained as a solution to maintain the grid stability in power systems where the level of penetration of converter-based generation is relatively low. However, quantifying and defining what is "low" is very difficult since it depends on a huge number of variables. Some of them are: The neighboring generators, the equivalent line impedance between the converter and the stiff source voltage, the own stiffness of the grid or even another variables like the number of generators available in the system have to be addressed. An example of this last case is on the Orkney islands. There, it exists a high proportion of renewable energy leading to a high value of LoP. However, its number of generators is limited and therefore, every system including the non-renewable or not converter-based must remain connected in case of any grid event [1].

Thus, in order to answer properly and give an exact number, this question has to be addressed in a case by case basis and, even so, it is very complicated. As a reference, in [2], one of the first books where the grid supporting functions were explained, a level

of penetration of 10% is considered high; value which has been widely exceeded in the countries where, primarily thanks to the wind energy, there is a growing number of power generation based on converters.

Some studies, taking into account several premises, have tried to quantify which is the limit when the ancillary functions are not a solution to provide grid stability. These studies, made on the simulation scope, set these limits between 40% and 60% [3], depending again on a huge number of variables such as the capacity factor of the generators, their technology, the situation of these in the grid, etc. However, although it seems quite clear that is very difficult or almost impossible to provide an exact number, it is also clear that there is a limit where these ancillary functions are not effective as solution anymore, exposing power systems to multiple catastrophic risks.

This chapter attempts to evaluate and assess which are the events or variables of the system that trigger the instability of power systems when converter-generation is not only a minority fraction of the system (like the previous chapter), but they are the primary source of energy. To do so, strategic scenarios are recreated in the laboratory to expose the weaknesses of actual converter systems, proposing solutions to achieve, in the end, a stable 100% converter-based power system based on the GFN solution explained in Chapter 1 section 1.5.

5.2 Additional ancillary functions necessary for converter-dominated grids

In Chapter 4, it was observed that the definition of an exact number and specific performance of the so-called grid supporting functions or ancillary function is vague and they are defined depending on the TSO which requires them, having a high disparity between countries. In any case, since there is a limit for converters where the system is facing or it is close to a complete black-out, it seems that these tasks are not covering the number of functions provided by a synchronous machine, or these tasks are not well defined.

In reality, synchronous machines contribute to the stability with additional func-

tions, not explicitly mentioned in any ancillary function or grid code but critical at this level of penetration. First, they behave as voltage sources behind an inductance. This simple fact has tremendous implications throughout the complete grid stability. As it was already explained in Chapter 2, conventional controlled converters behave as current sources, not voltage, having a passive role in the system and following the voltage imposed by the remaining synchronous generators. Within converter-dominated grids, only a minor fraction of the generators (the remaining synchronous machine connected to the system) may provide voltage regulation, resulting in a weaker voltage stiffness. Since conventional-controlled converters are especially sensitive to the voltage quality and its noise content, the entire power system can be compromised if nothing is done.

Second, synchronous machines provide synchronizing torque/power. Against a sudden change of frequency created by a grid event, some of the synchronous generators can suffer a sudden change of the instantaneous angle at the connection terminals. Following the well-known swing equation for synchronous generators, a sudden variation of the active power injected to the grid will occur and, as it was explained in Chapter 3 section 3.5.2, following the power-synchronization mechanism, the remaining synchronous generator will pull to make the singular synchronous machine to stay in synchronism. In a 100% converter-based grid, this is not an issue; since there are no rotating elements or inertias to respect in this case, converters can do instantaneous changes of their voltage angles if needed as long as the voltage stiffness is assured. However, if there is only a tiny amount of synchronous generators in the system, they will need some synchronizing torque to remain connected in case of any grid event. If converters fail to provide this service, the number of generators that can actually supply synchronizing torque may be too low. Consequently, the remaining synchronous machines will suffer of rotor angle instability having now a higher probability of disconnecting against a grid event (higher as higher is the level of penetration)and with it the remaining DQCI converters. Within DQCI-converter-dominated grids, only a minority of elements in the system are actually contributing to the grid stability, thus, losing some of the remaining synchronous generators of the system which supplies them does not seem like a good idea. Finally, this provides evidence that more synchronizing

torque must be supplied from converters to assure the requested rotor angle stability that synchronous generators need.

Converters can provide this synchronizing torque whenever they make use of any of the control strategies explained in Chapter 2 classified as Virtual Synchronous Machine or VSM. As soon as these control strategies get rid of the PLL to obtain a reference of synchronism, they automatically need the power synchronization mechanism which underpins the creation of synchronizing torque. However, this torque can be delivered with different profiles depending on the specific VSM control strategy used.

Although these are theoretical indications of what are the weaknesses of converter-dominated grids and why the ancillary functions cannot provide an unlimited stability, it is necessary to recreate an experiment in the laboratory where these evidence can be confirmed. Additionally, an attempt to evaluate the maximum tolerable level of penetration for a converter-dominated grid will be addressed. These results are extracted from the conference paper presented by the author in the 16th Wind Integration Workshop in Berlin [4].

5.3 Experimental setup

The system used as a converter-dominated power network is presented in Figure 5.1. This can be observed by the ratings of the synchronous set and the converter installed. Alternatively, from the equation 1.4 in Chapter 1 the LoP of this network can be computed obtaining a value of 81%. Value much higher than the 10% already considered as high in previous references [2].

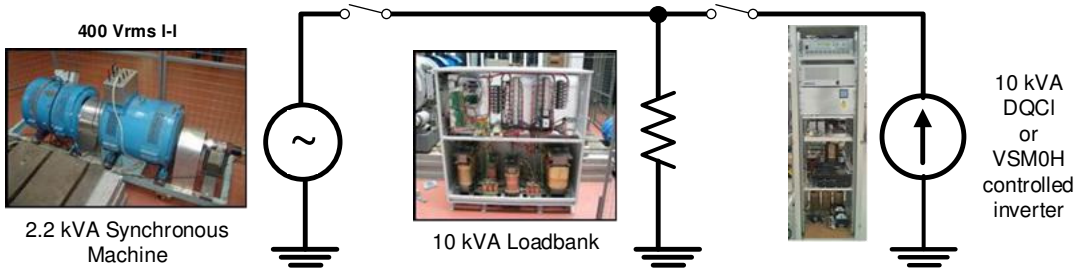

Figure 5.1: Main diagram of the converter.

Although in Figure 5.1 the converter has been represented as a current source, this is only valid if the converter is controlled using the conventional DQCI algorithm. This symbol has to be replaced by a voltage source if the VSM0H control strategy is used.

The scenario recreated consists of a synchronous set consisted of a motor and a generator with a rated power of 2.2 kVA representing the aggregate power of the remaining synchronous generation, a configurable load bank of 10 kW, and the tailor-made converter of 10 kVA with exchangeable algorithm explained in Chapter 3 representing the aggregate power of the converter-based generation.

Being more exact, although the synchronous generator has a rated power of 2.2 kVA, the motor can only provide 1.5 kW, thus, its active-power limit value is this last.

5.4 Experimental Results

5.4.1 Experiment 1: Level of Penetration experiment

In this chapter and the previous one, it has been mentioned the incapability of DQCI converters to produce their own grid and how PLLs make the inverters to behave as passive systems in the grid. Also, it has been cited that countries with a high level of penetration of converter-based generation are facing problems, triggering several studies in academia with industrial collaboration ([3], [5], [6]). These evaluations aim to calculate which is the limit value where power systems can face complete instability by the lack of management on the grid. However, there is no experimental assessment which evaluates the key variables of the system or why there is such a limit. However, it is straightforward to think that this assessment cannot be complete without an experimental validation which is the main subject under study during this experiment. The simulation study made in [3] initially predicted a maximum level of penetration of between 40 and 60 %, depending on the variables. This value will be assessed and additionally, a comparative experiment with the chosen VSM0H algorithm behaving as GFN will be made.

In order to compute a maximum level of penetration, the experiment cannot simply set some values and observe if the grid is stable. The experiment has to go through

a process similar to the one followed by a grid blackout. This procedure is explained as follows: The evaluation starts with the scenario presented in Figure 5.1 having all the elements disconnected. Then, the synchronous set is connected in islanded mode, building its own voltage and frequency. Following, the loadbank is connected with a load of approximately 700 W. The synchronous generator, as the voltage source that it is, satisfies this demand easily since this value is lower than the 1.5 kW which is able to supply. Later, the converter connects to the grid created (it does not matter which is the algorithm used), producing 500 W. This liberates the synchronous set and now it only has to produce the remaining 200 W of power to keep the balance between production and demand. Next, the demand is increased to 1200 W. Automatically, the synchronous generator reacts again increasing its production up to 700 W whilst the converter remains to inject 500 W. A new step in the converter active power is then executed injecting a total of 1000 W. This, again, liberates the synchronous set from injecting power. This procedure is repeated until the system becomes unstable or the maximum load has been reached in the load bank.

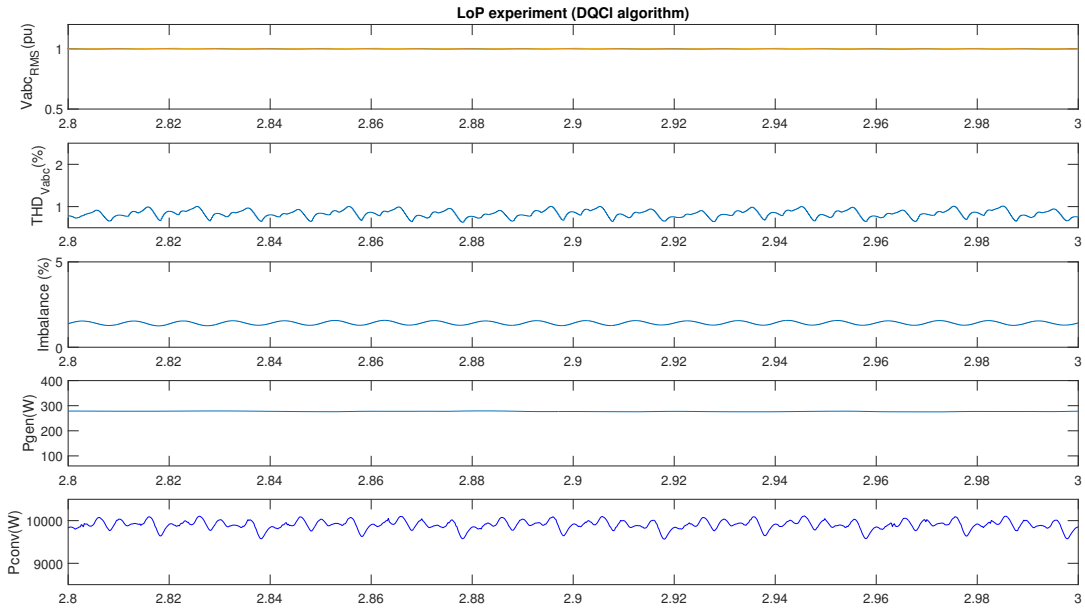

Figure 5.2: Level of Penetration experiment for the DQCI algorithm

Figure 5.2, presents an excerpt of the experimental results obtained using the DQCI control strategy. From top to bottom it is presented the voltages magnitude

for every phase($Vabc_{RMS}$), the Total Harmonic Distortion (THD) and the unbalance of these voltages in percentage, the active power produced by the synchronous machine (P_{gen})and the contribution of power supplied from the converter (P_{conv}). The unbalance and THD are presented here to confirm that the power quality is not affected during the experiment since these scenarios suppose to evaluate extreme conditions.

Naturally, in order to be able to compare both control strategies, the previously explained process has been repeated for the VSM0H algorithm and its results are presented in Figure 5.3, presenting the same signals.

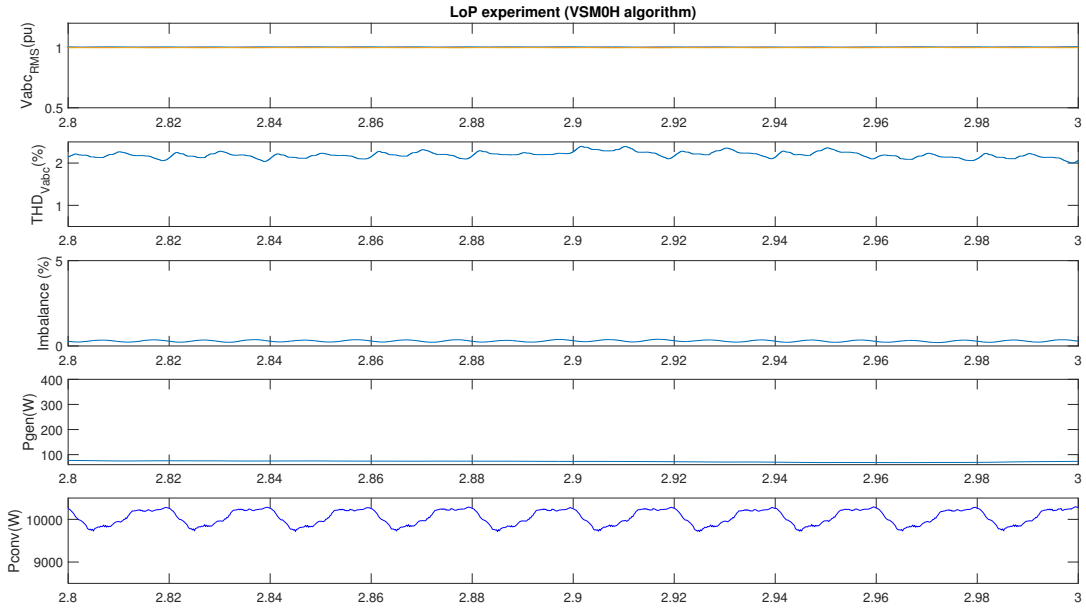

Figure 5.3: Level of Penetration experiment for the VSM0H algorithm

Figure 5.2 and 5.3 show unexpectedly similar results. For both scenarios, the converter is supplying power to the load almost entirely for the maximum value of the load bank. In addition, the power quality has not been compromised. Taking as reference the grid code from National Grid in UK [7], here THD is limited to 5% and the unbalance lower than 3%. Observing the extracted results, these values are never exceeded in any case confirming the grid is stable and clean.

At this moment, the equations already presented in Chapter 1 section 1.4 can be used for the calculation of a Level of Penetration for the particular case of this experiment. In that section, three equations were represented: LoP (equation 1.2),

LoP_{exp} (1.3) and the new proposed in this thesis as LoP_{conv} (1.4) which takes its meaning as result of the conclusions extracted from this experiment. Table 5.1 shows the resulting values using the three different formulas.

Level of Penetration obtained			
	LoP (eq 1.2)	LoP_{exp} (eq 1.3)	LoP_{conv} (eq 1.4)
DQCI	97 %	97 %	81.6 %
VSM0H	99.3%	99.3%	81.92 %

Table 5.1: Results obtained for the Level of Penetration experiment using the two control strategies evaluated.

Since there is no HVDC in this experiment, LoP and LoP_{exp} give identical results. In both cases, the number obtained is very close to 100%. These values produce an unexpected result, the amount of active power generated by the synchronous machine is not the main contributor to the grid stability; instead, it is the natural regulation capability of the synchronous machine which, imposing a voltage and a frequency reference, provides the stability to the grid. In other terms, the main grid stabilizer of this grid is the synchronous machine just because it is connected to the grid behaving as a voltage source. Thus, the main variable which dictates the stability of a grid is not the active power that is being supplied by the synchronous generators, it is the rating in kVA of the synchronous set. Therefore, this is the variable which must be taken into account to define a proper level of penetration. This is the reason why a new equation of LoP has been suggested in this thesis encapsulating this idea in the definition of LoP_{conv} and reducing the level of penetration to 81%.

5.4.2 Experiment 2: Loss of Mains experiment

Since the previous experiment gave a surprising value close to 100%, a logical question is what would happen if the scenario becomes literally a 100% converter-based grid. Additionally, the capability of islanding for both strategies can be evaluated. The results of this experiment using both algorithms are presented in Figures 5.4 and 5.5.

In both scenarios, the following signals are plotted: the instantaneous grid voltage ($Vabc$, the currents injected by the converter ($Iabc_{conv}$), the currents supplied by the

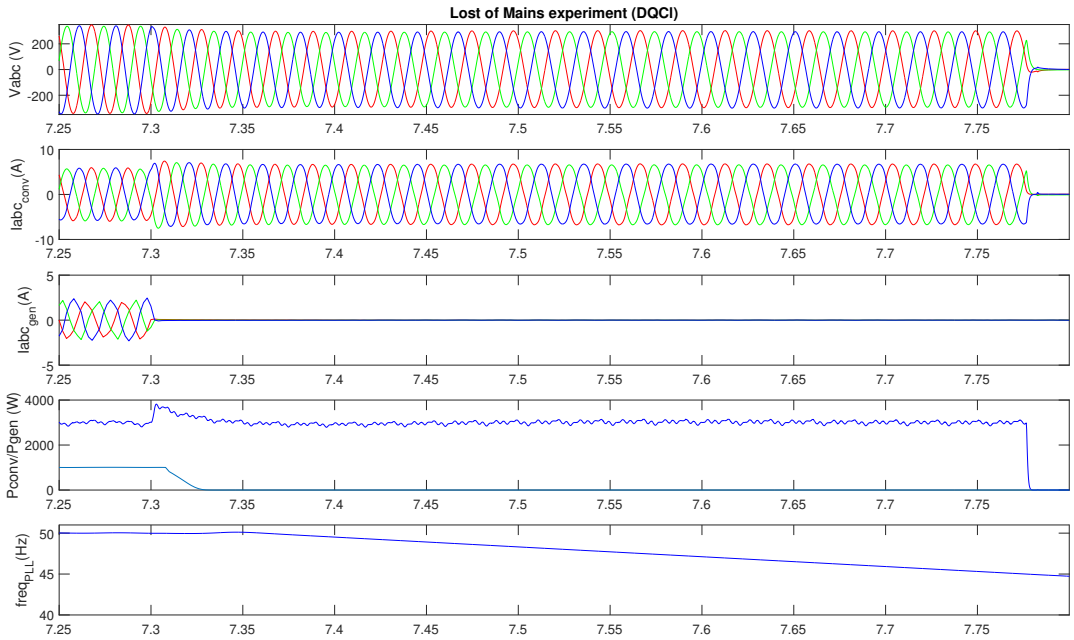

Figure 5.4: Lost of Mains experiments using the DQCI control strategy

synchronous generator ($Iabc_{gen}$); then, in the same plot the active power supplied by the converter and the machine (P_{conv} and P_{gen}) drawn in dark and light blue respectively, and finally the frequency obtained from the converter's PLL in the case of the DQCI experiment, or the internal estimated frequency from the control algorithm in the case of the VSM0H control strategy.

The results obtained for the DQCI control (Figure 5.4) begin with both generators, converter, and machine connected to the scenario created and feeding together a load of approximately 3.5 kW; 3 kW supplied by the converter and the remaining 0.5kW by the synchronous generator. At 7.3 sec the synchronous set is disconnected from the system, leaving the converter isolated with the load. Initially, the converter remains injecting power to the load and, after an initial overshoot, the reference returns to the previous value before the fault occurred. However, at this moment, it is only the converter the one which is injecting current and thus, it is the only one which is producing a voltage in the grid. This fact causes a conflict in the control algorithm which eventually results in the disconnection of the converter.

Analyzing what has triggered the converter disconnection it is evident that, at

$t = 7.3s$, the control algorithm enters into conflict since it needs a synchronization reference to operate but this is obtained measuring the grid voltage that is also produced by the DQCI algorithm. Eventually, this conflict gives as result a fast random increase or decrease of the grid frequency. For the case plotted in Figure 5.4, from the moment when the synchronous generators disconnect, frequency continues decreasing until approximately 7.7 sec. At this moment, the frequency goes lower than 45 Hz, a value which is set in the protection system as the limit for under-frequency (see section 3.4.2), disconnecting the converter from the system.

The waveforms shown in Figure 5.4 are very clear, smooth and free of noise because the load applied, linear and balanced. For the same reason, after the synchronous generator disconnects, the converter manages to stay connected up to 0.3 seconds, longer than what usually a DQCI would be capable of. Under the presence of much more challenging loads, events like the disconnection of the entire synchronous generation would have provoked a much faster degradation of the power quality and the resilience of the grid. Later, in this thesis (Chapter 6) unbalanced and non-linear loads are explored.

It is worth remarking that the event cannot be fixed if droop slopes are added to the control logic. If these would have been applied, against a drop in frequency, the converter would react injecting more active power executing primary regulation. However, from the moment the synchronous generator is disconnected from the system, the resulting power system turns into a grid exclusively sourced by converters. Therefore, the power synchronization mechanism which underpins the primary regulation is not valid anymore and an increase in P_{conv} would only provoke an increment of the converter output current, increasing with it the load voltage. The opposite effect is observable on the load voltage when the synchronous generator disconnects. From that moment, the voltage reduces slightly due to the absence of synchronous generator current.

The same scenario is replicated for the experiment using the VSM0H algorithm (Figure 5.5). Here, at approximately 4.67 sec, the generator disconnects again, letting the converter isolated. In this case, since the VSM0H technique operates the converter as a real voltage source when the machines disconnect, only an almost unnoticeable

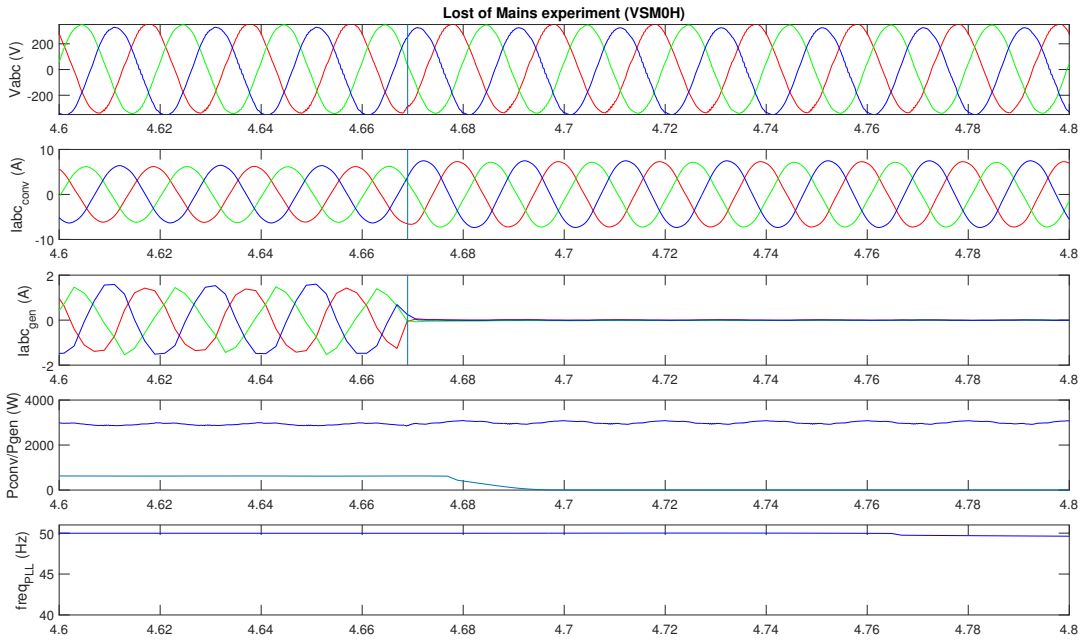

Figure 5.5: Lost of Mains experiments using the VSM0H control strategy

oscillation is observed on the load voltage (a thin line has been overlapped to detail the moment when the disconnection occurs).

From the moment the converter is the only generator and is able to supply the load with robustness, the grid is completely being fed by converters, achieving a true and feasible level of penetration of 100%. Additionally, the power quality has not been affected and the differences of voltage pre and post-fault are almost none, proving that a converter-controlled with VSM0H can build its own grid if it is necessary.

5.4.3 Experiment 3: Dynamic performance against a change of load

Taking a closer look at the moment when the synchronous machine disconnects in Figure 5.5 it is possible to observe that, in order to maintain the voltage between terminals, the converter reacts naturally increasing the output current, providing the power previously supplied by the synchronous generator without any transitory event. This step in current occurs naturally and thanks to that, the step does not suffer any oscillation typical from the synchronous generators. This behavior represents a significant advantage in terms of transitory events and motivates an additional experiment to confirm

and exploit this advantage.

The scenarios under study which will face a load step are two. In the first scenario a single VSM0H-controlled-converter, forming its own grid, is connected to the load bank (scenario 1); for the second case an additional synchronous generator will be connected in parallel and both will be connected to the load bank (scenario 2). This time the VSM0H will act as a reference node and the synchronous machine will connect to it using the power synchronization mechanism.

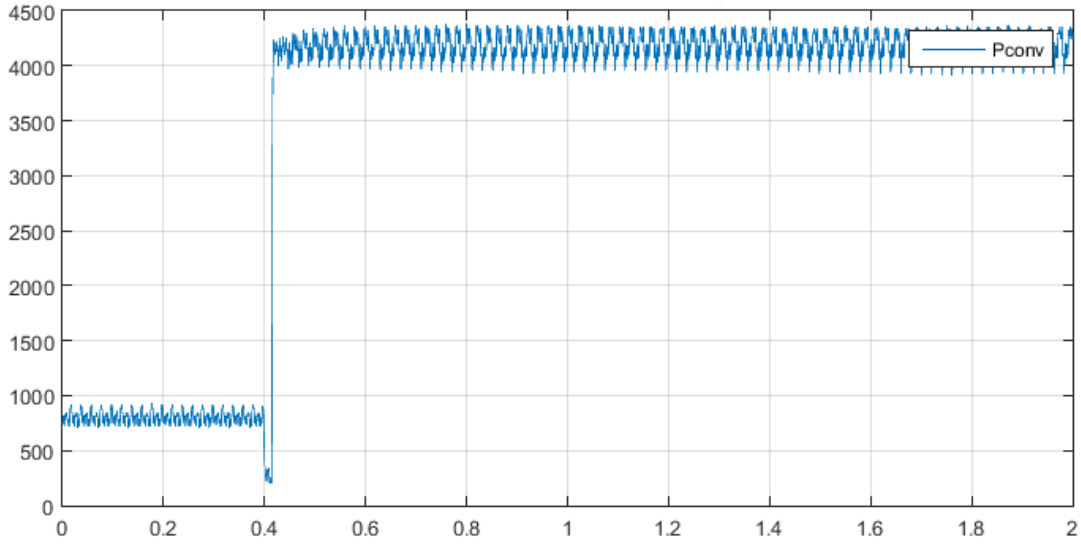

Figure 5.6: Load step using only VSM0H converters.

Figure 5.6 presents the scenario when only the VSM0H converter is connected to the load bank. In this figure, the active power injected by the inverter is represented facing a load step. Since the generator has no physical inertia to respect, its dynamics are mainly set by the control strategy embedded in the converter. As it has been mentioned in the introduction, the particularity of the VSM0H algorithm is the lack of an inertia that other VSM strategies have (this is the reason why it is called VSM Zero Inertia). Thus, with no inertia from the physical side and no inertia from the control strategy, the response in active power against a load step can be as ideal as the extracted from the results in Figure 5.6. Technically speaking, this square-shaped response is better than the one traditionally provided by a synchronous generator (see Figure 2.2 for an example of the latter) because it does not introduce power oscillations into the system.

However, in reality, VSM0H do have some "inertia". Paying attention to its control algorithm, the boxcar filters embedded in its control introduce a delay of between one to half grid cycle (depending on the settings of the filter) since they need this time to compute the filtering. This will be better observed in the second scenario.

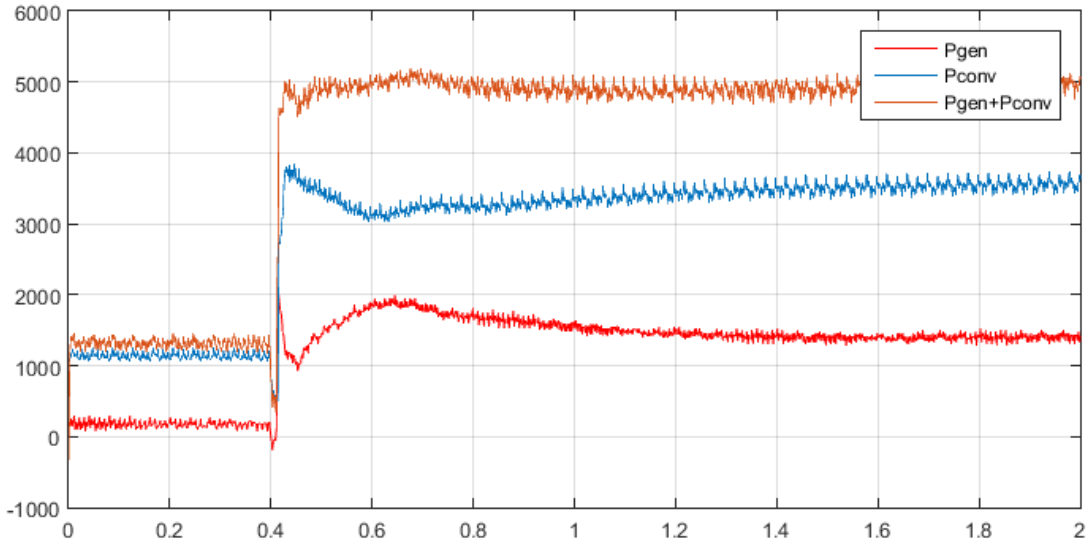

Figure 5.7: Load step using a VSM0H converter and a synchronous generator.

Figure 5.7 shows the active power signals of the VSM0H-controlled converter, the synchronous generator, and the sum of both for the second scenario for later illustration's sake. As it can be observed, before the load-step is applied, the converter and the synchronous machine are supplying power to a load of approximately 1kW. At 0.4 sec, a load step is executed in the system. Evaluating the response of both scenarios against the load step, it is obvious that the responses are quite different with respect to the first scenario where only the VSM0H converter was the only generator.

When the load step is executed, this load change automatically introduces a sudden drop of the voltage at the point where the measurements are taken (this is common for both scenarios). This voltage drop is caused by the parasitic elements inside the converter filter demanding a slightly higher value of reactive power when the load is increased. Because during this initial time the boxcar filters are still not aware of the load step, the net power injected suffers a small decrease.

Using droop control in the synchronous machine, it is possible to set which is the

contribution of the synchronous machine against the load step. For this case and in order to improve the explanation, this droop has been set high (46% for the synchronous machine and 3% for the converter) to maximize the machine response against the load step (it deliberately goes from a contribution of almost zero before the load step to nominal power after the event).

However, many events occur during the first 200 ms which are not shown in Figure 5.7. Therefore, a zoomed view of the same load step is represented in Figure 5.8. The dynamics present during the load step have also been divided in this figure in three stages for a better understanding.

Stage 1 only lasts for roughly 10 μs (this is just an estimation). Immediately after the load increase, both generators react automatically as the voltage sources that they are providing power to the load. The actual value of active power injected depends solely on the equivalent inductance of both generators. In the case of the converter, this value will mainly depend on the main filter inductor (Lf) whereas in the synchronous set this value will correspond with the direct axis transient reactance (Xd'). The arrows present in Figure 5.8 close to the mark of stage 1 represent the actual values of both generators during this initial stage.

Throughout the stage 2, two events are happening at the same time. From the

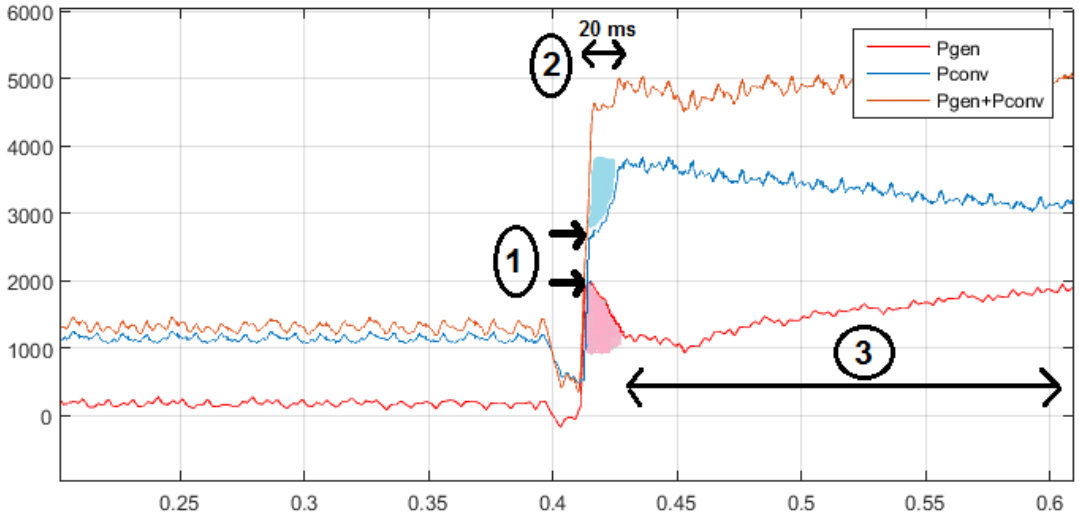

Figure 5.8: Zoomed view of the load step with the converter and the generator.

converter side, the boxcar filter contained in its algorithm is beginning to process the new value of active power and the new grid angle. This takes approximately 20 ms, exactly the time needed to process one grid cycle. Additionally, the exponential shape of this part of the signal is a clear evidence of this too. During this time, the synchronous generator is regulating the grid, compensating for the lack of power provided by the VSM0H converter. This energy comes from the physical inertia contained in the rotating machine. Furthermore, it seems that the synchronous generator could contribute with even more energy to the system but, since, as it was mentioned before, at this moment it is regulating the system, its contribution is limited. This can be evaluated by paying special attention to the signal and observing that it corresponds to second-order response truncated. The aforementioned events can also be confirmed realizing that the two shaded areas are approximately equal.

After 20 ms have passed, the boxcar filters have produced an updated set of their internal signals. At this moment stage 3 begins, VSM0H is fully engaged and the converter takes its master role into the system as a voltage regulator (or an oscillating node in other terms) making use of its fast internal droops calculation. From this moment it compensates any power oscillation and will maintain a stable value of active power observed by the load. The synchronous generator, on the other side, will begin to attempt counteracting the load step using its prime mover which has a relatively slow response compared to the converter. The dynamics of the governor and how VSM0H compensates can be better observed in Figure 5.7.

From stage 3 the converter is capable to compensate any power divergences in the grid to maintain a stable value of $P_{gen} + P_{conv}$. The resulting signal corresponds clearly to something very similar to the square-shaped step from the first experiment. These signals confirm several pieces of evidence:

- *VSM0H can correct power deviations.* Due to its almost lack of inertia compared to the dynamics of the prime mover, the converter is now free to inject power at any moment without having to respect certain inertias or lag caused by the control algorithm used or the specific VSM strategy used. This fact permits the converter to act as a compensator for the remaining elements of the system,

correcting its deviations.

- Although this evidence can be contained in the previous one it deserves a separated mention, *VSM0H can provide synchronizing torque*. As it has been observed and demonstrated in Figure 5.6-5.8, VSM0H provides the energy necessary to compensate power oscillations. Consequently, it inherently provides synchronizing torque to the remaining synchronous machines in the system contributing to the entire grid stability. Furthermore, since this torque is delivered instantaneously, worse events in the grid are avoided contributing further to the system stability, its robustness, and its resilience.

- *These features are unique for the VSM0H control strategy* since this algorithm is the only one which does not contain any inertia or at least one so short that can be negligible. Thanks to its lack of inertia, the converter capabilities can be truly exploited, increasing the generators speed and responsiveness as it is demanded.

5.5 Discussion

From the results obtained in the Level of Penetration (LoP) experiment, it can be observed that an almost 100 % converter-based production can be achieved with the standard DQCI algorithm as well as with VSM0H in a very idealized environment. Nonetheless, these results are caused by the lack of impedances between generators and loads. Since the elements of the experiment are connected between lines with low electrical impedances, the corrections in voltage which the synchronous generator has to realize in order to keep the stability are very seldom. This is something which is very difficult to demonstrate in the laboratory since there is no equipment necessary to corroborate it. However, the experiments have been translated to the simulation scope done in [3], obtaining similar results and confirming that the resulting level of penetration for any scenario has strong dependences with the inductances situated between generators and loads. Special emphasis must be made to the synchronous generator impedance, or more specifically the direct axis transient reactance (Xd'), since it will set the machine capability to impose its voltage to the neighboring elements

of the system providing more grid stiffness for lower values of Xd'. Since Xd' is lower as higher is the rating of the synchronous machines both sentences may be considered as equivalent.

However, from the Lost of Mains (LoM) experiment, it has been observed that some synchronous generation has to be always connected imposing a reference of frequency and voltage for the DQCI converters connected to the grid. From the LoP experiment it also can be extracted that the stability and the power quality of the grid remain unaffected by the lack of active power generated by the synchronous machine. Therefore, there is no connection between the active power generated by synchronous machines and the level of penetration limits nor there is any limit when the power quality at the load is compromised. It is the nominal rating of the machines connected to the grid which provides and contributes to this limit, since this value will indicate how much capability the grid has to compensate diversions of voltage and/or frequency out of the nominal values. Thus, a correct definition of the level of penetration must take into account, not the active power generated by synchronous generators (P_{gen}), but the nominal rating of the machines connected to the grid (S_{gen}) whether they are actually injecting power or not. Therefore, for the case analyzed on this project, the definition LoP_{conv} (see section 1.4) is the most consistent since it takes into account the cited dependence and, additionally, the fact that a converter operating as GFN, it stills contributes positively to the LoP value.

Throughout these experiments, it has been mentioned, observed and remarked that one of the main contributions which synchronous machines supply to the grid stability is derived from its master role in the system. In other terms, since they impose a voltage and frequency, they can act as active regulators of the system; something that does not happen in DQCI converters. Therefore, if the conventional control algorithm installed in the inverters is replaced by one which makes the converter to behave as a true voltage source of power like conventional generation do, more converter-based generation is possible without compromising the network stability nor the power quality.

This change of behavior can be obtained using any of the VSM control strategies. However, as it has been tested in the last experiment, VSM0H converters not only can

replace synchronous generators in terms of stability contribution. They can provide, if they have the energy necessary in the DC bus, even better performance than these machines, removing power oscillations, providing synchronizing torque and smoothing any transient in the grid.

This ideal response and power regulation are in this case exclusive from the VSM0H algorithm. Other VSM control strategies use a synchronous generator model and therefore, they are attached to the dynamics of these machines. Thereby risking power oscillations in the grid via virtual rotor oscillations which have to be mitigated by the remaining regulators of the system or power system stabilization devices. Accounting that within DQCI converter-dominated grids this synchronizing torque is almost nonexistent, this advantage can take a pivotal role in the system since this algorithm not only does not demand this synchronizing torque but also contributes positively to it.

Obviously, in this chapter, it has been evident that no conventional ancillary function can provide the services which this kind of grid need and thus, converter-dominated grids where the Level of Penetration is quite high have to be assessed in a completely different way. As soon as the lack of active regulators in the system can compromise the system stability, conventional grid ancillary functions cannot fight the excursions suffered in the grid. However, it is very difficult to estimate what is a low level of penetration and what is high, and thus, when the ancillary functions are an effective solution and when they are not. Since the study made here is intended to be extended for high interleaved networks with an almost number infinite of variables this task is even more complex. However, according to the experiences obtained in the laboratory during the experiments, it can be considered that from a LoP_{conv} of 50%, solutions enclosed within converter-dominated grids should begin to be introduced in order to keep the grid stable. This number must be taken with precaution, it must not be taken as a technical limit (this is the 81% that was observed in section 5.4.1 in the most idealized experimental conditions). It must be taken as the starting point from which VSM-type converters have to begin to be installed into the system to guarantee the grid stiffness and therefore, the stability of the entire grid. As a reference, Eirgrid the TSO

in Ireland, has already put its network to 50-60 % with DQCI converters providing ancillary functions; therefore, depending on the size and characteristics of the electric grid under study this limit is set between 50 and 81%.

Finally, it is worth remarking that often frequent stability is taken as the main variable to assess the robustness of the grid. Usually, system operators tend to think that against the imminent loss of inertia, the network can suffer huge and fast diversions so violent that can end in a complete black-out. As result, many efforts have been done to quantify and measure the instantaneous ROCOF or even mitigate its drop using the synthetic or virtual inertia. This search for a higher inertia is correct in a system primarily based in synchronous machines where, without inertia, the generators can suffer from rotor angle stability. However, as it was already mentioned in section 1.1, as the proportion of converter-based generation increases, the grid stability is less dependent of the rotor angle stability. Furthermore, the artificial methods for the creation of virtual or synthetic inertias have been demonstrated useless (see Chapter 3). In the last experiment, it has been explained that what traditionally has been called inertia should more precisely defined as synchronizing torque or at least more focus should be taken into this parameter as a very relevant contributor to the stability within converter-dominated grids.

Bibliography

[1] Orkney Renewable Energy Forum. Internet: http://www.oref.co.uk/ [Consulted in April 2018].

[2] T. Ackermann et all. *Wind Power in Power Systems*. UK: Ed. Wiley. 2005 pg. 144

[3] M. Yu et al., "Instantaneous penetration level limits of non-synchronous devices in the British power system." *IET Renewable Power Generation*, vol. 11, no. 8, pp. 1211-1217, 6 28 2017.

[4] L. Reguera, A.J. Roscoe, "Experimental Stability Assessment of Converter-Dominated Electrical Grids," presented at the 16th International Wind Integration workshop, Berlin, 2017.

[5] Ierna, R., Zhu, J., Urdal, H., Roscoe, A., Yu, M., Dysko, A., and Booth, C. "Effects of VSM Convertor Control on Penetration Limits of Non-Synchronous Generation in the GB Power System" presented at the 15th Wind Integration Workshop, Vienna, Austria, 2016.

[6] Yu, M., Dysko, A., Roscoe, A.J., Booth, C., Ierna, R., Urdal, H., and Zhu, J.: "Effects of Swing Equation-Based Inertial Response (SEBIR) Control on Penetration Limits of Non-Synchronous Generation in the GB Power System." presented at the IET Renewable Power Generation (RPG), Beijing, China, 2015.

[7] National Grid codes: Internet: http://www2.nationalgrid.com/uk/industryinformation/electricity-codes/grid-code/the-grid-code/ [Consulted in May 2018].

Bibliography

Bibliography

Chapter 6

Guaranteeing the stability of converter-dominated power systems facing unbalanced and non-linear loads

6.1 Introduction

Chapter 4 and 5 have focused on how to achieve absolute grid stability explaining several solutions depending on the level of penetration of the specific grid. These investigations and all known public domain studies to date assumed linear and balanced loads on the demand side. However, this is not true in a high, complex and interleaved electrical grid with multitude types of demand such as; power electronic devices, electrical vehicles chargers, constant power loads, compact fluorescent or LED lighting to cite some of them. Taking into account the progression of converter-based systems into the grid, if a replacement of the technology generation is going to be done substituting the conventional DQCI algorithm by the GFN solution, it is worth to study how these new algorithms will react against real loads that do not demand such ideal currents. Since, as it has been explained along this thesis, converter-dominated grids present a shortage of voltage regulation, any load which does not demand a perfect balanced

and linear current can potentially have a very distorting potential into the grid voltage signal. Therefore, in this chapter, using the converter already built, several converter-dominated scenarios will be recreated to assess the response of both strategies under the presence of unbalanced and non-linear loads, evaluating its impact into the grid stability and the power quality to, ultimately, propose solutions to mitigate them.

6.2 Unbalanced Loads

Many events can trigger an unbalanced phase in the electric grid at the transmission or distribution level. From switching on a simple kettle on the consumer side to large single-phase railway supplies, both elements, and for different reasons, can lead to an uneven voltage magnitude between phases.

This, in principle, is not a major problem in a conventional electrical grid where generation is dominated by synchronous generators. These machines, in the presence of unbalanced loads or voltages, reacts inherently as sources of positive sequence voltage. Consequently, they will naturally supply the necessary unbalanced current to, if not remove, at least mitigate the unbalance on voltage. However, this uneven generation will be done in the exchange of some stress on the generator bearings due to the ripples in the active power production (at twice the grid frequency) and torque. This stress will be present in the form of vibrations which magnitude will increase with the unbalance current injected into the grid.

Within conventional grids, the natural contribution of the synchronous machines to the voltage stiffness tends to be enough to maintain its homogeneity among electrical phases. However, its voltage capability is limited and there are cases, even nowadays, where still there is voltage unbalance in the grid, particularly at the ends of long rural Medium Voltage (MV) lines. These events are also fairly common at the distribution level and when a voltage unbalance is detected, DNO's can attempt to redistribute the loads between phases in order to maintain the voltage balance [1]. In rare cases, and only in low and medium level voltages, singular voltage regulators based on small tap changers are installed [2]. These devices adjust the specific phase voltage magnitude varying the tap changer of a singular phase making a slight increase/decrease of the

voltage magnitude to stay in range. Naturally, this improves the unbalance voltage from the customers perspective but does not address the aforementioned second order ripple problem.

However, nowadays these unbalanced loads have been even more present with the possibility of installing rooftop PV generation or small wind turbines on the household property. Due to the stochastic and intermittent nature of the emerging PV or wind generators, very fast power shifts can occur, leading to swings in the voltage magnitude of a singular phase and, thus, producing unbalanced grid voltages. Naturally, these events can be so transitory that single phase voltage regulators cannot be capable to even detect them.

Translating these events into a converter-dominated grid where there is a shortage of voltage regulation, the potential impact of an unbalance production and its consequences require careful consideration. Since the vast majority of converters are DQCI controlled, these systems will behave as sources of positive sequence currents, not voltage, regardless of the grid event (as it was already described in Chapter 2). Thus, against an unbalanced load, they do not provide, by default, negative sequence current injection. Since voltage magnitudes have to stay always balanced, this task is displaced to the remaining synchronous generators in the system. Within an almost 100% DQCI-controlled-converter-based scenario, an unbalanced energy production between phases simply may not be possible; compromising with it the grid voltage balance.

In order to have a reference about the maximum tolerable limit which has to be respected, the voltage unbalanced has been limited to 3%. This value is common among several TSOs in Europe [3], [4], [5] as an upper limit. However, normally this value is limited to 2% as mean 10 minutes RMS value according to EN-50160 standard, and the IEC 61000-2-12 [6] [7] for LV and MV. It is set at 3% as the highest punctual value.

6.2.1 Theoretical study

Unbalanced loads are present in the system when the current demanded by the three-phase system is not even. Under the presence of such load, if any of the phases are not correctly sourced injecting the requested uneven current for each phase, the voltage

magnitude between phases will be unbalanced. Translating this scenario to sequence diagrams, this reduction or increase in any singular phase current will be observed as a finite voltage on the negative sequence, in addition to the positive sequence voltage.

To start the analysis, the unbalanced load will be translated to the sequence frame. Assume R_B as the equivalent resistance that represents the balanced load across the three phases and R_I as the resistance that is coupled in parallel to only one of the phases (see Figure 6.1a) therefore, creating the unbalanced load scenario. This scenario can be represented in its matrix form as (6.1).

$$\left[V_{abc}\right] = \left[R\right]\left[I_{abc}\right] \tag{6.1}$$

$$where \quad \left[R\right] = \begin{bmatrix} 3R_B \parallel R_I & 0 & 0 \\ 0 & 3R_B & 0 \\ 0 & 0 & 3R_B \end{bmatrix} \tag{6.2}$$

where V_{abc} is the voltage observed by the loads and the converter in the Point of Common Coupling (PCC). Then, it is possible to translate these equations to the sequence frame using the symmetrical components transformation matrix:

$$A = \begin{bmatrix} 1 & 1 & 1 \\ 1 & a & a^2 \\ 1 & a^2 & a \end{bmatrix} and \quad A^{-1} = \frac{1}{3}\begin{bmatrix} 1 & 1 & 1 \\ 1 & a^2 & a \\ 1 & a & a^2 \end{bmatrix}$$

Then equation (6.1) can be translated into the sequence diagram [8]:

$$A^{-1} \cdot \left[V_{abc}\right] = A^{-1} \cdot \left[R\right] \cdot A \cdot A^{-1}\left[I_{abc}\right] \tag{6.3}$$

$$\left[V_{o+-}\right] = \left[R_{o+-}\right]\left[I_{o+-}\right] \tag{6.4}$$

$$where \quad \left[R_{o+-}\right] = A^{-1} \cdot \left[R\right] \cdot A = \frac{1}{3}\begin{bmatrix} R_1 & R_0 & R_0 \\ R_0 & R_1 & R_0 \\ R_0 & R_0 & R_1 \end{bmatrix}$$

$$and \quad R_1 = \frac{R_I R_B}{R_I + 3R_B} + 2R_B, \quad R_0 = \frac{-3R_B}{R_I + 3R_B}$$

Equation (6.4) can be simplified since zero sequence load currents and voltages occur in Wye connected systems, however, for the case of this project a delta-Wye winding transformer is used, therefore zero sequence is inherently removed. Expanding the remaining two equations the result is presented as follows:

$$\begin{aligned} V_+ &= R_1 I_+ + R_0 I_- \\ V_- &= R_0 I_+ + R_1 I_- \end{aligned} \tag{6.5}$$

Equation (6.5) shows how an unbalanced load can be seen, translated to the components frame, as an equivalent circuit for each component where there are a resistor and a cross-coupled term. This term can be represented as a dependent voltage source. See Figure 6.1

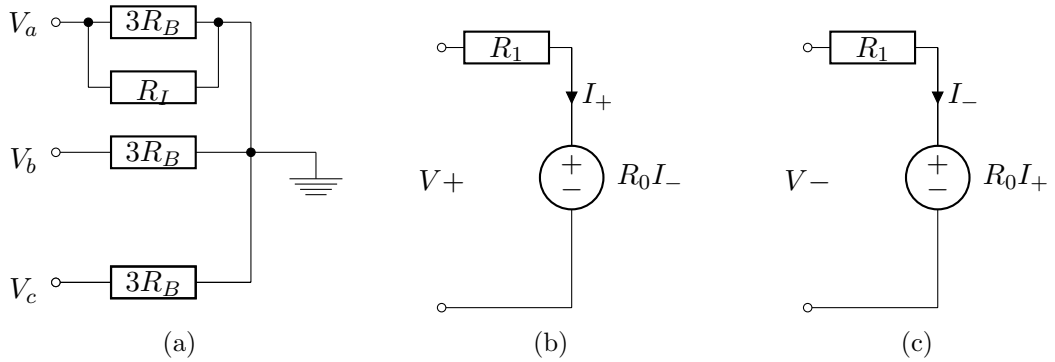

Figure 6.1: Representation of an unbalanced load in the sequence components frame.

Having the loads already translated to the sequence frame, it is necessary to know how to represent the generators which will be represented in the microgrid. For every scenario created in the following experiments, the same physical converter will be used.

However, different control strategies are used and thus, different behaviours will be observed from the grid's perspective. As it will be confirmed later, this takes on vital importance under the presence of unbalanced loads. DQCI converters, for instance, behave as a source of positive sequence current since they impose an active and reactive power reference following the voltage signal imposed by other generators present in the system under a current control loop [9]. On the contrary, VSMs algorithms behave as sources of positive sequence voltage, setting its own voltage reference regardless of the grid events.

Once the equations of the unbalanced loads in the sequence frame (6.5) and the theoretical behaviour of the converters working under the DQCI and VSM algorithm are understood, a circuit diagram of a converter connected using the DQCI or VSM control strategy can be obtained. This is represented in Figure 6.2 for the DQCI

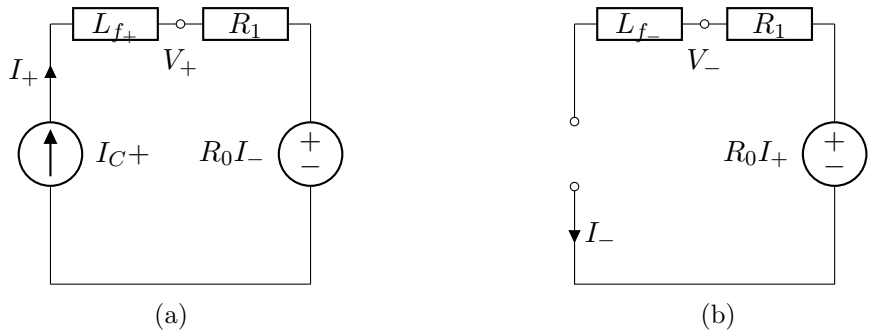

Figure 6.2: DQCI-controlled converter facing unbalanced loads in the symmetrical components frame.

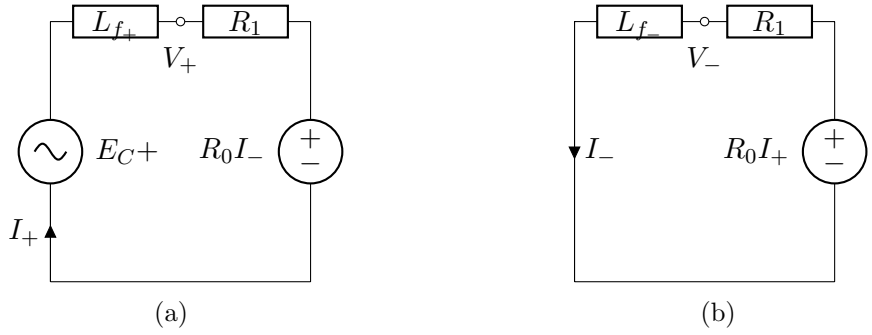

Figure 6.3: VSM-controlled converter facing unbalanced loads in the symmetrical components frame.

case and 6.3 for the VSM. Following the principle of superposition, since there is no action on the negative sequence component, current sources (DQCI converter) can be replaced by open circuits and voltage sources (VSM converter) by short-circuits. I_C+ is the positive current source of the DQCI converter, E_C+ is the positive sequence voltage source of the VSM inverter and L_{f_+} L_{f_-} are the positive and negative sequence converter impedance which, for the particular case of a converter are the same.

Balanced loads	**Unbalanced loads**				
	0 W	**600 W**	**1.2 kW**	**1.8 kW**	**2.4kW**
0 W	N/A N/A	N/A N/A	N/A N/A	N/A N/A	N/A N/A
2 kW	0 0	0 18.7	0 27.3	0 32.14	0 35.3
4 kW	0 0	0 11.5	0 18.8	0 23.7	0 27.3
6 kW	0 0	0 8.3	0 14.3	0 18.7	0 22.2
8 kW	0 0	0 6.5	0 11.5	0 15.2	0 18.7
	I_{unbal} V_{unbal} (%)	I_{unbal} V_{unbal} (%)	I_{unbal} V_{unbal} (%)	I_{unbal} V_{unbal} (%)	I_{unbal} V_{unbal} (%)

Table 6.1: Expected voltage and current unbalanced using the DQCI control strategy.

Additionally, knowing the resulting schematic, it is possible to calculate the expected amount of voltage and current unbalanced at the PCC depending on the algorithm used. To do so, the number of possible combinations of balanced and unbalanced loads is delimited to a finite number. For the DQCI-controlled inverter case, equations (6.5) can be used replacing $I_+ = I_{C_0}+$ and $I_- = 0$ where $I_{C_0}+$ corresponds to the nominal value of the current necessary to supply the balanced load at nominal voltage (1 pu). Having obtained V_+, V_- and I_+, I_-, a voltage and a current unbalance in percentage can be calculated as the ratio between the negative and the positive com-

ponent. Table 6.1 shows the predicted values for a finite number of scenarios. These configurations match the corresponding scenarios which will be experimentally assessed in section 6.2.3. 'N/A' are scenarios where the calculations get a division by zero. The values used for these calculations are: $V_{base_{ll}}$= 400 RMS, S_{base}=10 kVA, Lf=0.15 pu.

For the VSM case, the calculation to obtain the predicted values of V_+ and V_- is different. First, the currents I_{abc} must be calculated to compute a new resulting I_+ and I_- taking into account L_f in the circuit.

$$\left[E_{abc}\right] = \left[R'\right]\left[I_{abc}\right] \tag{6.6}$$

$$\left[R'\right] = \begin{bmatrix} j\omega L_f + (3R_B \parallel R_I) & 0 & 0 \\ 0 & j\omega L_f + 3R_B & 0 \\ 0 & 0 & j\omega L_f + 3R_B \end{bmatrix}$$

where E_{abc} is the voltage imposed by the converter bridge. Following a similar procedure

Balanced loads	**Unbalanced loads**				
	0 W	**600 W**	**1.2 kW**	**1.8 kW**	**2.4kW**
0 W	N/A N/A	N/A N/A	N/A N/A	N/A N/A	N/A N/A
2 kW	0 0	22.9 1.5	37.1 3.1	46.7 4.6	53.7 6.1
4 kW	0 0	12.9 1.5	22.6 3	30.1 4.47	36.1 5.8
6 kW	0 0	8.93 1.5	16.1 2.9	22.1 4.4	27 5.7
8 kW	0 0	6.83 1.55	12.5 3	17.4 4.3	21.6 5.6
	I_{unbal} V_{unbal} (%)	I_{unbal} V_{unbal} (%)	I_{unbal} V_{unbal} (%)	I_{unbal} V_{unbal} (%)	I_{unbal} V_{unbal} (%)

Table 6.2: Expected voltage and current unbalanced using the VSM control strategy.

as in equations (6.3-6.5), a new matrix $\left[R'_{o+-}\right]$ can be computed. Knowing a VSM controlled converter behaves as a positive sequence voltage source ($E_C+ = 1\text{pu}$, $E_C- = 0$), the currents I_+ and I_- can be obtained. Finally, the voltage observed by the VSM-controlled converter at V can be obtained since:

$$\left[V_{+-}\right] = \left[E_{+-}\right] - j\omega L_f \left[I_{+-}\right] \tag{6.7}$$

The expected results are presented in table 6.2. Here it can be observed how the short-circuit introduced by the VSM technique in the negative sequence offers a low path impedance which leads to a reduction of the voltage unbalance. However, there are still cases where the unbalance exceeds the limit of 3%.

Therefore it is straightforward to think which is the amount of unbalanced current necessary to remove completely the negative sequence voltage operating as an ideal voltage regulator. The set of equations (6.5) can be used again for this purpose since

Balanced loads	**Unbalanced loads**				
	0 W	**600 W**	**1.2 kW**	**1.8 kW**	**2.4kW**
0 W	N/A N/A	N/A N/A	N/A N/A	N/A N/A	N/A N/A
2 kW	0 0	23 0	37.5 0	47.4 0	54.6 0
4 kW	0 0	13.1 0	23.1 0	31 0	39.5 0
6 kW	0 0	9.1 0	16.7 0	23.1 0	28.6 0
8 kW	0 0	7 0	13 0	18.4 0	23.1 0
	I_{unbal} V_{unbal} (%)	I_{unbal} V_{unbal} (%)	I_{unbal} V_{unbal} (%)	I_{unbal} V_{unbal} (%)	I_{unbal} V_{unbal} (%)

Table 6.3: Expected voltage and current unbalanced using an ideal voltage regulator.

an ideal regulator shall force $V+ = 1\text{pu}$ and $V- = 0$. Replacing these variables $I+$ and $I-$ can be found to obtain a resulting expected voltage and current unbalance. These values are presented in table 6.3.

Note the small differences between the resulting values of unbalanced current for the VSM technique in table 6.2 and the ones for the ideal regulator presented in table 6.3. This provides an insightful connotation; a small shortage of the unbalanced current can lead to excessive levels of voltage unbalance. Another possible explanation is vector error, or in other terms, an error in the phase of the $I-$ applied, even if the exact amplitude may be correct.

6.2.2 Experimental setup with unbalanced loads

A schematic diagram of the system used for this project is shown in Figure 6.4. This scenario is very similar to the already described in the previous chapter for another experiment with the singularity that, in this case, it adds the capability of applying unbalanced loads of up to 2.5 kW to the microgrid. Full details of the internal converter values and the synchronous generator can be found in the appendix.

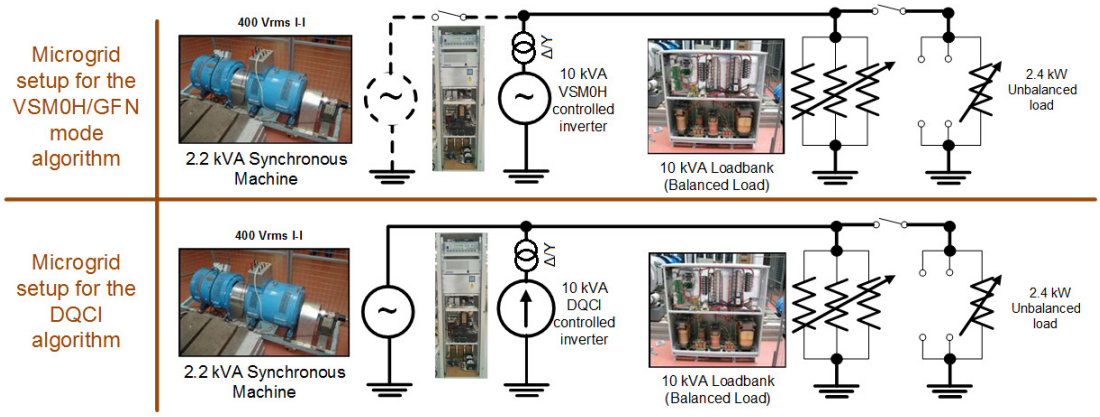

Figure 6.4: Experiment with unbalanced loads.

Depending on the control algorithm used for the converter, the synchronous set has a different role in this scenario. If the converter is operating in GFN/VSM mode, the machine is just required for an initial synchronization with the grid. Once it is synchronized, the synchronous set can be disconnected and the converter will remain islanded creating its own grid, and able to supply the load totally by itself. Since the

experiments that follow this project start with the converter being completely islanded, the synchronous set is represented in dashed lines in Figure 6.4. On the contrary, DQCI converters will compulsorily need, at least, a minor proportion of synchronous generators in the system to stay grid-connected [9]. Therefore, the performance evaluation will be assessed taking into account the synchronous generator is still connected.

6.2.3 Experimental results of a converter-dominated grid facing unbalanced loads

Another variable to take into account during the experiments is the proportion of unbalanced/balanced present into the system. The converter response and the capability to mitigate these faulty scenarios will not be the same if, for instance, the system is facing 0kW/1.8kW of balanced/unbalanced load than if the converter is supplying 6kW/1.8kW of balanced/unbalanced loads. If the vast majority of the energy involved in the experiment is balanced (6kW/1.8kW case), the voltage will suffer less distortion. Therefore, the task of regulating this voltage balance will be easier in that case than if the energy involved into the experiment is completely unbalanced (0kW/1.8kW case) where the grid voltage will suffer deep sags in magnitude. However, as it has been observed in tables 6.1 and 6.3 this effect takes more or less weight in the resulting voltage unbalance depending on the algorithm used. For the DQCI case, this proportion between the balanced and the unbalanced load is crucial, due to its equivalent open circuit on the negative sequence, the resultant unbalanced voltage relies predominantly on the load characteristics. For the VSM0H, the equivalent short-circuits offers a low impedance path which smooths the dependence between the resulting unbalanced voltage and the proportion of balanced/unbalanced loads. As result, for the same unbalanced load, the resulting expected voltage unbalance has similar numbers for different values of balanced loads.

DQCI algorithm

Table 6.4 contains the results of the unbalanced experiment under the DQCI control strategy for a variety of balanced and unbalanced loads. Cells noted with 'UNS' are

scenarios when the converter is marginally stable. 'OUT' are scenarios when the nominal power of the synchronous machine is lower than the actual unbalanced load, leading to the disconnection of; first the synchronous generator and, with it, the own converter. Finally, 'N/A' are conditions that can not be recreated with this strategy since DQCI converter cannot operate without loads.

As it was mentioned before in section 6.2.2, during these scenarios there are two generators: the synchronous machine and the converter. Since DQCI converters are theoretically incapable of providing negative sequence current, the most reliable strategy to follow in case of an unbalanced load is to start with the DQCI converter supplying almost a 100% of the linear load and, at that moment, apply the unbalanced load. Thereby, before the unbalanced is applied, the synchronous machine gets almost idle in terms of energy production and, thus, it will have the highest margin to regulate the voltage. However, because the synchronous generator is present in the experiment and it is the one which is providing in its majority the unbalanced current, the values

Balanced loads	**Unbalanced loads**				
	0 W	**600 W**	**1.2 kW**	**1.8 kW**	**2.4kW**
0 W	N/A N/A	N/A N/A	N/A N/A	N/A N/A	N/A N/A
2 kW	1 0.9	7 2.1	14 3.4	20 5	UNS
4 kW	0.9 0.8	6.5 2.3	13 3.7	UNS	OUT
6 kW	1 0.9	UNS	UNS	OUT	OUT
8 kW	0.9 0.9	UNS	OUT	OUT	OUT
	I_{unbal} V_{unbal} (%)	I_{unbal} V_{unbal} (%)	I_{unbal} V_{unbal} (%)	I_{unbal} V_{unbal} (%)	I_{unbal} V_{unbal} (%)

Table 6.4: Result for the unbalanced loads experiment using the DQCI control strategy.

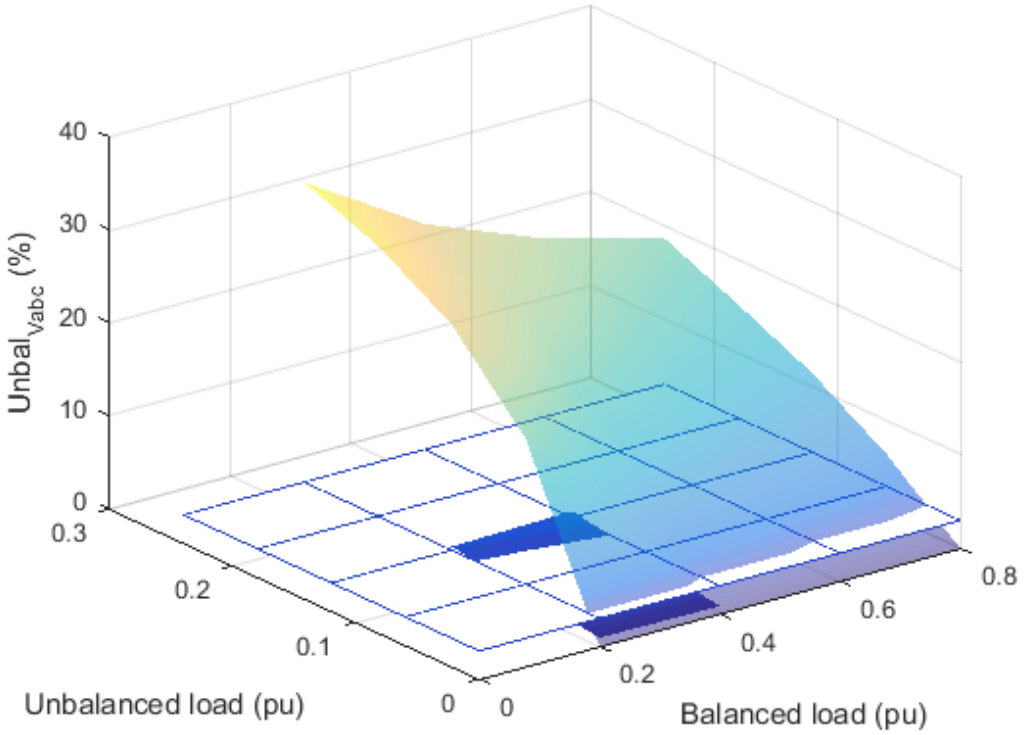

Figure 6.5: Comparison of the expected unbalanced voltage (faded) with the results obtained (solid) for the DQCI control strategy.

are shown in table 6.4 do not match with the ones of table 6.1. This comparison can be better observed in Figure 6.5 where the expected and resulting unbalanced voltages are presented with the aforementioned limit of 3%.

The difference of the unbalanced current provided by the ideal generator in table 6.3 and the ones registered in the laboratory is approximately the amount of unbalanced current injected by the synchronous machine. In any case what it is clear is that table 6.4 shows a system with a poor resilience and, for many setups, the microgrid is inviable. Note for instance the unstable case where 6kW of linear load and only 9% of the load is unbalanced (600W). This scenario led to an unstable situation where the synchronous machine was ineffective at regulating the voltage.

A reference scenario where 2 kW of balanced load with 1.8 kW of unbalanced load will be used in this section in order to provide an insightful comparison of the algorithms

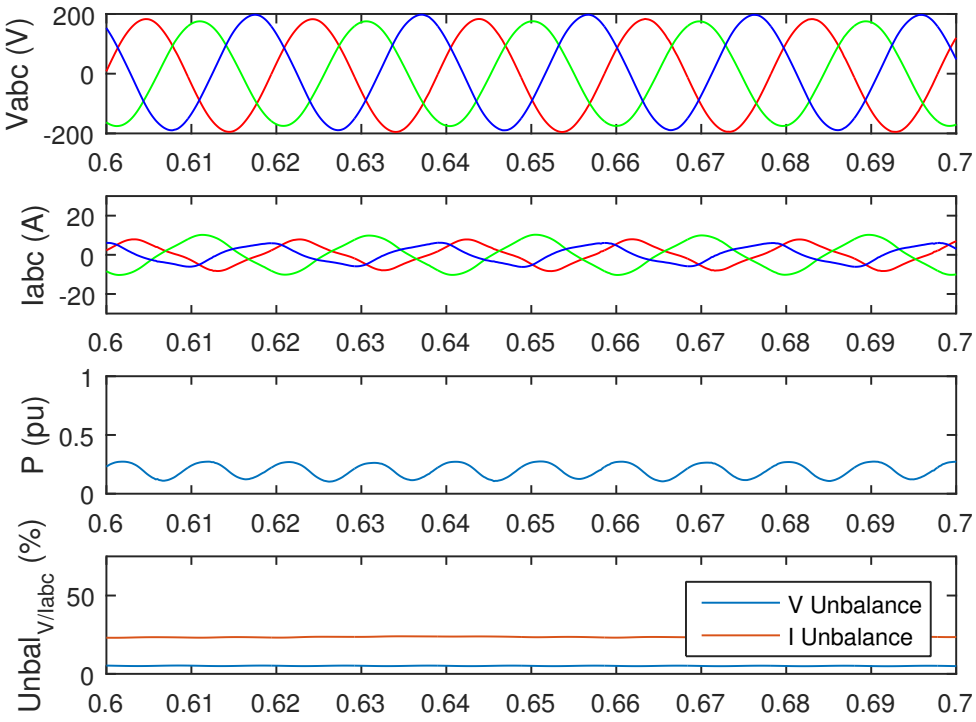

Figure 6.6: Results for 2kW/1.8kW of balanced/unbalanced load under the DQCI control strategy.

presented in this paper. Figure 6.6 shows a higher detailed picture of this scenario using the DQCI control strategy.

In this figure are presented, from top to bottom, the voltages observed by the converter (expressed here as V_{abc} but equivalent to V_c in section 6.2.1), currents injected by the converter (I_{abc}), active power (P) and the voltage/current unbalance. As it can be observed, although the voltage seems to be consistent, the current is only a 20% unbalanced; a value which is far from the expected 47.4%. Actually, taking into account the distortion present in the current injected (this may be caused by an interaction with the -1 order harmonic [16]), this value may be misinterpreted by the unbalance calculation process. In any case, the shortage of unbalanced current leads to a voltage unbalance of 5%, exceeding the tolerable limit of 3%.

Additionally, it is worth to mention the 2nd order harmonic ripple on the active

power signal. In this case, since there is a significant amount of voltage unbalance present in the system, part of this oscillation is caused by the voltage itself and the remaining is due to the unbalanced current. This ripple has to be considered for a real system connected to the grid which has a limited amount of collected energy in the DC bus. Therefore, DC capacitors and voltage will have to be controlled fast enough that these swells do not affect the converter normal operation [16].

VSM0H algorithm

The main feature of the VSM0H algorithm is the imposition of a voltage value regardless of the grid conditions. Opposite to other VSM algorithms, the VSM0H control strategy uses exclusively the synchronization mechanism of the traditional synchronous machines [19, 20]. Additionally, the boxcar filtering removes all unbalance and makes the voltage source completely stable during an unbalanced load situation, whereas a

Balanced loads	**Unbalanced loads**				
	0 W	**600 W**	**1.2 kW**	**1.8 kW**	**2.4kW**
0 W	6.7 1.1	46.7 2	65.5 4	72.2 5.6	77.5 7.3
2 kW	3.4 0.5	21.7 1.5	36.9 3.2	46.9 5	53.7 6.6 b
4 kW	1 0.4	13 1.2	24.1 2.6	32.4 4	38.6 5
6 kW	1.8 0.4	8.4 1.2	16 2.6	22.5 4	27.7 5
8 kW	2 0.45	6.85 1	12.9 2.2	18.2 3.4	OUT
	I_{unbal} V_{unbal} (%)	I_{unbal} V_{unbal} (%)	I_{unbal} V_{unbal} (%)	I_{unbal} V_{unbal} (%)	I_{unbal} V_{unbal} (%)

Table 6.5: Result for the unbalanced loads experiment using the VSM0H control strategy.

synchronous generator rotor will actually be perturbed by a small amount due to the second-order transfer function response of a physical rotor. Table 6.5 shows the results of the converter using the VSM/GFN algorithm against unbalanced loads.

The results obtained in this table show a microgrid much more stable than the previous one. This leads to more setups where the converter not only remains connected but also is able to regulate, to some extent, a lot of the unbalances present in the system. The representative scenario where 2kW/1.8kW of balanced/unbalanced loads were applied is presented in Figure 6.7. Although this has been already commented in Chapter 3, it is worth to mention again that the converter contains a Delta-Wye transformer and this is the reason why, although the unbalanced load is applied to a single phase, the observed currents contain two of the phases with more amplitude instead of only one.

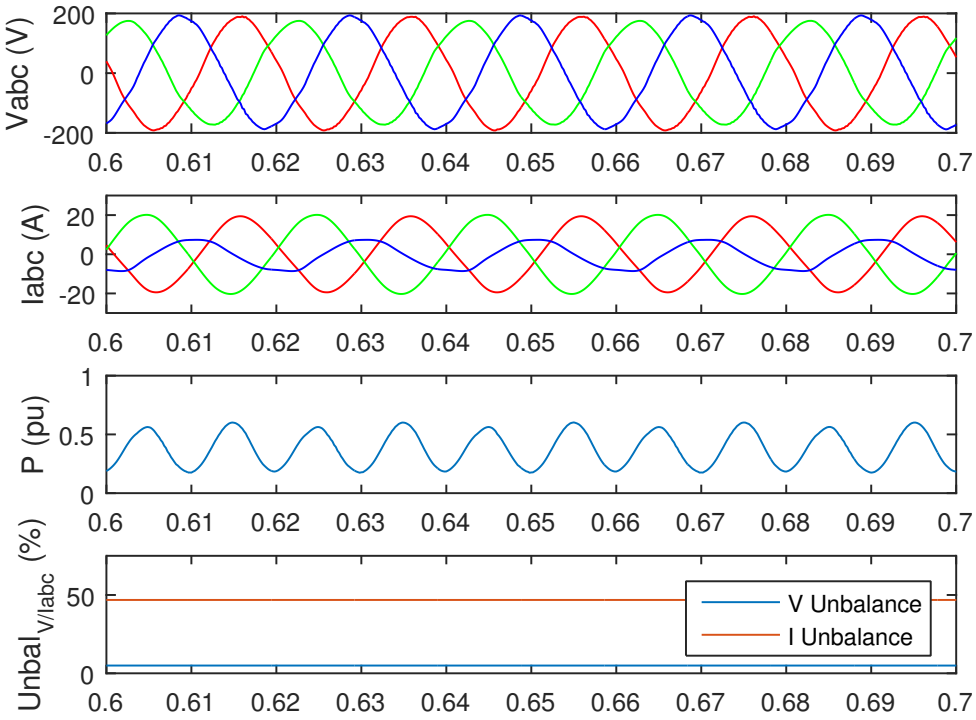

Figure 6.7: Results for 2kW/1.8kW of balanced/unbalanced load under the VSM0H control strategy.

Translating these numbers to percentage results in a 47.3% of unbalanced load. Since the resistances are linear loads, the current injected by the converter for a perfect regulation has to be equally unbalanced (this number also matches with the expected results for an ideal regulator in table 6.3) and, as it can be observed in fig. 6.7 and table 6.5, the measured unbalanced is 46.9%. This value is also very close to the predicted 46.7% from table 6.2. This comparison can be extended to every scenario finding in all of them very similar values with respect to the predicted previously not only on the currents but also in the resulting voltage unbalance. Again, this can be better observed presenting a surface plot of the expected and resulting values of unbalanced voltage from Table 6.2 and 6.5 ()Figure 6.8).

In Figure 6.8 there are small differences between the expected unbalanced voltages and currents which can be caused by small measurement errors. However, the trend and the limit points where the resulting unbalanced voltage reaches the limit of 3% are very similar. To confirm the validation between the prediction and the results 6.9 is presented too. This figure represents the expected and resultant values of unbalanced

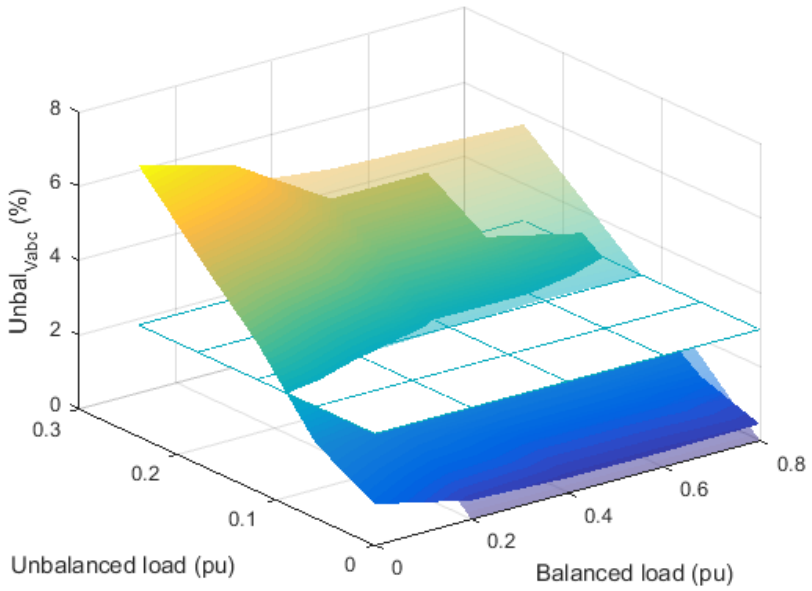

Figure 6.8: Comparison of the expected unbalanced voltage (faded) with the results obtained (solid) for the VSM control strategy.

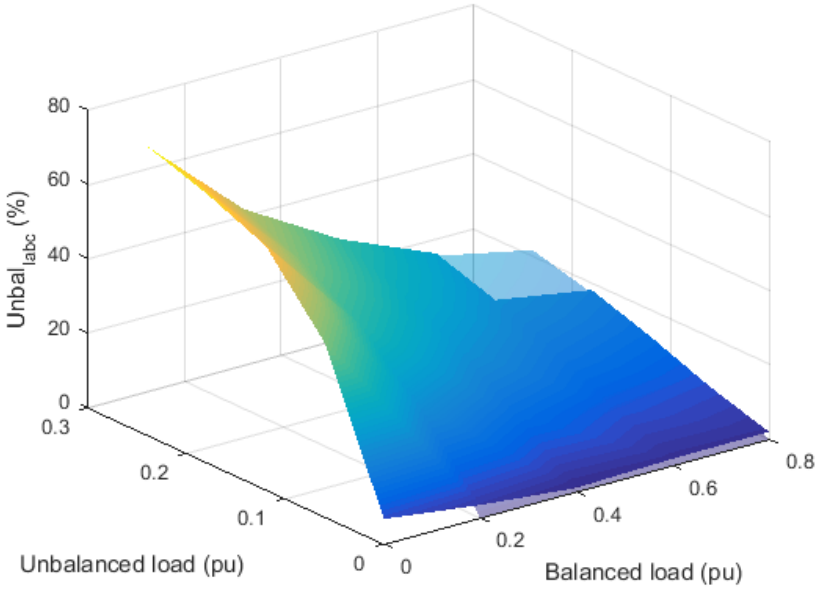

Figure 6.9: Comparison of the expected unbalanced current (faded) with the results obtained (solid) for the VSM control strategy.

current. Both plots are practically identical confirming that a VSM controlled converter behaves as an equivalent positive sequence voltage source of power.

However, there are still cases where the converter is unable to keep the unbalance present in the system lower than 2 or 3%. Actually, every scenario where the unbalanced load is equal to 1.8 kW or higher has resulted in values which exceeded the voltage unbalance limit imposed by the majority of TSOs of 3%. A discussion about this contradiction can be found in section 6.4.1. In any case, table 6.5 shows a system that is capable to regulate the voltage but can not, by default, mitigate completely the unbalanced scenario. If an enhanced voltage regulation is necessary, it is possible to explore further the VSM0H capabilities designing a specific control to regulate unbalanced voltages. The details about this technique and its results are explained in the following section.

VSM0H+ algorithm

The control design for this improvement over the actual VSM0H algorithm starts resuming the work done in Chapter 3, section 3.5.4. In this section the final commanded voltage magnitude and angle are transformed into IGBT firing signals, however, some modifications had to be made to make these commands practical in a real converter. Now, an additional improvement presented thereupon makes a further modification over the VSM0H algorithm; now to mitigate the unbalanced scenarios obtained improving the voltage regulation capabilities of the original VSM0H algorithm (VSM0H+). Figure 6.10 shows these aforementioned changes. In red dashed lines, it is framed the specific alterations made over the block *Driving the voltage reference* (explained with further detail in [10] and section 3.5.4).

Theoretically, as it was presented in section 6.2.1, an ideal generator E would be able to impose a negative sequence voltage or current to remove the finite voltage at

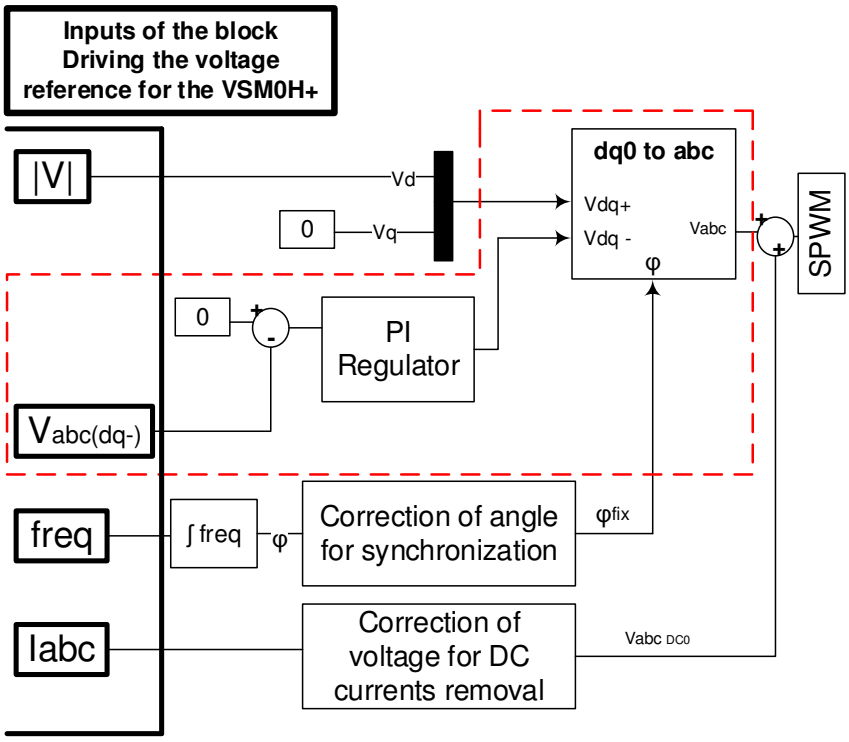

Figure 6.10: Block diagram of the modified VSM0H+ control strategy.

Balanced loads	**Unbalanced loads**				
	0 W	**600 W**	**1.2 kW**	**1.8 kW**	**2.4kW**
0 W	24 0.2	35 0.2	61.3 0.2	72.3 0.3	83.5 0.2
2 kW	5.6 0.1	20.9 0.2	37.8 0.2	49.2 0.2	57.4 0.2
4 kW	1.6 0.1	13.3 0.2	25.3 0.2	35 0.2	42.3 0.2
6 kW	1.9 0.2	8.9 0.2	17.3 0.2	24.9 0.1	30.9 0.2
8 kW	2 0.2	7.15 0.1	14.2 0.2	OUT	OUT
	I_{unbal} V_{unbal} (%)	I_{unbal} V_{unbal} (%)	I_{unbal} V_{unbal} (%)	I_{unbal} V_{unbal} (%)	I_{unbal} V_{unbal} (%)

Table 6.6: Result for the unbalanced loads using the VSM0H+ control strategy.

V_{-} under the presence of unbalanced loads. Since the VSM0H control strategy behaves as a voltage source, it is possible to alter the control in such way that the converter is able to provide, if necessary, a negative sequence voltage, permitting the complete mitigation of unbalanced scenarios.

Obtaining the sequence diagrams of the voltage measured from the converter in the rotatory dq frame ($V_{abc(dq-)}$), it is possible to design a dedicated control loop which objective is to remove any negative sequence voltage at the PCC. The outcome of this control is a signal called $Edq-$ which corresponds to the necessary negative sequence voltage driven by the converter to mitigate the unbalance. Following, a customized *dq0 to abc* block combines the original voltage product of the standard VSM0H control algorithm, $Edq+$, with the negative sequence command $Edq-$ from the unbalance mitigation control. Combining $Edq+$ with $Edq-$ and translating the resultant signal from the dq0 rotatory frame to abc, the converter driving voltages ($Eabc$) are produced. Lastly, these signals are modulated to create the IGBT firing signals.

The results of the VSM0H+ algorithm for the unbalanced scenarios are presented in table 6.6. Here, the obtained values of unbalanced voltage for any scenario are equal or below 0.3%, even during heavily unbalanced conditions. This is caused because the VSM0H+ converter behaves very similar to the ideal voltage regulator. In fact, it is possible to compare in a surface plot the values of unbalanced current expected from Table 6.3 from the ideal regulator and the ones obtained from Table 6.6 for the VSM0H+ in Figure 6.11, finding that both are very similar.

Another interesting comparison can be done between the measured current unbalance for the VSM0H and the VSM0H+ control strategy. This can be done observing these values in Table 6.6 and Table 6.5. It is noticeable the small differences in value between them. However, these tiny variations lead to a very positive effect on the net voltage balance. For instance, for the aforementioned case of 2kW/1.8kW of balanced/unbalanced scenario(see Figure 6.12), if the VSM0H strategy is used, a 46.9% of unbalanced current is measured whilst the VSM0H+ increases this value up to 49.2% unbalanced. Accordingly, 2.3% difference has caused a voltage unbalance reduction from 5 to 0.5%. This provides evidence of the magnitude of the small alterations made by the dedicated negative voltage removal control to the final driving voltage and how

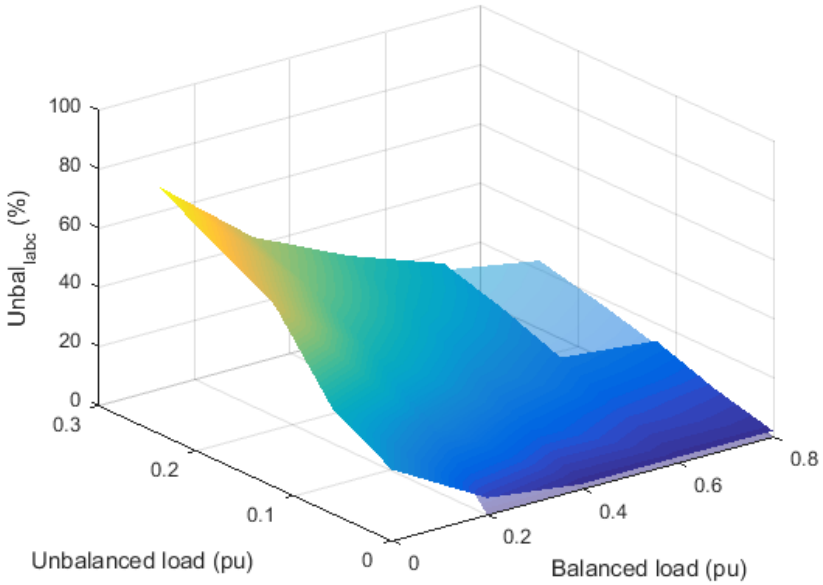

Figure 6.11: Comparison of the expected unbalanced current (faded) for the ideal regulator with the results obtained (solid) for the VSM0H+ control strategy.

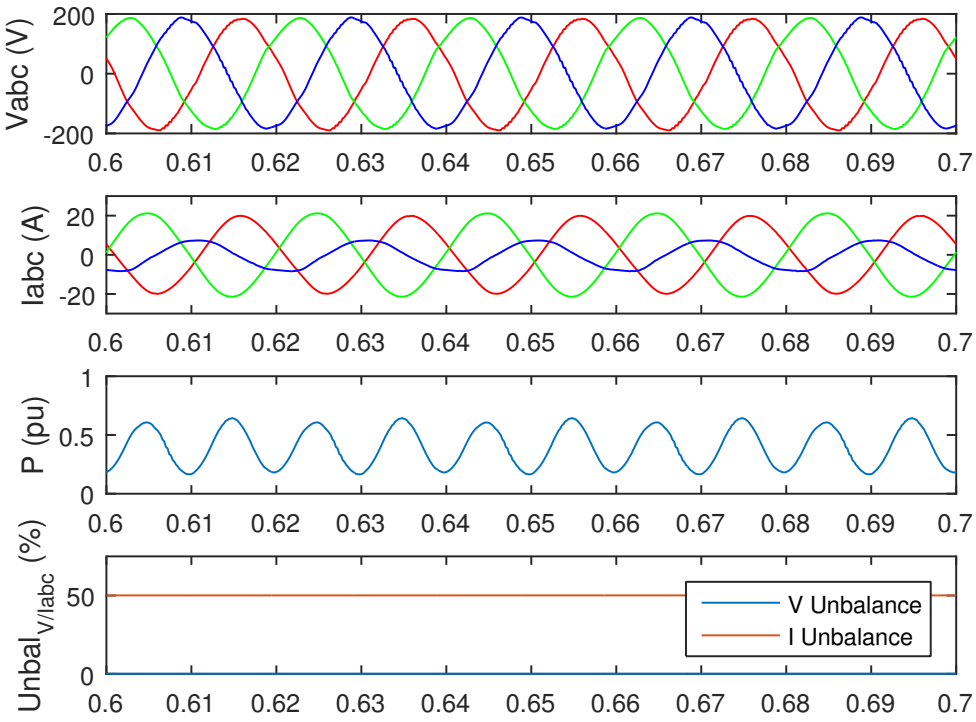

Figure 6.12: Results for 2kW/1.8kW of balanced/unbalanced load under the VSM0H+ control strategy.

this small modification has produced a notorious reduction on the voltage unbalance. Therefore, it does not seem to be necessary to install any further hardware to perform this enhanced control.

Comparing also the values obtained from unbalanced current and voltage with the ones of the ideal generator in table 6.3, VSM0H+ produces a slightly higher amount of unbalanced current than the expected. Since VSM0H+ algorithm objective is to remove completely the unbalanced voltage, the small asymmetries present between the grid filter elements across the three phases are also taken into account in the control loop and removed. As result, a slightly higher amount of current unbalance is produced.

6.3 Non-linear loads

The loads nature is also changing on the demand side. Typical linear resistive loads such as light bulbs are being replaced by solid-state devices which have an initial power stage that transforms the AC voltage to DC or simply operate producing non-linearities on the grid. As individual load, these elements do not represent any harm to the system, however, the aggregate power of these elements plus the latent progression of electric vehicle chargers into the system can lead to disturbances into the grid voltage. Either a passive rectifier from the low power digital load or an active converter from an electric vehicle charger, both elements demand non-linear currents which contains harmonics out of the fundamental. The harmonic content of any of these systems will depend on its nature and control method. In any case, if the demand of such currents is high enough, generators may be not able to cope with the demanded current, affecting to the grid voltage signal and, in consequence, to the Total Harmonic Distortion (THD) of the grid voltage. This parameter is key for this study and it will be used along this section since the vast majority of the European grid codes of Transmission System Operators (TSO) do not tolerate a higher value of THD in the grid voltage than 5% [4, 5] and 8% at the customer level [6].

6.3.1 Expected values

A non-linear load is by definition, any load which demands a current not proportional to the voltage applied. Naturally, this comprises a wide variety of elements, from a simple diode to complex power stages which need passive or active converters to operate properly. For the purpose of this study, a 6 pulse non-linear load like the one presented in Figure 6.13 has been used. It consists of a three-phase passive rectifier attached to a coil and a variable resistor. However, there are many types of non-linearities (and consequently, many types of non-linear loads). This non-linear load has been chosen due to its highly distorting characteristic and simplicity. Nonetheless, the following analysis is still valid for any type of non-linear load as long as the demanded current has a periodic response.

The aforementioned load has been simulated in Matlab/Simulink [17] and its de-

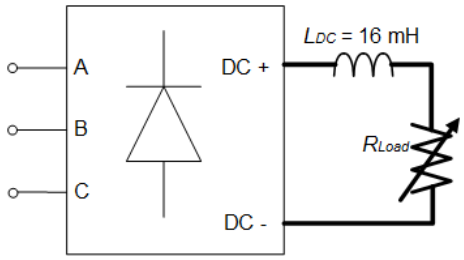

Figure 6.13: Schematic of the non-linear load

mand in current has been plotted in Figure 6.14. As it can be observed it does not have the shape of a sinusoidal wave. However, if a spectrum analysis is made (see the bottom of the same figure), its harmonic content can be observed, having significant harmonics with relevant magnitude at every $6\mathbf{n}\pm1$ order of the fundamental one.

This simulation has been correlated with the measurements taken in the laboratory using a PQ-meter. The results plotted in Figure 6.15 present the THD of the current demanded showing similar results. The only remarkable difference is the magnitude of

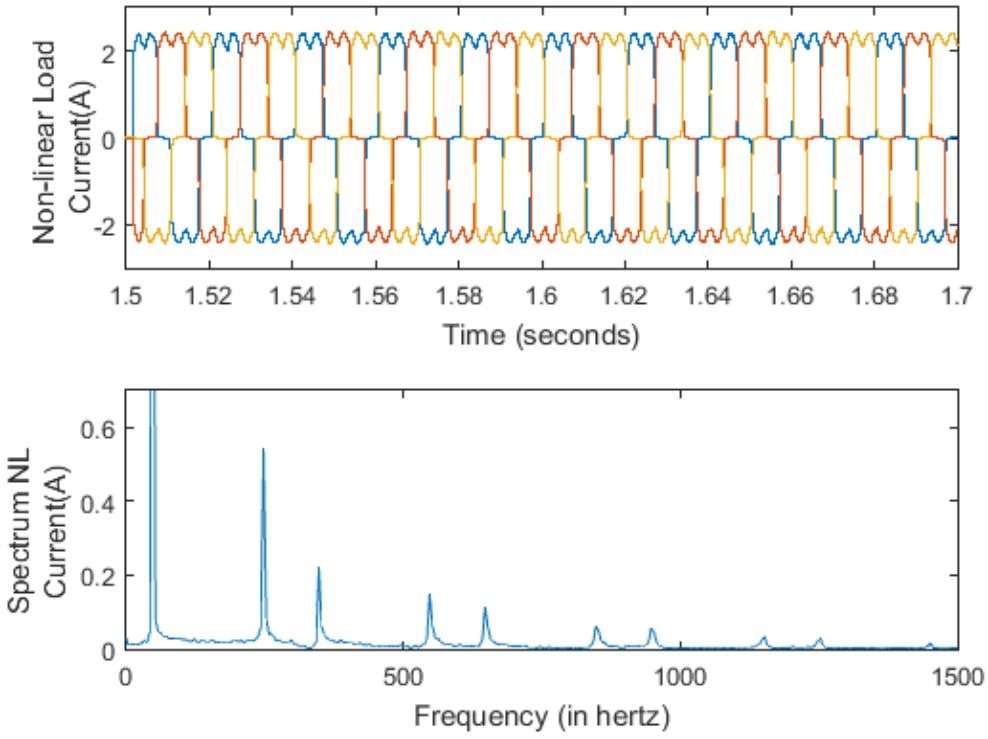

Figure 6.14: Current demanded from the non-linear load obtained in simulation in the time (top) and the frequency domain (bottom).

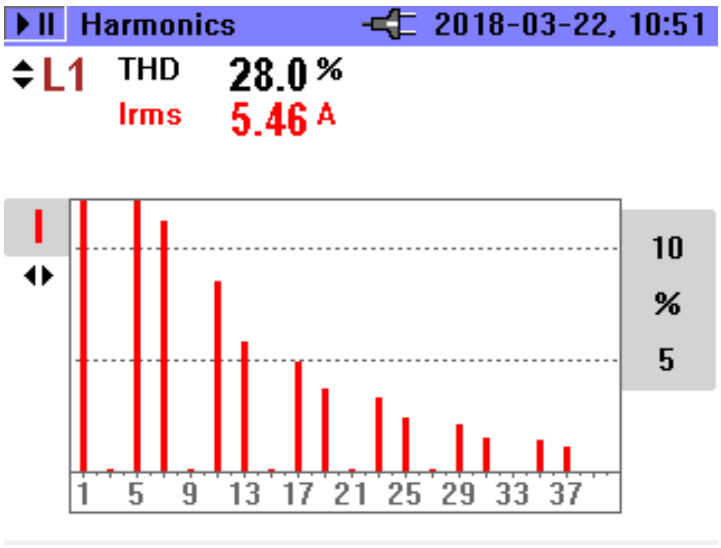

Figure 6.15: Harmonic content of the current demanded from the non-linear load obtained in the laboratory using a power quality meter.

its harmonics which is slightly less than the simulated one.

Knowing the harmonic content of the current demanded, the non-linear load can be expressed as a linear combination of demand in current for each harmonic. Then, the individual effects caused by this demand can be evaluated individually and combined to compute the resulting effect on the Total Harmonic Distortion (THD) of the grid voltage. This analysis is represented in Figure 6.16 where a combination of linear and non-linear load are present in the grid and shown as a demand in current. Also, the grid impedance Lg is represented here since, as it will be seen later in this chapter, this impedance is necessary for the circuit analysis.

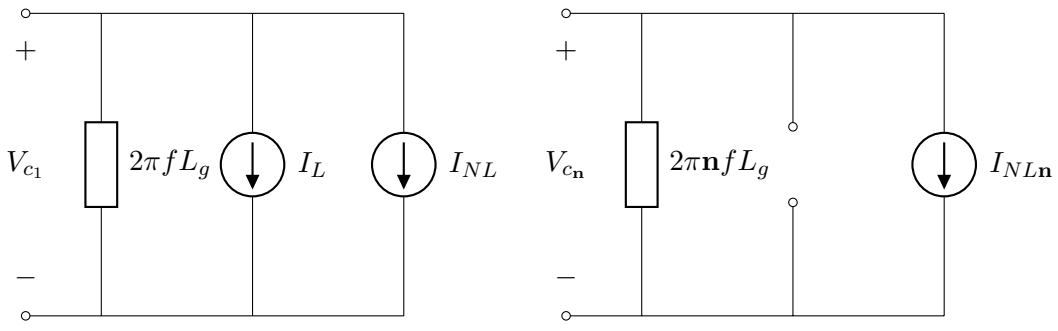

Figure 6.16: Equivalent circuit of the linear and non-linear load as a demand in current for the fundamental frequency (left) and for the **n**th harmonic.

For the fundamental frequency (left side of the figure), the linear load is represented in conjunction with the part of the non-linear load which demands a current at specifically grid frequency. On the right, it is represented the current demanded from the non-linear load for the harmonic **n**. Since the linear load does not demand any current out of the fundamental, here it is represented as an open-circuit.

Therefore, the net effect of the voltage observed by the converter (V_c) can be seen as the sum of the voltages present at any harmonic as long as the load demands it:

$$V_c = V_{c_1} + V_{c_5} + V_{c_7} + V_{c_{11}} ... = \sum_{6\mathbf{n}\pm1}^{\infty} V_{c_n} \tag{6.8}$$

If a proper voltage regulation is required, V_c will have a THD of zero. In order to obtain this value, every harmonic demanded from the non-linear load will have to be supplied with opposite sign contributing positively to the current THD injected by the converter. However, the exact number and magnitude of each harmonic demanded is

Linear loads	**Non-linear loads**					
	0 W	**1.1 W**	**2.3 kW**	**3.4 kW**	**4.5kW**	**5.6kW**
0 W	2.2 0	2.3 29.2	2.8 28.5	3 28.1	3.5 27.8	3.9 27.1
2 kW	2.2 2	2.3 10.2	2.6 15.3	3 18	3.4 19.6	3.8 20.3
4 kW	2.2 2.2	2.4 5.6	2.6 10	3 12.7	3.4 14.8	3.8 16
6 kW	2.2 1.9	2.3 3.2	2.6 6.6	3.2 9.2	3.4 11	3.9 12.5
8 kW	2.2 2	2.3 2.2	2.6 5.2	2.9 7.4	3.4 9.1	3.8 10.5
	THD_V THD_I (%)	THD_V THD_I (%)	THD_V THD_I (%)	THD_V THD_I (%)	THD_V THD_I (%)	THD_V THD_I (%)

Table 6.7: Expected values of THD for the injected current and the grid voltage when connected to a stiff grid.

difficult to calculate.

Contrarily to the unbalanced experiments where a theoretical calculation was performed previous to the experiment, here, it is possible to connect the load to a stiff grid for every scenario where each one of them contains a certain value of the non-linear and linear load. This stiff voltage source will actuate as an ideal regulator. Then, the currents which satisfy the non-linear load will be characterized making use of a power quality meter to obtain a resulting current and voltage THD (since the grid is not an ideal generator and therefore contains some harmonics) for each case. Following, the same process will be followed when, instead of a stiff voltage, the converter will be the main generator of the system working with the DQCI algorithm and the VSM0H. Table 6.7 contains the registered values of THD currents by the stiff grid to achieve a successful voltage regulation including the grid voltage's THD. As it can be observed, the levels of THD_V never exceed 5%.

Theoretically, similarly to the previous experiment with unbalanced loads, if the

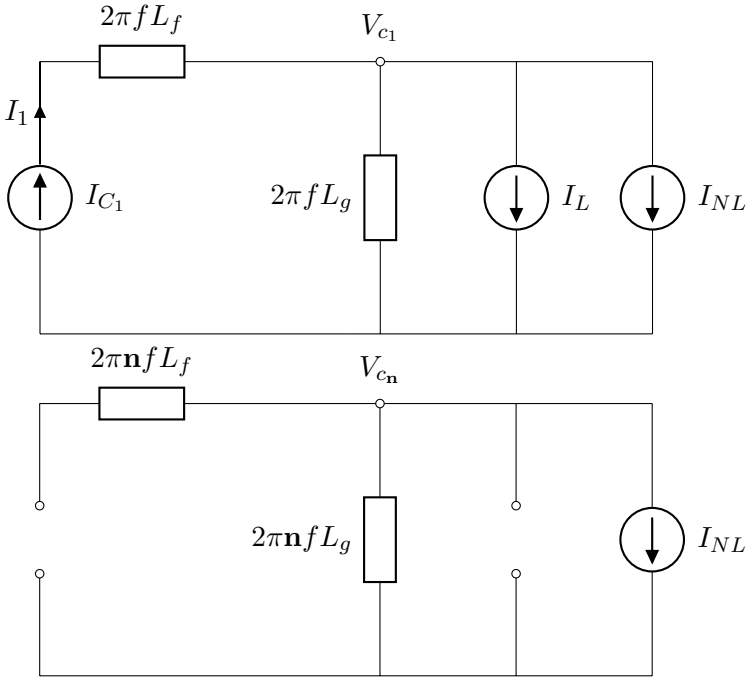

Figure 6.17: Equivalent circuits of the linear and non-linear load connected to the DQCI-controlled converter for the fundamental frequency (top) and for the **n**th harmonic (bottom).

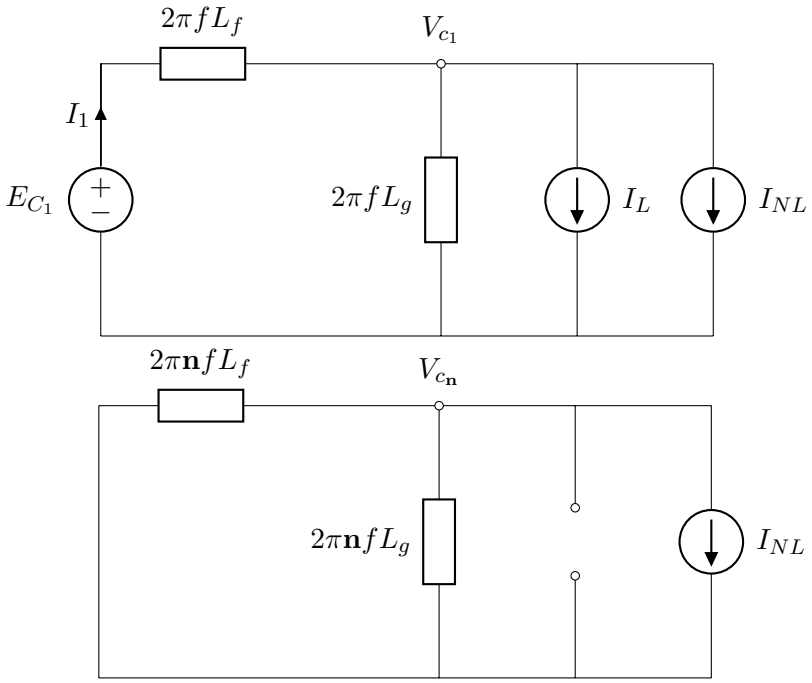

Figure 6.18: Equivalent circuits of the linear and non-linear load connected to the VSM0H-controlled converter for the fundamental frequency (top) and for the **n**th harmonic (bottom).

DQCI strategy is used under the presence of non-linear loads, the converter will actuate providing only positive sequence current, ignoring any other harmonic out of the fundamental one and, following the principle of superposition, behaving as an open circuit in any harmonic out of the fundamental. On the other hand, the GFN/VSM algorithm should impose a positive sequence voltage at 50 Hz and, following again the principle of superposition, behaving as a short-circuit in any harmonic out of the fundamental. Both behaviors are represented in Figures 6.18 and 6.17.

6.3.2 Experimental setup with non-linear loads

The setup for this experiment is very similar to the already presented in the previous section replacing the unbalanced load by a non-linear load.

The schematic of the non-linear load connected here was already presented in Fig. 6.13. It consists of three-phase diode rectifier VUO 62-16NO7 from the brand IXYS [18] in combination with an inductance of 16 mH and a load bank which permits the

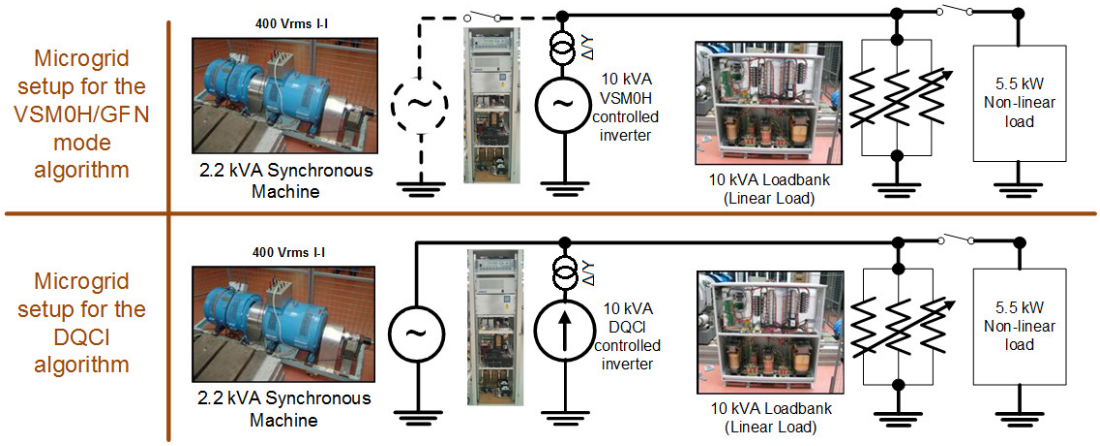

Figure 6.19: Experiment with non-linear loads

modification of the current demanded from this load. The ratings and main parameters of these elements are presented in Table 6.8.

Although, as it will be observed later, this configuration is very disruptive, it is typical of an input power stage in any digital device and it is used due to its great performance (on the DC side) and the low cost of its elements.

Diode Rectifier			
Elem./Param.	**Description**	**Values**	**Units**
If	Maximum forward current	63	A
Vf	Voltage forward	1.7	V
V_{Isol}	Maximum reverse voltage	2500	V
Main Inductor			
L_{DC}	Inductance of the non-linear load	16	mH
$I_{L_{DC}}max$	Maximum current tolerable by L_{DC}	20	A
Loadbank			
$V_{R_{load}}$	Maximum voltage applied	700	V
$I_{R_{load}}$	Maximum current applied	15	A

Table 6.8: Ratings of the elements built as non-linear load.

6.3.3 Experimental results of a converter-dominated grid facing non-linear loads

DQCI algorithm

Standard DQCI control theory has two major difficulties here. First, it makes the converter to behave as a source of positive sequence current, hence, it cannot impose a voltage reference at its connection point. Second, this algorithm needs a synchronization reference which is usually provided by a PLL, being this block very sensitive to the noise present on the measured signal. If too much noise is present in the grid voltage, PLL can enter into instability compromising the stability of the whole converter.

The resulting THD values using the converter operating under the DQCI control strategy are presented in table 6.9; here 'UNS' means the converter lost its stability and had to disconnect and 'OUT' means the system disconnected because the synchronous generator was overloaded.

Linear loads	**Non-linear loads**					
	0 W	**1.1 W**	**2.3 kW**	**3.4 kW**	**4.5kW**	**5.6kW**
0 W	2.6 0	3.3 27.1	OUT	OUT	OUT	OUT
2 kW	0.6 0.3	2.7 7.7	OUT	OUT	OUT	OUT
4 kW	0.8 0.6	UNS	OUT	OUT	OUT	OUT
6 kW	0.7 0.8	OUT	OUT	OUT	OUT	OUT
8 kW	0.8 0.9	OUT	OUT	OUT	OUT	OUT
	THD_V THD_I (%)	THD_V THD_I (%)	THD_V THD_I (%)	THD_V THD_I (%)	THD_V THD_I (%)	THD_V THD_I (%)

Table 6.9: Result for the non-linear loads experiment using the DQCI control strategy

Table 6.9 presents a system very sensitive to the non-linear loads. Due to the incapability of the DQCI control to face any load that is non-linear, it cannot contribute to the stability in any way and hence, the vast majority of the scenarios led to a scenario where the synchronous generator has to face a load higher than its nominal power. Consequently, it has to disconnect, forcing with it the disconnection of the converter.

Taking the case where 1.1 kW non-linear load is present as a reference, the values shown for the observed THD grid voltage are very good but here, again, the main stability contributor is the synchronous generator, not the converter. This can be corroborated by comparing the THD value of the current injected with the expected one. Converter injects a current with a 7.7% of THD when 10.2% was expected. However, the voltage THD is still between operational margins. Furthermore, it has only increased 0.5% compared to the stiff voltage.

On the contrary, if the linear load exceeds 2 kW, since the non-linear load is so high and the DQCI converter cannot provide voltage regulation, the PLL suffers from voltage distortion losing the synchronism. As result, the whole system enters into the instability region and has to disconnect.

The situation where 2kW/1.1kW of linear/non-linear load was being supplied using the DQCI control strategy is depicted in Figure 6.20 for further evaluation. From top to bottom are plotted: The observed grid voltage from the converter V_{abc} (which corresponds to the voltage point at V_c in the previous theoretical analysis), the current injected from the converter, I_{abc}, the active power injected by the converter, P, and the THD coefficient for the observed grid voltage and the current injected. As it can be observed, the scenario is already marginally stable. Due to the voltage sensitivity of the PLL built in the converter, this system is becoming incapable of providing a voltage reference. Consequently, there are swings in power between the synchronous generator and the converter observable through P. However, since the synchronous set is acting in island mode and it can regulate the voltage accordingly, the voltage distortion is low (2.7%).

VSM0H algorithm

Theoretically, voltage source behaviour plays a big advantage in facing this type of loads. Its rigid voltage-source provision against any load, regardless of its nature, provides a voltage regulation effect to the network which contributes positively to the system stability. These scenarios and their corresponding THD values are presented in Table 6.10.

Table 6.10 presents a much more resilient system where the converter only trips because it gets overloaded (the sum of the linear and non-linear loads is higher than the converter nominal power). However, the power quality gets progressively distorted and almost as soon as the non-linear load present in the microgrid is more than 1.1 kW the observed THD grid voltage gets higher than the 5% limit. Therefore, VSM0H control strategy presents some weaknesses which will be further discussed in section

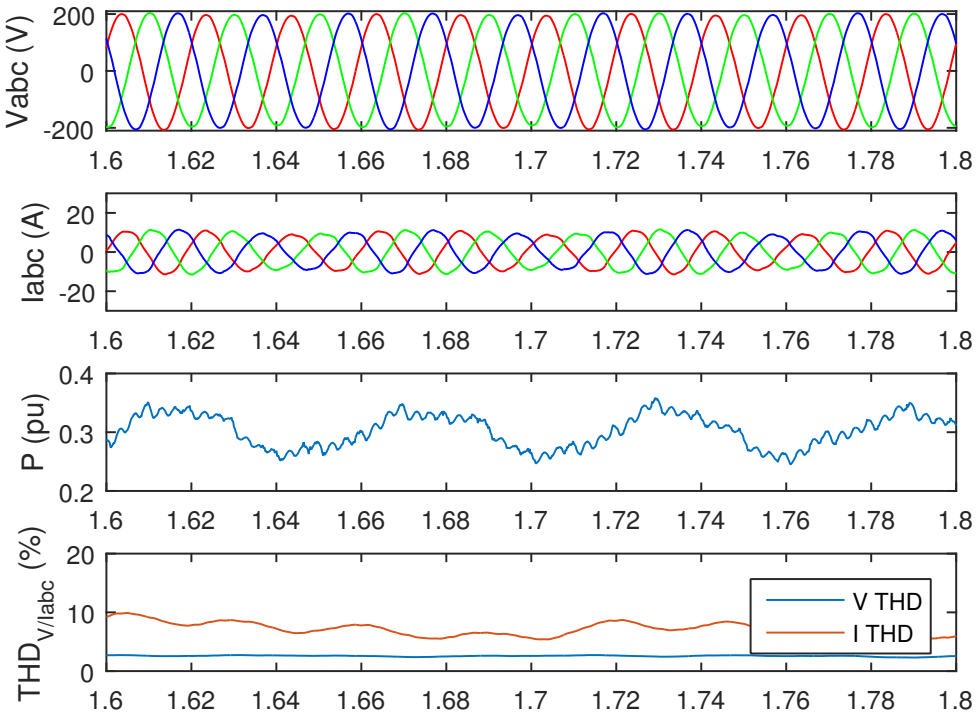

Figure 6.20: Results for 2kW/1.1kW of linear/non-linear load under the DQCI control strategy.

6.4.2.

Observing the measured THD values with the expected ones from table 6.7, it is possible to observe that when the THD stays between operational margins (<5%), the difference of THD between the current injected by the converter and the expected one are minor. However, for instance in the scenario where 2kW/5.6kW of linear/non-linear load is present in the microgrid, VSM0H controlled-converter injects a current with a THD of 12.9% when 20.3% were expected resulting in a distorted voltage with a THD of 16%, a value which exceeds widely the 5% limit.

To compare the results with the DQCI control strategy, the same scenario where 2kW/1.1kW of linear/non-linear load is connected by the VSM0H converter is presented in Figure 6.21. Here, the distortion of the observed grid voltage becomes more evident than in the DQCI case and this translates to an increased THD value of 4.6%. Comparing this scenario with the same for the DQCI algorithm, it is curious to observe that, although the resulting grid voltage THD in the DQCI case is lower than

Linear loads	**Non-linear loads**					
	0 W	**1.1 W**	**2.3 kW**	**3.4 kW**	**4.5kW**	**5.6kW**
0 W	2.6 0	5.4 26.3	9.8 23.6	13.5 22	16.6 20.6	19.3 19.5
2 kW	0.6 0.3	4.6 8.7	8.5 11.5	11.6 12.7	14 12.9	16 12.9
4 kW	0.8 0.6	3.6 4.5	7 7	9.7 8.1	11.8 8.7	13.3 9.3
6 kW	0.7 0.8	2.8 2.6	5.6 4.1	7.6 5.5	8.9 6.7	OUT
8 kW	0.8 0.9	2.4 1.9	4.4 3.6	OUT	OUT	OUT
	THD_V THD_I (%)	THD_V THD_I (%)	THD_V THD_I (%)	THD_V THD_I (%)	THD_V THD_I (%)	THD_V THD_I (%)

Table 6.10: Results for the non-linear loads experiment using the VSM0H control strategy

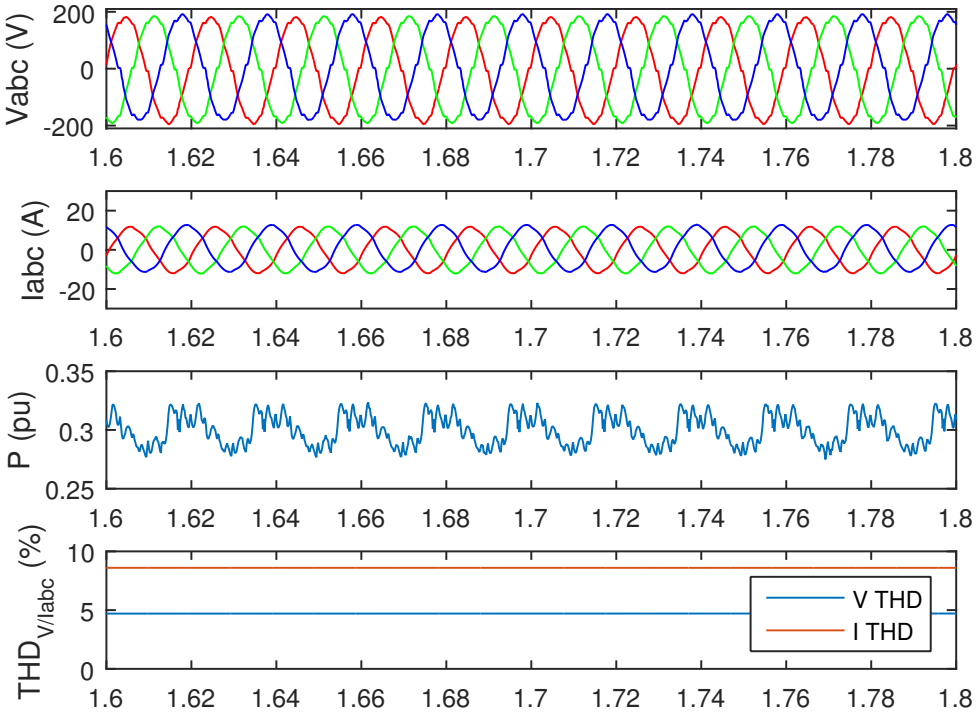

Figure 6.21: Results for 2kW/1.1kW of linear/non-linear load under the VSM0H control strategy.

in the VSM0H one, the converter provides better regulation when the latter is used. Observing the current injected THD in both cases, the VSM0H provides a current with a higher THD. Hence, contributing more to the voltage stiffness. The reason why the DQCI case provides better results is caused by the presence of the synchronous generator in this scenario and its good performance as voltage regulator.

VSM0H+ algorithm

It is tempting to think that, similarly as it was done in section 6.2.3 for the unbalanced case, making use of the voltage behavior of the VSM0H algorithm, it would be possible to design a specific control in charge of mitigating the harmonics contained in the grid voltage. This further modification over the previous one made for unbalanced loads is presented in Figure 6.22.

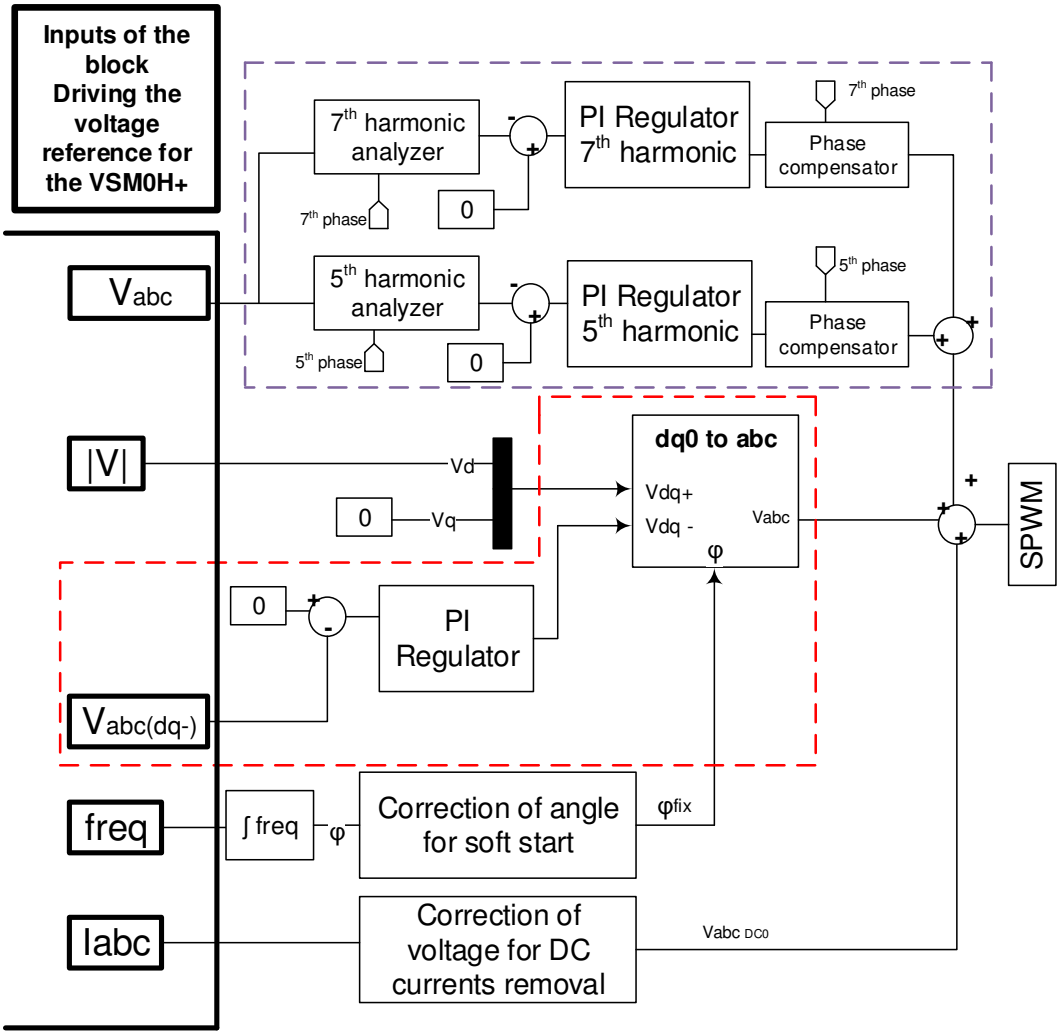

Figure 6.22: Modification of the driving the voltage reference block to mitigate harmonics (framed in purple).

This control evaluates the harmonic content of the grid individually and it has a dedicated control loop which objective is to remove the specific harmonic adding compensation terms at the final converter voltage. First, it has a block which evaluates the magnitude and phase of the specific harmonic to analyze. The resulting magnitude is driven as the measured signal to the PI regulator which sets the magnitude necessary to remove the harmonics present in the grid. Following, the phase compensator reconstructs the signal into a sine wave incorporating the phase previously measured in the **n**th harmonic analyzer. Finally, all the resulting signals are combined and incorporated

into the driving voltage.

This technique is enclosed within the Active Power Filters (APF). As it can be observed, theoretically, **n** control loops should be incorporated in parallel to mitigate the possible harmonic content present in the grid. However, this action is limited by the sampling frequency. For instance, for the case of the converter built for this thesis where 2 KHz is used as sampling and switching frequency. Following Nyquist theorem, it would possible to control up to the 20th harmonic. However, in reality beyond the 7th harmonic, the block in charge of extracting the phase and magnitude cannot provide a correct measurement to the control loop. This is the reason why only the 5th and 7th harmonic control loop are presented in Figure 6.22.

Unfortunately, when this control has been integrated into the converter, the results have been unexpected. All the scenarios presented previously have ended into a disconnection of the converter due to overcurrents. The explanation of this can be seen clearly as follows. The equivalent circuit of the scenario where this control strategy is used and a combination of linear and non-linear load at the **n**th harmonic is present together with the harmonic content of the current spectrum using a stiff grid. Both plots are presented in Figure 6.23. As it can be observed, the equivalent effect is the incorporation of a voltage at the **n**th harmonic which creates a current of opposite sign to the one demanded from the load. If both currents would be the same, the resulting voltage at V_{c_n} would be zero, being this the aim of this control.

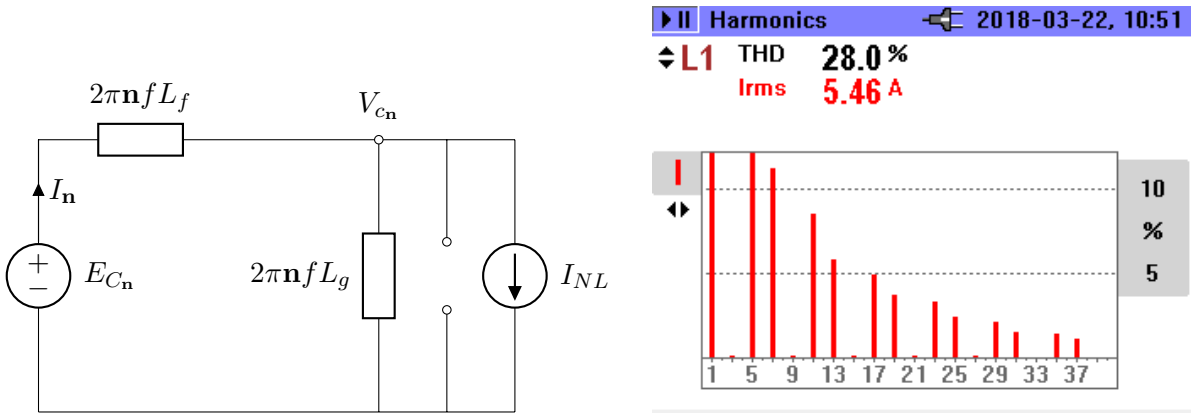

Figure 6.23: Study with the **n**th harmonic

Taking a look now to the power quality meter measurement (plot on the right of Figure 6.23), focusing only in the voltage magnitude and one harmonic, there seems to be among other a 7th harmonic which has a magnitude higher than 10%. Ignoring the angle component, this would mean that, if the converter acts as a perfect voltage regulator it would have to produce a current at the 7th harmonic which will have a magnitude of 10% (for the sake of this explanation its value will be approximated to 10%) of the fundamental one. In other terms, if the load requires 10 Amps at 50 Hz it will require 1 Amps at 350 Hz. As it will be explained as follows, this implies several difficulties.

The problem centers into the two impedances represented in Figure 6.23 between the converter and the load (L_f and L_g). If 10 Amps would be required at 50 Hz and also at 350 Hz the voltage that should be forced for the fundamental frequency (**n**=1)at E_1 would be:

$$E_1 = (X1_{L_f} + X1_{L_g})I_1 \tag{6.9}$$

where $X1_{L_f}$ and $X1_{L_g}$ corresponds to the converter and grid reactance at the fundamental frequency respectively and I_1 to the current demanded at 50 Hz. For the 7th harmonic (350 Hz) the equation is very similar:

$$E_7 = (X7_{L_f} + X7_{L_g})I_7 \tag{6.10}$$

where $X7_{L_f}$ and $X7_{L_g}$ corresponds to the converter and grid reactance at the fundamental frequency respectively and I_7 to the current demanded at 350 Hz. And also:

$$7 * (X1_{L_f} + X1_{L_g}) = X7_{L_f} + X7_{L_g} \tag{6.11}$$

Equations 6.9-6.11 show that for the same current, since the reactance value relies on the frequency, E_7 has to be 7 times higher than E_1, generalizing this for any harmonic **n**:

$$E_{\mathbf{n}} = \mathbf{n}E_1 \tag{6.12}$$

Although equation 6.12 is obvious, it needs to be put into this context to continue the explanation. Now, characterizing the harmonic content from using the power quality meter it is possible to obtain table 6.11 with the magnitude of every harmonic contained in the current demanded.

n=1 (50Hz)	**5**	**7**	**11**	**13**	**17**	**19**
100%	14%	12%	8%	6%	5%	4%

Table 6.11: Harmonic content of the current demanded by the non-linear load

Knowing equation 6.12 and the magnitude of the harmonics, it is possible to estimate (ignoring the angle component of the harmonics) which is the magnitude of the converter voltage which will have to be imposed in order to achieve voltage regulation.

$$\vec{E} = \sum_{\mathbf{n}=1}^{\infty} \mathbf{n} \cdot \vec{I_{\mathbf{n}}} \cdot j(X1_{L_f} + X1_{L_g}) \tag{6.13}$$

where E is the voltage imposed by the converter, $\mathbf{n}$ is the specific harmonic under study and I_n is the magnitude of the current demanded by the non-linear load (their values as it was mentioned, are in table 6.11). As it can be observed from equation 6.13, the factor of $\mathbf{n}$ in this equation makes E value very high. Obviously, this is partially mitigated by the fact that as the harmonic order gets higher its magnitude is lower, however, the $\mathbf{n}$ factor in the equation is much higher making the converter prone to the disconnection.

This study has shown that, although theoretically a harmonic compensation is possible, this technique is very difficult to develop since it can put the converter in risky situations where the DC bus voltage does not have enough value to set a value so high at the output of the converter bridge. However, these results will be later discussed in section 6.4.2 where possible solutions and mitigation techniques are explained.

6.4 Discussion about the obtained results

6.4.1 Unbalanced loads

The experiments made along this chapter can produce several conclusions which can help to understand the behavior of converters depending on the control strategy used in each case. For instance, the DQCI converter implemented has shown a poor performance against unbalanced load being very sensitive to them and prone to disconnect as soon as the unbalanced loads cannot be supplied by other generators. However, unexpectedly they have provided a small amount of negative sequence current when none was predicted. This unbalanced current production is caused by the limited bandwidth of the internal control dynamics. DQCI converter's objective is to achieve an active and reactive power command. To do so, it implements an inner current control loop with a finite bandwidth. If this bandwidth would be high enough to fully mitigate the 2nd order harmonic perturbation created by the unbalanced scenario, the inverter would be able to react fast enough against it and therefore, it would behave as an ideal positive sequence current source. On the other hand, if the control bandwidth would be lower than 50 Hz, the regulators would not be able to observe the perturbation and they would not react to counteract it, giving as result a much higher negative sequence current component on the expense of losing some controllability. Since, in this case, the control bandwidth is 200 Hz, only some of this 2nd order harmonic signal gets into the internal variables of the inner control loop. As result, some unbalanced production is obtained but much lower than the necessary to mitigate the faulty scenario. This result is also consistent with the ones presented in [21].

Additionally, it was observed in the experiments that the Phased-Locked-Loop (PLL) system implemented inside the DQCI control strategy is very sensitive to these unbalanced scenarios, destabilizing the converter and finally leading it to the disconnection. However, if the conventional Synchronous Reference Frame PLL (SRF-PLL) is replaced by advanced PLL configurations, the converter tolerance to the unbalanced scenarios can be much improved. For instance, the Double Second Order Generalized Integrator PLL (DSOGI-PLL) has already provided very good results for unbalanced

scenarios [15], improving vastly the converter resilience against these events. However, although the converter could stay connected to the grid, it would remain playing a passive role, displacing (mostly) the responsibility to mitigate the faulty scenario to the remaining synchronous generators connected in the system. This would concentrate a significant amount of mechanical stress in structural and rotating elements of the generator. Consequently, this accumulated fatigue damage would lead to higher maintenance costs, discouraging present and new synchronous generators to connect to the grid, promoting with it an even higher absence of active regulators in the system [16]. This detriment on voltage regulation could be mitigated by dividing the voltage measured into the positive and negative sequence and then, implement a dedicated negative sequence control capable of injective negative sequence current. However, this has been left for future work.

Regarding the experiments using the VSM0H control strategy, it seems that (coming back to the analysis made in Figure 6.3), the VSM/GFN converter permits the continuity of I_n in the negative sequence circuit. This shortcircuit causes only a small voltage of V_- which leads to a visible unbalanced voltage. V_- value will depend on the current injected into the positive sequence and the impedance of the converter. Since the only controllable parameter from the converter side is L_f its value will dictate the converter capability to force a stiff voltage reference. In other words, if a converter is intended to work as GFN, the equivalent impedance of the converter grid filter will have to be reduced as much as possible. This may be achieved by reducing the filter inductance as long as the harmonic content of the current injected does not increase substantially. If this reduction is simply not possible or further voltage regulations are required, the explained VSM0H+ algorithm can be used as a solution to mitigate the faulty scenario. Imposing a voltage on the negative sequence reference frame, (E_{C-}) this control strategy counteracts the current I_n created by the cross-coupled term $R_0 I_+$. Naturally, for lower values of L_f, lower magnitudes of E_{C-} will be required to remove the negative sequence voltage.

To perform this control strategy the only requirement necessary is to have a linear operation margin enough to impose a voltage slightly higher than the usual. In order

to provide the voltage support against the unbalanced scenario, the specific control reacts increasing the voltage of the specific faulty phase. To be able to perform this task, it requires a DC voltage high enough that the converter does not enter into PWM over-modulation and, thus, losing the linear operation mode. Although this margin has not been found significantly high, this has been the reason why in table 6.6, for the case of 8kW/1.8kW of balanced/unbalanced load, the converter using the VSM0H+ algorithm disconnected and using the standard VSM0H (observe table 6.5), it did not.

Another important factor to consider is the dimensioning of the DC bus. Throughout the experiments, the DC bus has always been considered as an almost infinite source of power since it has been supplied by a high-performance DC power supply. However, a real converter may be connected to a limited source of DC energy. For instance, a grid side connected converter from a wind turbine with a fully rated back-to-back converter has a limited energy available in the DC bus. In this case, the energy collected by the DC capacitors and available to be injected into the grid is directly dependent, in its majority, on the wind resource available and the rectifier-side converter performance. Consequently, if VSM0H or VSM0H+ control strategies are going to be used into a real system, the DC buses may need some resize or even the addition of external energy storage elements such as super-capacitors or batteries depending on the converter response required.

Finally, in order to extend the GFN solution to large complex electrical grids, it is necessary to think about how these solutions will be implemented in a real system which is dynamic and has to be designed with a certain resilience against any event. The studies done using GFN converters, including this, have considered a singular GFN converter which provides the stiff voltage needed. However, if for any reason, the GFN converter would have to disconnect, at least the local stability would be highly compromised. Naturally, this responsibility can not be left to only one generator, thus, at least two of them must be connected at the same time providing these ancillary services. Consequently, two converters would attempt to impose both their own voltage reference creating possible conflicts in the network. This scenario is especially critical if VSM0H+ is being used since this algorithm provides an active response against

the presence of negative sequence voltage. However, this action can be also limited by introducing a gain smaller than 1 between the measured signal and the error calculation or just transform the PI regulator into a proportional regulator operating in open loop. This last case is equivalent to establish a droop control.

6.4.2 Non-linear loads

During the experiments undertaken along section 6.3.3 the weaknesses of the DQCI algorithm have been exposed, showing that this control strategy tends to be unstable when noisy grid voltages are present because of the PLL sensitivity to these signals. This may be enhanced with the aforementioned DSOGI-PLL structure or any other configuration which includes a filter inside. However, there may be possible implications due to the time response of the filter into the entire converter stability. Additionally, some tuning can be done in the PLL dynamics to face systems very prone to noise. There is evidence [22] which shows that a reduction in the PLL's internal PI gains can lead to a more stable converter in the exchange of some transient performance. This adjustment can be possible depending on the Short Circuit Ratio (SCR) of the grid to which the converter is connected and the nominal power of this.

On the other hand, VSM0H experiments have shown that, although the converter behaves as a stiff source of positive sequence voltage, there are limitations in terms of voltage regulation when the system is facing non-linear loads. This is caused by the impedance L_f and its increasing reactance value when the harmonic order increases. As it was explained in the VSM0H+ section, for every increase in the harmonic order, the current gets divided by this same factor, subtracting capability to regulate the voltage at V_c.

Since no further action has been considered it is interesting to calculate which is the maximum limit in the percentage of non-linear load which the microgrid can tolerate to stay with a grid voltage lower than 5%.

Figure 6.24 shows the values of table 6.10 in a 3D plot. A plane at 5 % shows here the boundary conditions where the system reaches this limit value of THD. The intersection of both planes can be found and plotted on top of Fig 6.25. These boundary points

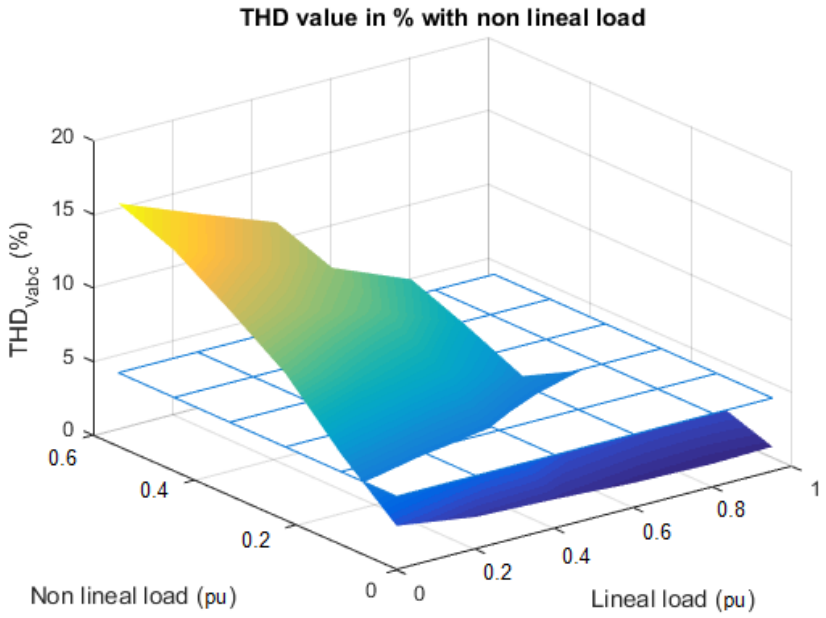

Figure 6.24: Surface plot of the Voltage THD (%) Vs linear and non-linear load using the VSM0H/GBN control strategy

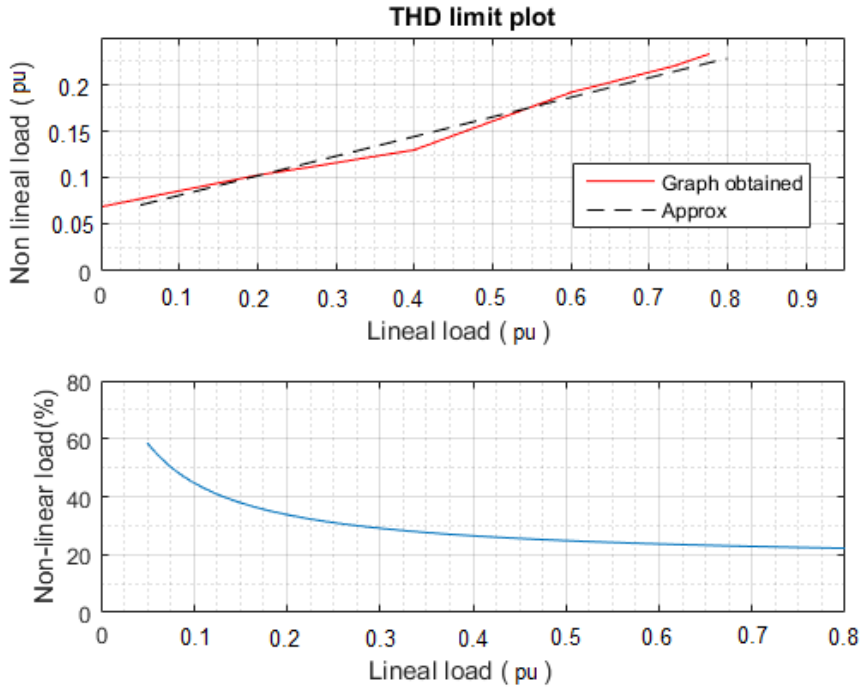

Figure 6.25: Limit conditions for THD = 5% (top) and corresponding percentage of non-linear load (bottom)

can be approximated to a straight line which equation can be found and consequently translated into percentages of non-linear load (bottom of the same plot). As it can be observed, the non-linear percentage curve has an asymptote that also can be calculated as operating limit. The result is 17.35% which is the percentage of non-linear load for a converter filter inductance of 0.18 pu to stay viable within limits for any value of linear load present in the system.

6.5 Final discussion

The value previously obtained in section 6.4.2 must be taken as the most favorable of the cases since, extrapolating the results obtained in the microgrid where the only generator in the system, the converter, was operating under the VSM0H control strategy. Therefore, the entire energy was being supplied with active voltage regulators. Extending this analysis to large grids, this would mean that all the generators of the system would behave as voltage source, something that is very unrealistic. Thus, this value is a boundary that, for sure, must not be exceeded in any kind of grid if specific measures to suppress the harmonics are not considered. Since basically, any digital device demands a more or less disruptive non-linear current, to limit its amount to 17.35% of the total load demonstrates the distorting capability of these loads in the system and the magnitude of the problem for which future large grids have to entail.

Similarly to the unbalanced case, the impedance L_f seems to be the main factor for the converter capability to regulate the grid voltage. However, for the unbalanced case, this can be overcome by the specific control implemented in the VSM0H+ algorithm, however, this option, as it was explained in section 6.3.3 is not recommended for the non-linear load, at least for the case shown in this thesis.

If the harmonic mitigation is mandatory, all the efforts should focus on reducing the value of L_f. Three solutions in order to reduce its value are suggested here:

- *L_f reduces its value with power.* Since for different converters L_f has similar values in per unit, this inductance gets smaller with the nominal power of the generator. This would justify a delegation of these duties to the large generators present

and connected to the grid since they have smaller impedances and therefore, they have more capability to mitigate the harmonics present in the grid voltage.

- *Use Modular Multilevel Converters (MMC) as Active Power Filters (APF).* Due to its structure, MMCs can produce a voltage that does not require much filtering, having a net L_f very low (in some cases it can be even zero). This provides them with a higher capability to compensate harmonics in addition to its well-known performance under unbalanced loads. This fact makes them ideal candidates for voltage regulation [11]- [14].

- *Encourage the usage of linear loads.* As it has been observed the proportion of linear and non-linear load play also a role in the system. This is caused by the damping effect that these loads have in the system. Linear loads, or more specifically, resistive load provide a natural damping to the system which helps to mitigate any transitory event, therefore, they should be encouraged or, if not, demand from the operation loads which do not request a disruptive current as the one presented in Figure 6.19.

Bibliography

[1] D. H. Harrison. "Connecting renewable generation to rural 11kv networks with high levels of voltage unbalance," presented at the IET Conference on Renewable Power Generation (RPG 2011), Edinburgh, 2011, pp. 1-4.

[2] S. M. Fernndez, S. M. Garca, C. C. Olay, J. C. Campo Rodrguez, R. V. Garca and J. V. Lpez, "Electronic Tap Changer for Very High-Power Medium-Voltage Lines With No SeriesParallel Thyristors." *IEEE Transactions on Industrial Electronics*, vol. 65, no. 7, pp. 5237-5249, July 2018.

[3] Energinet. "Regulations for grid connection. Document: 'Technical regulation 3.3.3 for PV/Wind Power Plants Above 11 kW." Internet: https://en.energinet.dk/Electricity/Rules-and-Regulations/Regulations-for-grid-connection [Consulted March 2018].

[4] Red Electrica de Espana. "Procedimientos de operacion." Internet: http://www.ree.es/es/actividades/operacion-del-sistema-electrico/procedimientos-de-operacion [Consulted March 2018].

[5] National Grid. "National Grid Code". Internet: https://www.nationalgrid.com/uk/electricity/codes/grid-code?code-documents [Consulted March 2018].

[6] Voltage Disturbances Standard EN 50160. "Voltage Characteristics in Public Distribution systems." July 2004.

[7] IEC 61000-2-12:2003. "Electromagnetic compatibility (EMC) - Part 2-12: Environment - Compatibility levels for low-frequency conducted disturbances and signaling in public medium-voltage power supply systems", 2013.

[8] Edith Clarke. *Circuit Analysis of A-C Power Systems*. General Electric Company. 1943

[9] L. Reguera Castillo, A.J. Roscoe, "Experimental stability assessment of converter-dominated electrical grids". presented at the 16th Wind Integration Workshop, Berlin, Germany, 2017.

[10] L. Reguera Castillo, A.J. Roscoe. "Experimental validation of a novel inertia-less VSM algorithm". presented at the IEEE Innovative Smart Grid Technologies North America, DC, United States, 2018.

[11] M. P. Nandankar and D. S. More. "Performance analysis of transformer-less hybrid active power filter using different inverter topologies," presented at the International Conference on Intelligent Computing, Instrumentation and Control Technologies (ICICICT), Kerala State,Kannur, India, 2017, pp. 892-897.

[12] V. Tummakuri, B. Das, P. R. Kasari and A. Chakraborti, "Grid connected five level cascaded H bridge inverter as shunt active power filter," presented at the National Power Electronics Conference (NPEC), Pune, 2017, pp. 60-65.

[13] S. Ray, N. Gupta and R. A. Gupta, "Improved single phase SRF algorithm for CHB inverter based shunt active power filter under non-ideal supply conditions," presented at the IEEE PES Asia-Pacific Power and Energy Engineering Conference (APPEEC), Bangalore, 2017, pp. 1-6.

[14] K. Karaarslan, B. Arifoglu, E. Beser and S. Camur, "A novel 7-level cascaded inverter for series active power filter," presented at the 18th International Scientific Conference on Electric Power Engineering (EPE), Kouty nad Desnou, 2017, pp. 1-5.

[15] P. Rodriguez, R. Teodorescu, I. Candela, A. Timbus, M. Liserre, and F. Blaabjerg, New positive sequence voltage detector for grid synchronization of power converters under faulty grid conditions, in *Power Electronics Specialists* and presented at the IEEE 37th Conference on, 2006, pp. 14921498.

[16] A. J. Roscoe, S. J. Finney and G. M. Burt, "Tradeoffs Between AC Power Quality and DC Bus Ripple for 3-Phase 3-Wire Inverter-Connected Devices Within Microgrids." *IEEE Transactions on Power Electronics*, vol. 26, no. 3, pp. 674-688, March 2011.

[17] Matlab. "Offical page of Simulink/Matlab". Internet: https://www.mathworks.com/products/simulink.html [Consulted Sep 2018].

[18] IXYS. "Offical page of IXYS power corporation". Internet: http://www.ixyspower.com/ [Consulted Sep 2018].

[19] Q. C. Zhong and G. Weiss, "Synchronverters: Inverters That Mimic Synchronous Generators." *IEEE Transactions on Industrial Electronics*, vol. 58, no. 4, pp. 1259-1267, April 2011.

[20] H. P. Beck and R. Hesse, "Virtual synchronous machine," presented at the 9th International Conference on Electrical Power Quality and Utilisation, Barcelona, 2007, pp. 1-6.

[21] M. Yu, A. J. Roscoe, A. Dyko, C. D. Booth, R. Ierna, et al., "Instantaneous Penetration Level Limits of Non-Synchronous Generation in the British Power System." *IET Renewable Power Generation*, vol.11, pp. 1211-1217, 2016.

[22] J. Z. Zhou and A. M. Gole, "VSC transmission limitations imposed by AC system strength and AC impedance characteristics," presented at the 10th IET International Conference on AC and DC Power Transmission (ACDC 2012), Birmingham, 2012, pp. 1-6

Bibliography

Bibliography

Chapter 7

Conclusions & Future Work

7.1 General conclusions

Converter-dominated grids is a topic with a growing interest for both academia and industry. From small industrial microgrids to large country-sized electrical grids, converters are playing a pivotal role in contemporary networks taking the role of primary generators system at the expense of the traditional synchronous machines. With this change, stability studies have been triggered due to the awareness of an alarming loss of inertia of large electrical systems where the renewable energy, and hence the converter proportion, is not negligible.

This thesis provides a better understanding of converter-dominated grids behaviour, proposing scenarios where their main weaknesses have been studied and exposed. Once these are understood, several solutions to achieve a feasible and robust power system where the generation is solely based on converters have been explored, proposed and validated in the laboratory.

In order to perform representative scenarios along this thesis, a converter of 10 kVA has been built on purpose (further details in Chapter 3). This system has the particularity of allowing the change of the control logic embedded in it. Thus, it can operate as the conventional vectorial current control named along this thesis as D-Q axis Current Injection (DQCI). Or, on the other hand, it can work under the logic of control named Virtual Synchronous Machine with Zero Inertia (VSM0H). Being in this

thesis the first case, to date, where this algorithm has been implemented into a real converter. Special modifications over the theoretical algorithm have been developed to make its implementation viable. These changes have been explained and validated experimentally.

During the construction of this converter two additional contributions have been made. First, the improvement of the basic DQCI control algorithm dynamics due to the creation of a virtual parasitic resistor in series with the filter inductor. And secondly, the design and experimental validation of a novel control technique based on the standard DQCI which provides the converter with a distinct feature. A controllable speed response depending on the grid events. Due to this adaptive reaction, the robustness of the converter and the grid are mutually benefited (both contributions are explained in Chapter 3).

With the aforementioned converter already built, it is possible to recreate a converter-dominated grid into the laboratory. To do so, the 10 kVA converter is connected to a small controllable synchronous set of motor-generator rated in 2.2 kVA. Just connecting both generators supplying power to a load has provided interesting outcomes described as follows.

In this first experiment, it was understood that the main weakness of converter-dominated grid was the lack of voltage regulation, or more precisely, the lack of voltage stiffness. Since conventional-controlled converters behave as current sources, they are incapables of providing the necessary voltage regulation to the system, leading to a progress weakening of the grid voltage signal.

Because of the aforementioned reasons, the active contributors to the stability within converter-dominated scenarios are the voltage source of the system; the synchronous machines. Behaving as voltage sources, these generators can correct any deviation from the pure and balanced sinusoidal grid voltage signal. Taking into account this, the expressions traditionally used for the parameter Level of penetration (LoP) fail encapsulating this idea since they take into account the active power provided by the synchronous machine. Consequently, another contribution to this thesis is a new formula of LoP (LoP_{conv}). This expression aims to gather that the factor to

evaluate is not the active power injected by the synchronous machine, instead, it is the nominal power of the generator since this parameter quantifies the capability of the synchronous machine to regulate the voltage at its terminals.

Understanding that converter-dominated grids suffer from shortage of voltage regulation, the solution is straightforward. Transform the converters in a way such they behave as voltage sources of power, not current sources. Then, former synchronous machines could be replaced by this new type of converter.

This transformation from the grid point of view can be done by just replacing the control algorithm embedded in the converter and replace it by any of the techniques enclosed within the Virtual Synchronous Machine (VSM). As its name already advances, these algorithms base, totally or partially, on mimicking the behavior of a synchronous machine. Thanks to this new control, these VSM-controlled converters are observed as positive sequence voltage sources, contributing now to the voltage stiffness.

Extending this idea within to large-power systems dominated by converters, the term Grid Forming Node (GFN) has been coined in academia as the strategic nodes in a power system where the voltage signal integrity (or grid stiffness) is assured, usually making use of converters controlled by the aforementioned VSM control techniques. Once these points supply the necessary voltage stiffness, others DQCI/standard-controlled converters can follow this signal reference leading to a system which can work in a stable manner.

Additionally, it has been observed that, if the VSM0H control algorithm is used among the VSM-techniques, further regulations can be done. The VSM0H control algorithm has a special particularity, it has zero inertia. Due to this feature, it can exploit the control capabilities of silicon-based devices which do not need to respect any physical inertia like synchronous machine do. Thus, it can provide power with the best possible dynamics against events as typical as a load step. An additional experiment in Chapter 6 has been conducted to evaluate the VSM0H converter capabilities to improve the dynamics of the grid as a whole, proving that it is capable to mitigate any power oscillation caused by the neighboring synchronous generators present in the grid thanks to the provision of synchronizing torque/damping. As result, a clean voltage

signal without oscillations is observed by the load allowing the possibility to improve the stability of the grid even further than using real synchronous generators.

However, so far, it has been understood that the main weakness of converter-dominated grids is the lack of voltage regulation but there has not been evidence of this. Additionally, the GFN architecture suggests a drastic solution, the replacement on the control algorithms of many nodes of a high interleaved electrical system. Something that is difficult to assume for engineers and managers of such complex grids. Because of both reasons, additional experiments have been conducted in the laboratory along Chapter 6. These scenarios are set under the premise that it is necessary to evaluate the risks of an electrical grid that is not only changing on the generation but also on the demand side. To date, all the studies which assess the GFN solution assume linear and balanced loads on the demand side. Since, as it has been mentioned before, converter-dominated grids are electrical networks which suffer from voltage regulation shortage, it is advised to evaluate the sensitivity of this new type of architecture against loads which can demonstrate the lack of voltage regulation of converter-dominated grids. These are unbalanced and non-linear loads.

For the unbalanced case, a deep analytical study has been undertaken. The assessment has included the calculation of the theoretical response of the converter computing the expected unbalanced current and resulting grid voltage unbalance for the DQCI and the VSM0H control strategies. Later, the predicted values have been confirmed in the laboratory. This assessment has shown the sensitivity of the DQCI converter to this type of loads as well as its very limited capability to mitigate this event without further modifications. VSM0H, on the contrary, has proved to be a much more resilient generator with finite contributions to the correct voltage regulation. Additionally, the theoretical calculation presented along Chapter 6 and its following practical validation confirm that the DQCI-controlled converter can be modeled as a positive sequence current source and the VSM0H-controlled converter can be replaced as a positive sequence voltage source.

If further regulation is necessary in the presence of unbalanced loads, an improved version over the actual VSM0H control strategy has been purposed and validated in

this thesis with experiments (named VSM0H+ in Chapter 6). This control exploits the voltage source behavior of the VSM0H algorithm in order to remove completely any voltage unbalance. This is made by incorporating a specific control loop which measures and eliminates the negative sequence component present in the grid.

For the non-linear loads, a much more practical approach has been taken. Taking as a reference a stiff grid, it is possible to characterize the necessary currents demanded to achieve a voltage regulation within limits measuring the Total Harmonic Distortion (THD) of the current injected and the grid voltage for any scenario. Knowing how a correct regulator behaves, it is possible to compare the response of the DQCI and the VSM0H algorithm under each combination of linear and non-linear loads. DQCI converter has proved to be especially susceptible to this type of loads. This is caused by the PLL sensitivity to a polluted grid signal with harmonic content. VSM0H on the other side has behaved as a very resilient source of energy showing almost no scenario where the converter disconnects. However, it has been remarked the limited capability to regulate voltage within limits due to the reactance of the converter main filter inductor and its increasing value with the harmonic order.

A similar approach with the VSM0H+ technique has been explained to remove the harmonic content caused by the non-linear loads. Creating a dedicated control loop for every individual harmonic, it should theoretically be possible to remove every harmonic content from the grid providing the demanded current at the specific frequency in phase and magnitude. However, in this case, this action is very limited due to two reasons: First, there is a limited bandwidth available which depends on the sampling and switching frequency, conditioning the maximum harmonic order that is possible to regulate. And secondly, the voltage necessary to drive that current to the non-linear load is so high (due to the aforementioned increasing value of the filter reactance with the harmonic order) that the converter gets out of the linear operation due to lack of DC voltage margin. According to the results obtained it has been calculated that a maximum of 17.65% of nonlinear loads must be present in the grid to remain the microgrid within limits. This value must be taken as an absolute maximum under the most ideal conditions since 100% of the generators were voltage sources contributing

to the stability. However, taking into account the number of actual and future loads which demand a non-linear current, this experiment has demonstrated the distorting potential of non-linear loads, raising the awareness of how these type of loads may be limited in weak power systems.

7.2 Main contributions of this thesis

- The weaknesses of *converter-dominated grids* have been exposed and understood. Throughout this thesis the experimental assessments conducted confirm that converter-dominated power systems *lack of voltage regulation*. Solutions enclosed like GFN have proven to be effective for this type of grid but with some limitations directly dependent on the equivalent filter impedance of the converter filter.

- In this thesis, it has been presented, explained and validated a *novel technique based on the conventional DQCI control strategy to operate with adaptive speed response*. Depending on the grid conditions, the converter can provide a slow or a fast response. As result, the converter and the grid are mutually benefited leading to a more stable operation of both of them. See Chapter 4 for more details about this solution.

- *The virtual resistor*. Based on an stability assessment, it has been proven how the parasitic resistance of the main filter inductor contributes to the stability of the entire inner control loop. A feed-forward compensation in the inner current loop was developed to simulate the presence of a larger value of this parasitic resistor than the real one, leading to a plant which is easier to control.

- *Further development and refinement of the VSM0H control strategy to behave better as local voltage regulators*. Several modifications have been made along this thesis of the initially theoretical algorithm VSM0H. First, two blocks have been added to make the algorithm practical into a real converter; One block which is charge of eliminating the DC current present in the grid, another one to permit the immediate synchronization with the grid voltage. Later, a second

modification have been done to face mitigate the side-effects caused by unbalanced and non-linear loads. For the unbalanced loads, this solution has been validated experimentally, however, for the non-linear loads this additional modification has only been purposed and explained since it has not been possible validating it due to limitations in the converter built.

- *VSM0H converters can replace synchronous machines* in terms of voltage regulation but, due to its lack of inertia, it also can provide at the same time *power compensation*. Consequently, any power oscillation present in the grid is mitigated.

- *The effects of non-linear loads* have been investigated. It has been observed that at a relative low levels, DQCI converters are very sensitive to the harmonics demanded from this type of loads, tampering the internal operation of its PLL and forcing them to disconnect. On the contrary, VSM0H has proven to be much more resilient with limited contributions to the voltage regulation, again, this contribution is directly dependent with the equivalent converter filter impedance.

7.3 Future Work

This project triggers many questions that still have to be solved and can be the start point for future work, some of them are exposed as follows:

- *GFN solution using two VSM converters*. The GFN solution is based on a master-slave configuration where the master VSM imposes a reference of voltage magnitude and angle which other converters can follow. In a real implemented power system, this task can not be performed by just one generator. If this unique GFN would have to disconnect, the entire microgrid would be highly exposed to a blackout. Thus, in a real power system, more than one generator will have to act as master trying to impose a voltage reference. This can lead to conflicts between them which can lead to swings in the grid voltage.

- Following with the previous point it can be that in real grids *solutions like*

VSM0H+ may be too restricted for large power systems. Forcing the negative sequence removal can be correct in a single master configuration but if two different converters would operate as VSM0H+, small differences in the negative sequence measured (for instance) could lead to voltage swings.

- Throughout the experiments, the DC bus has always been considered as an almost infinite source of power since it has been supplied by a high-performance DC power supply. However, a real converter may be connected to a limited source of DC energy. For instance, a grid side connected converter from a wind turbine with a fully rated back-to-back converter has a limited energy available in the DC bus. In this case, the energy collected by the DC capacitors and available to be injected into the grid is directly dependent, in its majority, on the wind resource available and the rectifier-side converter performance. Consequently, if VSM0H or VSM0H+ control strategies are going to be used into a real system, the DC buses may need some resize or even the addition of external energy storage elements such as super-capacitors or batteries depending on the converter response required.

Appendix A

Publications

1. L. Reguera Castillo, A.J. Roscoe, "Experimental stability assessment of converter-dominated electrical grids". presented at the 16th Wind Integration Workshop, Berlin, Germany, 2017.

Abstract:

With the inclusion of renewable generation into the electrical grid, traditional fossil-fueled plants based on synchronous generators have been gradually replaced by converterbased systems, controlled using the standard vectorial current control (DQCI). From the grid point of view, this control strategy makes converter behave as current sources that inject power to the grid but have limited magnitude or angle voltage regulation. The shortage of this task implies a detriment of the stability of key parameters for a stable grid, exposing the system to huge diversions of frequency and voltage. Ultimately, this can make generators to disconnect, compromising with it the stability of the whole system thanks to a cascade failure. However, as it will be seen in this paper, it is possible to transform the converter into a real regulating voltage source changing just the control algorithm. Thanks to this change, same converters can create now reference nodes (also called grid building nodes) in the grid which DQCI converters can follow. This scheme would allow the possibility to a robust system based completely on converters. This scenario is object of test in this paper where a power quality and stability assessment is conducted in the lab.

2. L. Reguera Castillo, A.J. Roscoe. "Experimental validation of a novel inertia-less VSM algorithm". presented at the IEEE Innovative Smart Grid Technologies North America, DC, United States, 2018.

Abstract:

For years, grid phenomena such as voltage stability, loss of inertia, voltage dips, etc. have been managed by well established solutions. Such solutions include on load tap changing transformers, and synchronous generators. Now, the increased penetration of load and generation interfaced by converter based systems has demanded changes in the way the grid is managed. If the aforementioned issues are not considered, local instability can lead to system-wide instability. One possible solution for the majority of these issues is to change the control logic of the converter, modifying it from the standard vectorial output current theory (DQCl control) to one where the traditional synchronous generator is emulated. These solutions are based within the so called Virtual Synchronous Machine or VSM algorithms. Among them, the so-called Virtual Synchronous Machine Zero Inertia (VSM0H) has been implemented in this paper. Due to its simplicity and efficacy, it has been chosen for experimental testing and analysis. The process to implement the VSM0H algorithm in the lab will be explained; with particular emphasis in the connection process since, with the VSM0H algorithm, the converter becomes a true voltage source, and this procedure can be particularly challenging. An explanation of the blocks added to provide this soft connection will be explained. Additionally, another experiment showing the behavior of the system against changes in the power references will be shown.

3. L. Reguera, A. Lazaro and A. Roscoe, "Experimental analysis of a fully compliant grid inverter with controllable response," presented at the IEEE 12th International Conference on Power Electronics and Drive Systems (PEDS), Honolulu, HI, 2017, pp. 1,167-1,171.

Abstract: *This paper continues on from previous work where a grid connected inverter with ancillary functions was explained, designed and simulated. In this paper, the project will continue implementing the converter in a microgrid; experiments have been conducted to evaluate the performance and fulfillment of a grid code compliant inverter. Before, the system had the capability of changing, automatically, the internal converter dynamics. Now, these functionalities have been exploited further and the it is able to adapt its response speed even when the system is already connected and injecting power to the grid. This characteristic makes the converter not only fully compliant with the most common grid codes of Spain, Denmark and the UK but also dynamic depending on the grid situation. As a result, the converter is more grid-friendly and easily customized and at the same time improves the stability of the converter itself.*

Appendix A. Publications